ESCUELA TÉCNICA SUPERIOR DE INGENIERÍA DE TELECOMUNICACIÓN
UNIVERSIDAD POLITÉCNICA DE CARTAGENA

**Proyecto Fin de Carrera**

# Análisis de discontinuidades de guía onda y filtros con resonadores guía onda con ridges asimétricos mediante el método Mode Matching

AUTOR: María Valverde Navarro
DIRECTOR(ES): José Luís Gómez Tornero

Cartagena, Mayo 2006


| | |
|---|---|
| **Autor** | María Valverde Navarro |
| **E-mail del Autor** | maria.valverde@gmail.com |
| **Director(es)** | Jose Luís Gómez Tornero |
| **E-mail del Director** | josel.gomez@upct.com |
| **Codirector(es)** | |
| **Título del PFC** | Análisis de discontinuidades de guía onda y filtros con resonadores guía onda con ridges asimétricos mediante el método Mode Matching |
| **Descriptores** | Filtros de microondas, guías de onda, filtros plano-E |

**Resumen**

El principal objetivo de este proyecto fin de carrera consiste en explorar las posibilidades de mejora de las características de los filtros plano-E con inserciones metálicas, incorporando guías de onda con ridges asimétricos.

En primer lugar se ha llevado a cabo el análisis de discontinuidades entre guías de onda mediante el método *Mode Matching*. Dicho método ha sido empleado para el modelado de filtros plano-E que incorporan secciones de guía de onda ridge actuando como resonadores. Tras el desarrollo de una herramienta rápida y eficiente de simulación, los resultados obtenidos han sido analizados y validados, obteniendo ventajas frente a configuraciones estándar, tales como el aumento de la selectividad y la reducción de las dimensiones del filtro. También es importante destacar la aparición de ceros de transmisión a frecuencias finitas. Además, tres prototipos han sido fabricados y medidos, obteniendo resultados aceptables para filtros con un resonador. Finalmente, son propuestas distintas líneas futuras que continúan el trabajo realizado a lo largo de este proyecto fin de carrera.

| | |
|---|---|
| **Titulación** | Ingeniero Superior de Telecomunicación |
| **Intensificación** | Sistemas y Redes de Telecomunicación |
| **Departamento** | Tecnología de la Información y la Comunicación |
| **Fecha de Presentación** | Mayo de 2006 |

*Agradezco a D. George Goussetis y a D. José Luís Gómez Tornero*
*su apoyo y dedicación a lo largo de este proyecto.*

# ÍNDICE GENERAL

# ÍNDICE PARTE I

# 1. INTRODUCCIÓN.

## 1.1. FILTROS DE MICROONDAS

Los filtros pasivos de microondas son componentes esenciales en la implementación de sistemas de telecomunicación. Su objetivo principal es dejar pasar las señales deseadas y atenuar las señales no deseadas.

Generalmente, los filtros de microondas están compuestos por líneas de transmisión o guías de onda. Las líneas de transmisión usadas frecuentemente para la fabricación de estos filtros son: stripline, línea microstrip, línea coaxial, guía de onda circular, guía de onda rectangular, guía de onda con ridge y guía de onda con dieléctrico.

Dependiendo de las especificaciones eléctricas, mecánicas y ambientales, algunas líneas de transmisión ofrecen mejor rendimiento que otras. Es responsabilidad del diseñador ser consciente de las propiedades de todas las líneas de transmisión para obtener un rendimiento óptimo del filtro.

La investigación ha aumentado particularmente en la última década con un gran crecimiento de los sistemas de telecomunicación wireless y vía satélite, los cuales requieren un alto rendimiento y fiabilidad en el diseño de los filtros.

## 1.2. FILTROS PLANO-E

Elementos inductivos, como strips transversales, son muy empleados en la industria para producir filtros pasa banda de guía de onda para una amplia variedad de aplicaciones. Sin embargo, es muy difícil producirlos a bajo coste y de manera masiva. Para resolver este problema, los filtros con inserciones metálicas (septum) en el plano E son propuestos en [1].

La configuración estándar de los filtros plano-E consiste en usar una guía de onda separada en bloques y situar obstáculos inductivos en el plano E de una guía de onda rectangular, separados entre ellos cerca de la mitad de la longitud de onda. La configuración estándar de los filtros plano-E es presentada en la *Figura 1-1*.

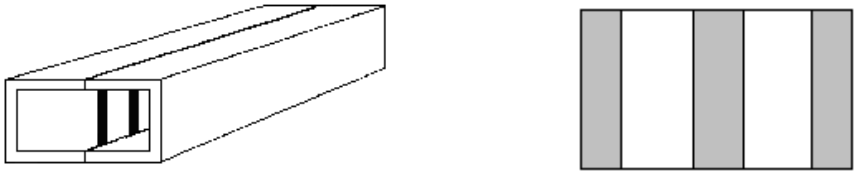

*(a)* *(b)*

*Figura 1-1: Geometría del filtro plano-E (a) y layout de la inserción metálica(b)*

Estas configuraciones tienen muchas características ventajosas, incluyendo bajo coste, no necesidad de puesta a punto y producción masiva. Otra ventaja de estos filtros es que las inserciones metálicas consisten en circuitos impresos que son muy fáciles de fabricar empleando para ello el proceso fotolitográfico.

No obstante, a pesar de estas ventajas, la banda de rechazo puede presentar características inapropiadas para determinadas aplicaciones, como en el caso de los multiplexores. La resonancia armónica de los resonadores que forman el filtro aparece como un espurio en la banda de paso del filtro plano-E a una frecuencia aproximadamente 1.5 veces la frecuencia central [2]. Este efecto limita el ancho de banda disponible o requiere componentes extra para eliminar dichos espurios.

Además, guías de onda con ridge pueden ser incorporadas en la tecnología de inserciones metálicas en el plano E, tal y como se muestra en la *Figure 1-2 (a)*, añadiendo finos ridges impresos sobre la inserción metálica sin aumentar la complejidad de fabricación. Tanto la longitud de onda guiada como la impedancia característica, en la propagación por la guía de onda con ridge, varían con respecto a la altura de los ridges. Por lo tanto, permite cambiar las características de propagación a lo largo de la misma guía de onda. Basándonos en este punto, [6] sugirió que el uso de secciones de guías de onda con ridges actuando como resonadores en un filtro plano-E podría optimizar la respuesta en la banda de rechazo sin incrementar la complejidad en su fabricación. El argumento de [7] fue que todas las secciones de guía onda resuenan a una frecuencia fundamental particular. Por lo contrario, no resuenan a la vez a frecuencias altas, siempre y cuando el gap entre los ridges sea diferente. Esto da lugar a diferentes longitudes de onda de la guía en las distintas secciones del filtro. Debido a esto, los armónicos de resonancia aparecerán desplazados a frecuencias mayores y la atenuación en la banda de rechazo generalmente será mejorada.

Uno de los objetivos de este proyecto es mejorar la selectividad de la respuesta del filtro. Para ello, se incorporan guías de onda con ridges asimétricos en la tecnología de inserciones metálicas en el plano E, como es presentado en la *Figura 1-2 (a)*, debido a que este tipo de configuraciones pueden dar lugar a la aparición de ceros de transmisión a frecuencias finitas cercanas a la banda de paso del filtro incrementando así la selectividad. Ésta es una de las principales ventajas encontradas con respecto a la configuración estándar de la *Figura 1-1*.

Cuando la onda que se propaga puede atravesar la guía por dos caminos diferentes, al final de la guía las ondas que van por cada camino pueden sumarse en fase o en oposición de fase. Como ejemplo, en la *Figura 1-2 (b)* se presentan las respuestas de dos filtros como los de la *Figura 1-2 (a)*, con resonadores en posiciones opuestas, donde se da el acoplo cruzado entre ellos y un cero de transmisión aparece cercano a la banda de paso mejorando con ello la selectividad del filtro.

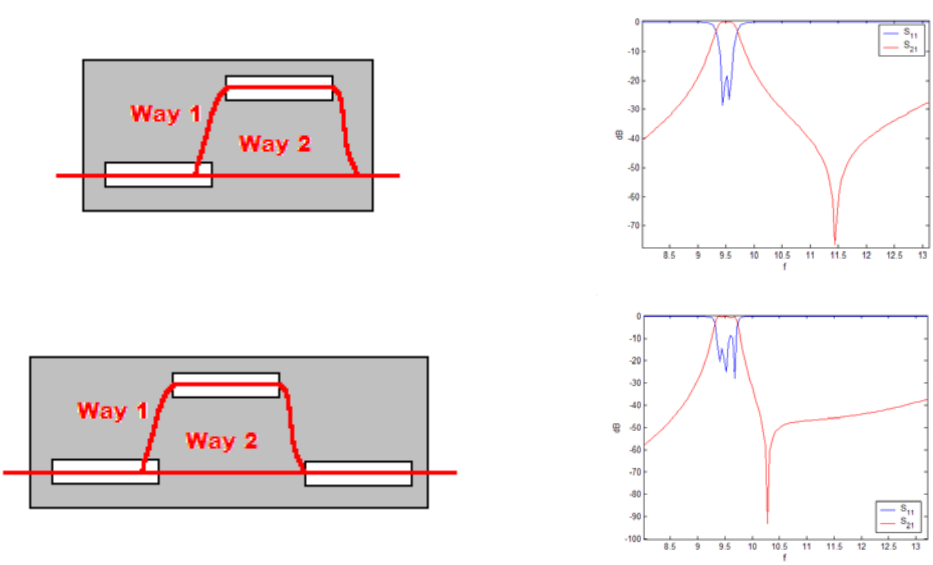


(a) (b)

*Figura 1-2: Inserción metálica de filtros plano-E con dos y tres guías de onda ridge asimétricas (a) y la correspondiente respuesta de dichos filtros (b)*

Además, como en todas las estructuras de guía de onda, siempre está presente la cuestión del peso. Es importante, por ejemplo en aplicaciones espaciales, donde las unidades de masa a bordo de los satélites son muy caras de poner en órbita. Varias sugerencias para la miniaturización de los componentes de guía de onda han sido comentadas en [3], [4], [5].

Una solución posible para conseguir la miniaturización es rellenar la guía de onda con dieléctrico. Esto reduce la longitud de onda en un factor inversamente proporcional a la permitividad del dieléctrico y la miniaturización es conseguida por el hecho de que una longitud física corta es vista eléctricamente más larga. Sin embargo hay una desventaja principal en esta propuesta, el hecho de que las pérdidas totales comparadas con la guía de onda estándar son significantemente mayores. Por lo tanto, a pesar de lo anterior, un campo considerable para la aplicación de la tecnología de las guías de onda en estructuras MIC y MMIC queda abierto.

Por tanto, otra solución es propuesta para resolver el problema del tamaño. Dicha solución será estudiada a lo largo de este trabajo, y consiste en incorporar guías ridge a la configuración estándar. En capítulos posteriores será demostrado que el tamaño total del filtro es reducido obteniendo la misma respuesta pero mejorando la selectividad y conservando bajas las pérdidas totales.

## 1.3. MODELADO DE FILTROS PLANO-E

La *Figura 1-3 (a)* presenta el layout de la inserción metálica de un filtro plano-E indicando las diferentes secciones que pueden formar un filtro. Como se muestra en la figura, un filtro esta constituido básicamente por acopladores inductivos y resonadores. Los bloques metálicos actúan como acopladores y consisten básicamente en secciones de guía de onda reducida. Además podemos encontrar diferentes tipos de resonadores: la guía de onda tradicional (WG) y la guía de onda con ridge actúan como resonadores simples, sin embargo, la guía de onda coaxial ridge se comporta como dos resonadores en paralelo. Por lo tanto, podemos decir que los filtros plano-E están formados por la unión de distintas guías de onda, como se muestra en la *Figura 1-3 (b).*

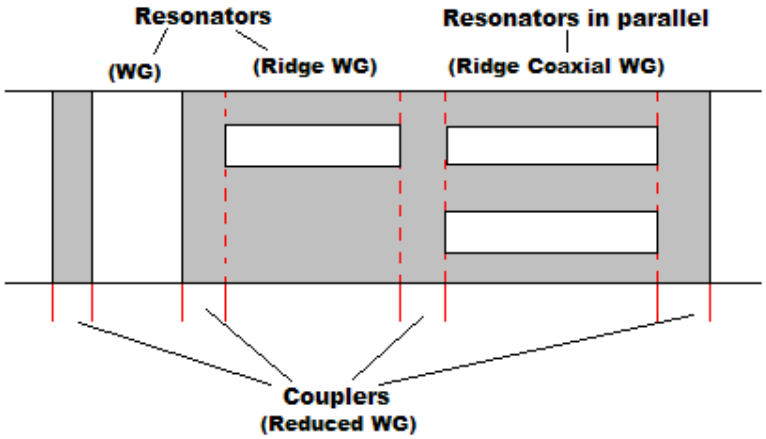


*(a)*

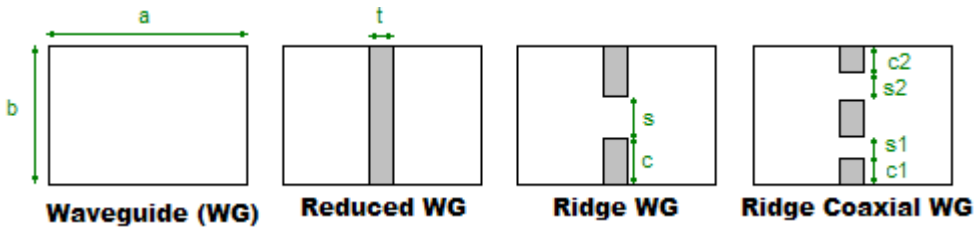


*(b)*

*Figura 1-3: Inserción metálica que indica las partes de un filtro plano-E (a), y la sección transversal de varias guías de onda*

Por lo tanto, para calcular la respuesta final del filtro es necesario resolver dos problemas diferentes.

El primero de ellos es estudiar la propagación en cada sección de guía de onda, principalmente calculado los modos que pueden existir en cada una de las secciones. En el caso de la guía de onda tradicional y de la reducida, el cálculo de los modos es analítico. Al contrario, para las guías de onda ridge y coaxial ridge, el cálculo no es analítico, por esta razón métodos como el de *Resonancia Transversa* y *Field Matching* son necesarios para obtener los modos en estas guías. El procedimiento para llevar a cabo esta tarea está explicado en [8], y también está resuelta la propagación en las guías ridge y coaxial con ridge.

El segundo problema, y uno de los principales objetivos del proyecto, es obtener el modelado completo de los filtros plano-E con inserciones metálicas que incorporan guías de onda ridge. Primero es necesario analizar las discontinuidades formadas por las diferentes secciones que forman el filtro. Principalmente, las discontinuidades que aparecen en la *Figura 1-3 (a)* son: Guía de onda- Guía de onda reducida, Guía de onda ridge- Guía de onda reducida y Guía de onda coaxial ridge- Guía de onda ridge. En [9] la primera de ellas fue estudiada y la segunda fue analizada pero para un caso particular en el que el resonador se sitúa en una posición simétrica. Por esta razón, la discontinuidad entre una guía de onda ridge general (resonador tanto en posición simétrica como en asimétrica) y una guía de onda reducida es estudiada en este proyecto por primera vez. La última de las discontinuidades nombradas anteriormente es mencionada en el capítulo nueve como una tarea futura interesante.

La matriz general de parámetros S de la discontinuidad entre una guía de onda ridge y una guía de onda reducida es obtenida aplicando el método *Mode Matching*. Básicamente, este método analiza los campos en la unión de dos guías con distinta sección transversal. El capítulo dos presenta la formulación general del método y su aplicación para caracterizar la discontinuidad bajo estudio. Una vez que las matrices generales de parámetros S de todas las discontinuidades están disponibles, la matriz general de parámetros S global del filtro puede ser obtenida usando el procedimiento de cascada de matrices.

## 1.4. PROPAGACIÓN EN FILTROS PLANO-E

Los filtros bajo estudio en este proyecto van a trabajar principalmente en la banda X, por lo tanto la frecuencia central más baja será 8 GHz y la más alta 12 GHz. Además, serán excitados con el primer modo TE de una guía de onda rectangular, el modo $TE_{10}$. La distribución de campo de este modo es presentada en la *Figura 1-4.*

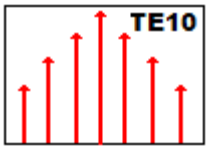


*Figura 1-4: $TE_{10}$ de una guía de onda rectangular*

Atendiendo a las frecuencias de corte de los modos en cada sección del filtro es posible saber qué modos se propagan. Si la frecuencia de corte del modo, $f_c$, es menor que la frecuencia central de trabajo del filtro, $f_o$, el modo se propaga.

| Condición de propagación | $fc < fo$ |
|---|---|

Por lo tanto, el número de onda de corte, $k_c = \frac{2 \cdot \pi \cdot f_c}{c_o}$, está relacionado directamente con la $f_c$ y es determinado por las condiciones de contorno a lo largo de los ejes x e y. Lo que quiere decir que $k_c$ permite sólo tener un conjunto de valores discretos, cada uno de los cuales corresponde a un modelo de distribución de campo en x-y que se propaga a lo largo de z según $e^{(j\omega t-\gamma z)}$ donde:

$$\gamma = \sqrt{k_o^{\,2} - k_c^{\,2}}$$

Un modo se propagará cuando $k_c < k_o$ , o, in otras palabras, cuando $\gamma$ sea real. Si $k_c > k_o$ , $\gamma$ es puramente imaginaria, por lo tanto el modo no se propaga. Estos últimos modos reciben el nombre de modos evanescentes o reactivos y están caracterizados porque se atenúan de manera exponencial y por el hecho de que presentan un desplazamiento de fase.

La *Tabla 1-1* da as frecuencias de corte de los dos primeros modos en las distintas secciones, como, guía de onda, guía de onda reducida, guía de onda ridge y guía de onda coaxial ridge.

A diferencia del caso de la guía de onda reducida, las frecuencias de corte de los primeros modos en cada sección son menores que las posibles frecuencias centrales de la banda X. Por lo tanto, el primer modo satisface la condición de propagación y se propagará.

Es de señalar, que si la guía de onda reducida es vista como una guía de onda con la mitad de la anchura, el primer modo de la guía de onda reducida tendrá una frecuencia de corte mayor que la de la guía de onda (donde $f_c = \frac{c_o}{2}\sqrt{\left(\frac{m}{a}\right)^2 + \left(\frac{n}{b}\right)^2}$). Este efecto es apreciado en la *Tabla 1-1*, donde $f_c^{WG}$=6,561679615 GHz y $f_c^{RedWG}$=13,18101898 GHz≈ $2 \cdot f_c^{WG}$.

En el caso del segundo modo de las secciones, las frecuencias de corte son mayores que las posibles frecuencias centrales de la banda X. Debido a esto, el segundo modo y otros modos de orden mayor no se propagan.

| | fc 1° modo TE (GHz) | fc 2° modo TE (GHz) |
|---|---|---|
| Guía de onda | 6,561679615 | 16,1562629 |
| Guía de onda reducida | 13,18101898 | 14,7637797 |
| Guía de onda ridge | 4,53617877 | 14,0478872 |
| Guía de onda coaxial ridge | 6,143415621 | 15,982071 |

*Tabla 1-1: Frecuencias de corte del primer y Segundo modo de diferentes guías de onda*

Dimensiones de la guía de onda en mm: a=22.86, b=10.16

Dimensiones de la guía de onda reducida en mm: a=22.86, b=10.16, t=0.1

Dimensiones de la guía de onda ridge en mm: a=22.86, b=10.16, t=0.1, s=2, c=1

Dimensiones de la guía de onda coaxial ridge en mm: a=22.86, b=10.16, t=0.1, s1=s2=2, c1=c2=1

La *Figura 1-5* muestra un ejemplo de filtro plano-E con diferentes secciones de guía de onda para explicar la propagación de los modos a través del filtro. Cuando el modo $TE_{10}$ viaja a través de la guía y llega a la guía de onda reducida es transformado en modos evanescentes. Estos modos son excitados con una amplitud que se va reduciendo exponencialmente a lo largo de la sección de guía de onda reducida hasta llegar a la siguiente sección. En algunas ocasiones, cuando la sección de guía de onda reducida es demasiado larga los modos evanescentes desaparecen antes de llegar a la siguiente sección, y por tanto, no tiene lugar ninguna propagación.

Cuando los modos evanescentes ven la discontinuidad con la guía de onda ridge, se transforman en el primer modo TE de esta guía. Si la siguiente sección es una guía de onda coaxial ridge, los modos que se propagan en esta sección son el TEM y el primer modo TE. El modo TEM es el modo fundamental de una guía de onda coaxial ridge, teniendo una frecuencia de corte nula. La energía total propagada en una guía de onda coaxial ridge será la combinación de ambos modos, el TEM y el $TE_1$, por encima del corte.

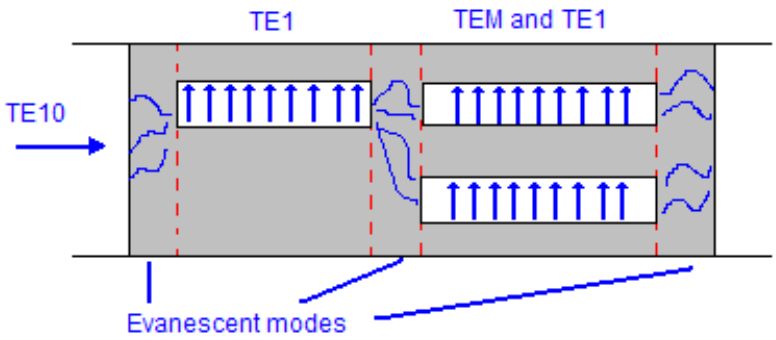


*Figura 1-5: Propagación de modos en un filtro plano-E excitado con el $TE_{10}$ de una guía de onda rectangular*

## 1.5. OBJETIVOS

El principal propósito de este proyecto consiste en explorar las posibilidades de mejora de las características de los filtros plano-E con inserciones metálicas incorporando guías de onda con ridges asimétricos. Uno de los objetivos más importantes es aumentar la selectividad y reducir las dimensiones del filtro conservando las ventajas que aporta este tipo de filtro, como bajo coste y producción masiva.

Para alcanzar el punto en el que la investigación sea factible, es necesaria una herramienta rápida y precisa para llevar a cabo la simulación de las estructuras bajo estudio.

Pero una de las tareas iniciales del proyecto, antes de llevar a cabo lo anterior, es formular en ecuaciones de matrices de autovalores los dos problemas que fueron comentados en la sección 1.3. El primero de ellos es la propagación en una guía de onda ridge que fue resuelto en [8]. Y el segundo de ellos es efectuado en este proyecto. Consiste en la aplicación del método Mode Matching para configuraciones plano-E. En particular se usa para caracterizar la discontinuidad entre una guía de onda ridge y una guía de onda reducida, y en una etapa superior para definir la matriz general de parámetros S global que genera la respuesta final del filtro.

También son investigados la mejora en la banda de rechazo, obteniendo incluso ceros de transmisión a frecuencias finitas, y el aumento de la selectividad del filtro para varias geometrías que incorporan la guía de onda ridge. Para llevar a cabo lo anterior se realiza un análisis que relacione la mejora de la respuesta con los parámetros geométricos que posiblemente le afecten.

Habiendo desarrollado la herramienta de simulación propuesta anteriormente, directamente puede empezar la investigación del primer propósito del proyecto, es decir, la exploración de las oportunidades de mejora de la respuesta de los filtros plano-E usando guías de onda ridge.

Además, como fue dicho previamente, siempre existe un compromiso con el peso de las configuraciones, en especial en aplicaciones espaciales. Por esta razón el segundo propósito principal es reducir el tamaño total del filtro conservando la mejora de su respuesta y las pérdidas totales en un nivel bajo.

# 2. TRABAJO DESARROLLADO

Este capítulo se encarga de resumir el trabajo llevado a cabo a lo largo del proyecto, resaltando las conclusiones y resultados más importantes.

## 2.1. MODE MATCHING

En esta sección se presenta el método Mode Matching (MM) para analizar el campo en la discontinuidad creada por la unión de dos guías de onda con distinta sección transversal y se realiza el cálculo de la matriz general de parámetros S en dicha unión entre las guías a partir del análisis MM. La matriz de parámetros S se dice que es general debido a que mide los parámetros S tanto para el modo fundamental como para los modos de orden superior. Por lo tanto, un circuito de microondas compuesto de distintas secciones de guías de onda puede ser descompuesto en términos de sus matrices generales de parámetros S y, posteriormente, pude ser calculada la matriz global de parámetros S del circuito mediante la cascada de dichas matrices.

Por lo tanto, combinando los métodos MM y el de cálculo de la matriz general de parámetros S obtenemos el análisis completo de los campos en un filtro pasa banda de guía de onda rectangular con ridges, cumpliendo así uno de los principales propósitos del proyecto.

El método MM es un método de discretización modal utilizado, antes que los de discretización en espacio o tiempo, cuando las estructuras tienen una forma geométrica simple debido a que se necesita menos memoria y menos tiempo de procesado para converger a la solución. Además de estas ventajas, es el más eficiente para una predicción precisa de la respuesta electromagnética de estructuras plano-E y para estructuras que consisten en la cascada de secciones de guía de onda homogéneas.

Las fórmulas que se presentan a continuación están basadas en [9] y son válidas para cualquier sección transversal.

El primer paso del método MM consiste en la descomposición de la estructura en dos secciones rectangulares de guía de onda, *WG-I* y *WG-II,* como muestra la *Figura 2.1-1*.

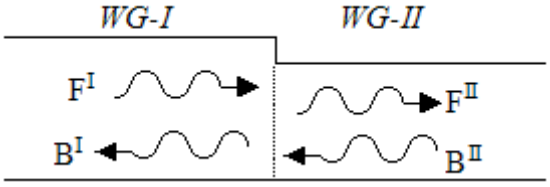


*Figure 2.1-1: Surface discontinuity*

Los campos eléctrico y magnético de cada sección se pueden expresar como la suma de sus componentes TE y TM:

$$E = E_{TE} + E_{TM} = \nabla \times A_h + \frac{1}{j\omega\varepsilon} \nabla \times \nabla \times A_e \qquad (2.1\text{-}1)$$

$$H = H_{TM} + H_{TE} = \nabla \times A_e - \frac{1}{j\omega\mu} \nabla \times \nabla \times A_h \qquad (2.1\text{-}2)$$

Donde $A_h$ and $A_e$ son los vectores potenciales eléctrico y magnético respectivamente, definidos como:

$$A_h = \sum_{q=1}^{\infty} \sqrt{Z_{hq}} \cdot T_{hq}(x,y) \cdot \left[ F_{hq} e^{-j \cdot K_{zhq} \cdot z} + B_{hq} e^{+j \cdot K_{zhq} \cdot z} \right] \cdot \hat{z} \qquad (2.1\text{-}3)$$

$$A_e = \sum_{p=1}^{\infty} \sqrt{Y_{ep}} \cdot T_{ep}(x,y) \cdot \left[ F_{ep} e^{-j \cdot K_{zep} \cdot z} - B_{ep} e^{+j \cdot K_{zep} \cdot z} \right] \cdot \hat{z} \qquad (2.1\text{-}4)$$

La matriz de parámetros S puede ser calculada, cuando las ondas incidentes son conocidas, mediante la siguiente expresión:

$$\begin{bmatrix} B^I \\ F^{II} \end{bmatrix} = \begin{bmatrix} S_{11} & S_{12} \\ S_{21} & S_{22} \end{bmatrix} \cdot \begin{bmatrix} F^I \\ B^{II} \end{bmatrix} \qquad (2.1\text{-}5)$$

Con el fin de conocer las ondas incidente, se iguala el campo transversal eléctrico a ambos lados de la discontinuidad, tomando z=0, y se realiza lo mismo con el campo magnético obteniendo:

$$diag\left\{\sqrt{Z_{hq}^I}\right\} \cdot \left(F_h^I + B_h^I\right) = J_{hh} \cdot diag\left\{\sqrt{Z_{hs}^{II}}\right\} \cdot \left(F_h^{II} + B_h^{II}\right) + J_{he} \cdot diag\left\{\sqrt{Z_{et}^{II}}\right\} \cdot \left(F_e^{II} + B_e^{II}\right) \qquad (2.1\text{-}6)$$

$$diag\left\{\sqrt{Z_{er}^I}\right\} \cdot \left(F_e^I + B_e^I\right) = J_{eh} \cdot diag\left\{\sqrt{Z_{hs}^{II}}\right\} \cdot \left(F_h^{II} + B_h^{II}\right) + J_{ee} \cdot diag\left\{\sqrt{Z_{et}^{II}}\right\} \cdot \left(F_e^{II} + B_e^{II}\right) \qquad (2.1\text{-}7)$$

$$J_{hh}^T \cdot diag\left\{\sqrt{Y_{hq}^I}\right\} \cdot \left(F_h^I - B_h^I\right) + J_{eh}^T \cdot diag\left\{\sqrt{Y_{er}^I}\right\} \cdot \left(F_e^I - B_e^I\right) = diag\left\{\sqrt{Y_{hs}^{II}}\right\} \cdot \left(F_h^{II} - B_h^{II}\right) \qquad (2.1\text{-}8)$$

$$J_{he}^T \cdot diag\left\{\sqrt{Y_{hq}^I}\right\} \cdot \left(F_h^I - B_h^I\right) + J_{ee}^T \cdot diag\left\{\sqrt{Y_{er}^I}\right\} \cdot \left(F_e^I - B_e^I\right) = diag\left\{\sqrt{Y_{et}^{II}}\right\} \cdot \left(F_e^{II} - B_e^{II}\right) \qquad (2.1\text{-}9)$$

Las matrices J se llaman matrices de acoplo y son definidas de la siguiente manera:

$$\left(J_{hh}\right)_{qs} = \iint_{SII} (\nabla T_{hq}^I \times \hat{z}) \cdot (\nabla T_{hs}^{II} \times \hat{z}) dS \qquad (2.1\text{-}10)$$

$$\left(J_{eh}\right)_{rs} = \iint_{SII} (-\nabla T_{er}^I) \cdot (\nabla T_{hs}^{II} \times \hat{z}) dS \qquad (2.1\text{-}11)$$

$$\left(J_{he}\right)_{qt} = \iint_{SII} (\nabla T_{hq}^{I} \times \hat{z}) \cdot (-\nabla T_{et}^{II}) dS = 0 \qquad (2.1\text{-}12)$$

$$\left(J_{ee}\right)_{rt} = \iint_{SII} (-\nabla T_{er}^{I}) \cdot (-\nabla T_{et}^{II}) dS \qquad (2.1\text{-}13)$$

Multiplicando (2.1-6), (2.1-7), (2.1-8) y (2.1-9) con $diag\left\{\sqrt{Y_{hq}^{I}}\right\}$, $diag\left\{\sqrt{Y_{er}^{I}}\right\}$, $diag\left\{\sqrt{Y_{hs}^{II}}\right\}$, $diag\left\{\sqrt{Y_{ey}^{II}}\right\}$ respectivamente, podemos escribirlas en forma de matriz como:

$$\begin{bmatrix} F_h^I + B_h^I \\ F_e^I + B_e^I \end{bmatrix} = M \cdot \begin{bmatrix} F_h^{II} + B_h^{II} \\ F_e^{II} + B_e^{II} \end{bmatrix} \qquad \begin{bmatrix} F_h^{II} - B_h^{II} \\ F_e^{II} - B_e^{II} \end{bmatrix} = M^T \cdot \begin{bmatrix} F_h^I - B_h^I \\ F_e^I - B_e^I \end{bmatrix} \qquad (2.1\text{-}14)$$

donde

$$M = \begin{bmatrix} diag\left\{\sqrt{Y_{hq}^{I}}\right\} \cdot J_{hh} \cdot diag\left\{\sqrt{Z_{hs}^{II}}\right\} & diag\left\{\sqrt{Y_{hq}^{I}}\right\} \cdot J_{he} \cdot diag\left\{\sqrt{Z_{et}^{II}}\right\} \\ diag\left\{\sqrt{Y_{er}^{I}}\right\} \cdot J_{eh} \cdot diag\left\{\sqrt{Z_{hs}^{II}}\right\} & diag\left\{\sqrt{Y_{er}^{I}}\right\} \cdot J_{ee} \cdot diag\left\{\sqrt{Z_{et}^{II}}\right\} \end{bmatrix} \qquad (2.1\text{-}15)$$

Volviendo a la expresión (2.1-5), obtenemos los parámetros S en la unión de dos guías de onda, tal y como se muestra a continuación:

$$\begin{aligned} S_{11} &= -W \cdot \left(U - M \cdot M^T\right) \\ S_{12} &= 2 \cdot W \cdot M \\ S_{21} &= M^T \cdot \left[U + W \cdot \left(U - M \cdot M^T\right)\right] \\ S_{22} &= U - 2 \cdot M^T \cdot W \cdot M \end{aligned} \qquad (2.1\text{-}16)$$

donde U es la matriz unitaria y W es dada como:

$$W = (U + MM^T)^{-1} \qquad (2.1\text{-}17)$$

El análisis anterior es válido para discontinuidades planas entre dos guías de onda. Pero los filtros estudiados en el proyecto consisten en la cascada de secciones de guía de onda con una longitud finita, tal y como se muestra en la *Figura 2.1-2*. Por lo tanto a continuación es presentado el método para obtener la matriz global de parámetros S que caracteriza al filtro.

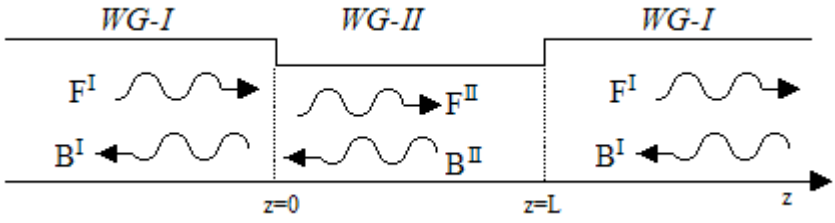


*Figura 2.1-2: Cascada de distintas secciones*

En primer lugar, para obtener la matriz S es necesario tener en cuenta el efecto de la propagación a lo largo de la sección de longitud L, según la siguiente expresión:

$$\begin{bmatrix} F \\ B \end{bmatrix} = \begin{bmatrix} \mathrm{diag}\left\{\exp\left(-jk_z L\right)\right\} & 0 \\ 0 & \mathrm{diag}\left\{\exp\left(+jk_z L\right)\right\} \end{bmatrix} \cdot \begin{bmatrix} F^L \\ B^L \end{bmatrix} \qquad (2.1\text{-}18)$$

Por lo tanto, la matriz de parámetros S en la sección vendrá dada por:

$$\begin{bmatrix} \begin{bmatrix} B_h^{II} \\ B_e^{II} \end{bmatrix} \\ \begin{bmatrix} F_{h\,L}^{II} \\ F_{e\,L}^{II} \end{bmatrix} \end{bmatrix} = \begin{bmatrix} 0 & \begin{bmatrix} D_h^{II} & D_e^{II} \end{bmatrix} \\ \begin{bmatrix} D_h^{II} & D_e^{II} \end{bmatrix} & 0 \end{bmatrix} \cdot \begin{bmatrix} \begin{bmatrix} F_h^{II} \\ F_e^{II} \end{bmatrix} \\ \begin{bmatrix} B_{h\,L}^{II} \\ B_{e\,L}^{II} \end{bmatrix} \end{bmatrix} \qquad (2.1\text{-}19)$$

donde

$$D_h^{II} = \mathrm{diag}\left\{\exp\left(-jk_{zh}^{II} \cdot L\right)\right\} \qquad D_e^{II} = \mathrm{diag}\left\{\exp\left(-jk_{ze}^{II} \cdot L\right)\right\} \qquad (2.1\text{-}20)$$

Ahora es cuando hay que superponer las matrices de parámetros S para obtener la matriz general que define la estructura, tal y como se muestra en las siguientes expresiones y en la *Figura 2.1-3*.

$$\begin{bmatrix} B_{IN} \\ F_{MED} \end{bmatrix} = \begin{bmatrix} S_{11}^F & S_{12}^F \\ S_{21}^F & S_{22}^F \end{bmatrix} \cdot \begin{bmatrix} F_{IN} \\ B_{MED} \end{bmatrix} \qquad \begin{bmatrix} B_{MED} \\ F_{OUT} \end{bmatrix} = \begin{bmatrix} S_{11}^L & S_{12}^L \\ S_{21}^L & S_{22}^L \end{bmatrix} \cdot \begin{bmatrix} F_{MED} \\ B_{OUT} \end{bmatrix}$$

$$\begin{bmatrix} B_{IN} \\ F_{OUT} \end{bmatrix} = \begin{bmatrix} S_{11}^F + S_{12}^F S_{11}^L V S_{12}^F & S_{12}^F \left(I + S_{11}^L V S_{22}^F\right) S_{12}^L \\ S_{21}^L V S_{21}^F & S_{22}^L + S_{21}^L V S_{22}^F S_{12}^L \end{bmatrix} \cdot \begin{bmatrix} F_{IN} \\ B_{OUT} \end{bmatrix} \qquad (2.1\text{-}21)$$

donde

$$V = \left(I - S_{22}^F S_{11}^L\right)^{-1} \qquad (2.1\text{-}22)$$

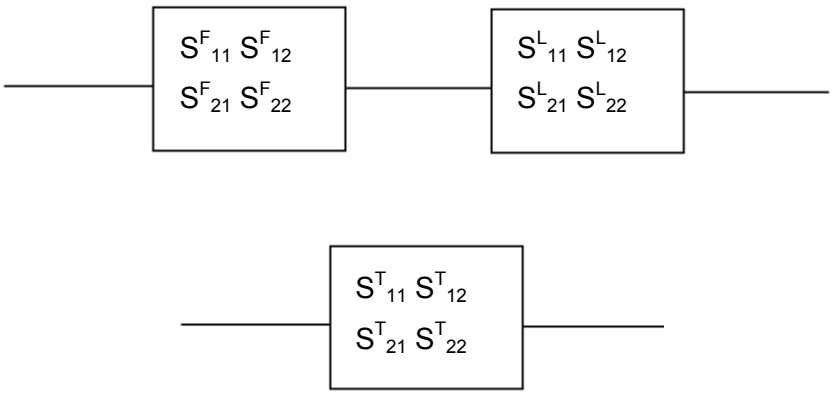


*Figura 2.1-3: Cascada de dos matrices de parámetros S*

Como caso particular se ha llevado a cabo el análisis de la discontinuidad creada entre una guía de onda ridge y una guía de onda reducida, quedando sus matrices de acoplo de la siguiente manera:

- n=0:

$$J_{hh} = A^I A^{II} \cdot (m\cdot\pi)^2 \cdot \frac{\sin(k^I e)}{b\cdot 2\cdot\sqrt{2}\cdot k^I} \qquad J_{eh} = A^I A^{II} \cdot m\cdot\pi \cdot \frac{\sin(k^I e)}{2\cdot\sqrt{2}\cdot k^I}$$

- m=0:

$$J_{hh} = A^I A^{II} \cdot (n\cdot\pi)^2 \cdot k^I \cdot \frac{b}{2} \cdot \frac{\cos(n\cdot\pi)\cdot\sin(k^I e)}{(k^I e)^2 - (n\cdot\pi)^2} \qquad J_{eh} = 0$$

- Otro caso:

$$J_{hh} = A^I A^{II} \cdot \pi^2 \cdot \frac{k^I}{2\cdot b} \cdot \frac{\cos(n\cdot\pi)\cdot\sin(k^I e)}{(k^I e)^2 - (n\cdot\pi)^2} \cdot \left((me)^2 + (n\cdot b)^2\right)$$

$$J_{eh} = A^I A^{II} \cdot \pi \cdot m \cdot \frac{\cos(n\cdot\pi)\cdot\sin(k^I e)}{2\cdot k^I}$$

Para todo m≥1:

$$J_{ee} = A^I A^{II} \cdot \pi \cdot \frac{n\cdot e}{2\cdot b} \cdot \frac{\cos(n\cdot\pi)\cdot\sin(k^I e)}{(k^I e)^2 - (n\cdot\pi)^2} \cdot \left((m\cdot\pi)^2 + (k^I \cdot b)^2\right)$$

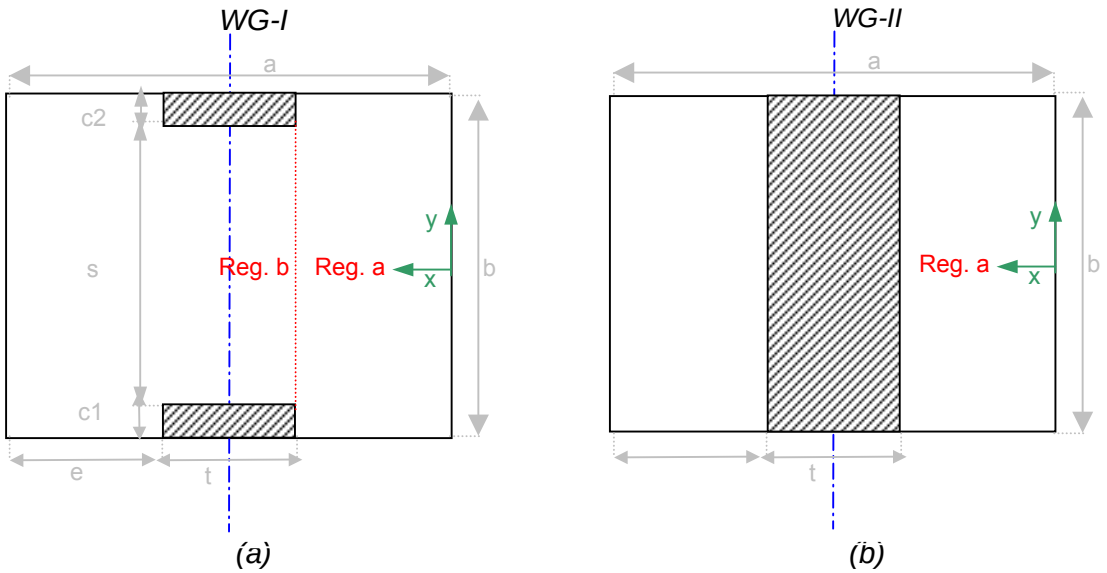


*Figure 2.1-4: Cross section of Ridge Waveguide (a) and Reduced Waveguide (b)*

## 2.2. PROGRAMACIÓN DEL MODELADO DE FILTROS PLANO-E EN FORTRAN Y MATLAB

FORTRAN [10] ha sido usado para resolver la formulación matemática presentada en la sección anterior debido a que su gran velocidad permite reducir el tiempo de ejecución. La principal función desarrollada recibe el nombre de *"GeneralFilter"* y se encarga de calcular la matriz global de parámetros S del filtro siguiendo el procedimiento descrito en la sección 2.2.

Además, ha sido desarrollada una interfaz interactiva en MATLAB [11] que se encarga de la representación de la respuesta final del filtro.

Por lo tanto, la combinación de ambos programas proporciona una herramienta rápida y fácil de utilizar que permite analizar de manera sencilla diferentes configuraciones de los filtros plano-E bajo estudio en este proyecto. En la *Figura 2.2-1* se muestra el aspecto de dicha interfaz.

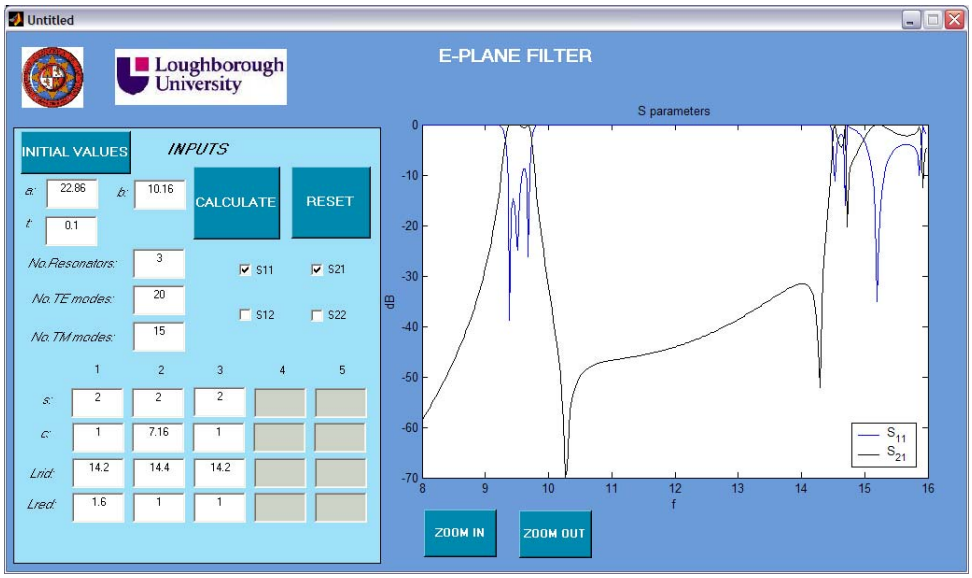


*Figura 2.2-1:Interfaz para la simulación de filtros plano-E*

Como se aprecia en la interfaz, es posible la simulación de filtros plano-E con hasta cinco resonadores, siendo el ejemplo mostrado para un filtro con tres resonadores posicionados de manera opuesta.

Hay que tener en cuenta que cuando se realizan programas de este estilo es necesario comprobar su precisión, y para ello es necesario realizar un estudio de la convergencia. En este caso, el estudio se realiza con respecto al número de modos TE y TM. Tras la realización de dicho estudio, buenos resultados han sido obtenidos escogiendo 20 modos TE y 15 modos TM.

## 2.3. ANÁLISIS DE FILTROS PLANO-E CON DISTINTO NÚMERO DE RESONADORES

Una vez completados el análisis matemático y la herramienta de simulación, la investigación de la mejora de la banda de rechazo y de la selectividad para distintas configuraciones de filtros plano-E puede ser llevada a cabo.

Las principales configuraciones estudiadas consisten en filtros plano-E con uno, dos y hasta tres resonadores situados tanto en posiciones simétricas como asimétricas. Finalmente, algunas conclusiones sobre la relación que guardan los parámetros geométricos del filtro con su respuesta final son comentadas a continuación.

En primer lugar, la longitud del resonador es uno de los parámetros que puede definir la banda de paso, ya que está directamente relacionado con la frecuencia. Otro parámetro importante es la altura de los resonadores. En general, la selectividad y la mejora de la banda de rechazo son maximizadas cuando la altura de los resonadores es estrecha. Además, la longitud de los acopladores es importante, porque cuando aumenta, la configuración es más reflectiva y el acoplo es más débil.

En segundo lugar, hay que tener en cuenta que uno de los objetivos principales es obtener una respuesta con un cero de transmisión cercano a la banda de paso mejorando con ello la selectividad. Por esta razón, hay que recordar que los resonadores tienen que situarse en posiciones opuestas cercanos a las paredes de la guía, que su altura debe ser pequeña y que los acopladores interiores deben ser cortos. Siguiendo estas indicaciones seremos capaces de obtener filtros con alta selectividad y con ceros de transmisión en frecuencias finitas.

También es importante destacar que dos factores importantes en la etapa de diseño han sido analizados. Dichos factores son el factor de calidad (Q) y el coeficiente de acoplo (K), estudiados en un filtro plano-E con uno y dos resonadores respectivamente. En la *Figura 2.3-1* se presentan Q y K en 3D observando sus variaciones.

La conclusión de Q es que aumenta a medida que el resonador se encuentra más cerca de las paredes de la guía y a medida que el acoplador es más largo. Por el contrario, K aumenta cuando los resonadores se encuentran cerca entre si y cuando la longitud de los acopladores internos es pequeña.

Es interesante señalar que los resonadores tienen que ocupar posiciones opuestas para que el acoplo sea débil y llevar a cabo el objetivo de aumento de la selectividad, como se ha dicho anteriormente. Por lo tanto, como en este caso la dependencia de K con respecto a la longitud de los acopladores internos es despreciable, tal y como muestra la

*Figura 2.3-1*, se pueden escoger valores pequeños de longitud para los acopladores internos y cumplir así con otro de los principales objetivos reduciendo el tamaño total del filtro.

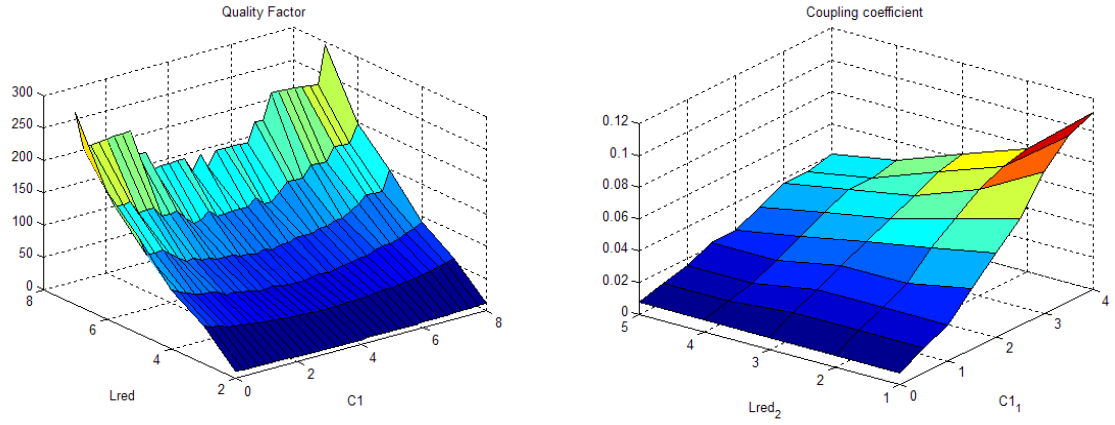


*(a)* *(b)*

*Figura 2.3-1: Factor de calidad (a) y coeficiente de acoplo (b)*

## 2.4. VALIDACIÓN DE LOS RESULTADOS

Después del análisis básico de los filtros plano-E, han sido simulados tres filtros con uno, dos y tres resonadores. Para la selección de las dimensiones del filtro, la respuesta simulada ha sido comparada con la de un prototipo con configuración estándar. Los resultados obtenidos han sido validados tomando como referencia el software comercial HFSS [12], tal y como se muestra en la *Figura 2.4-1*.

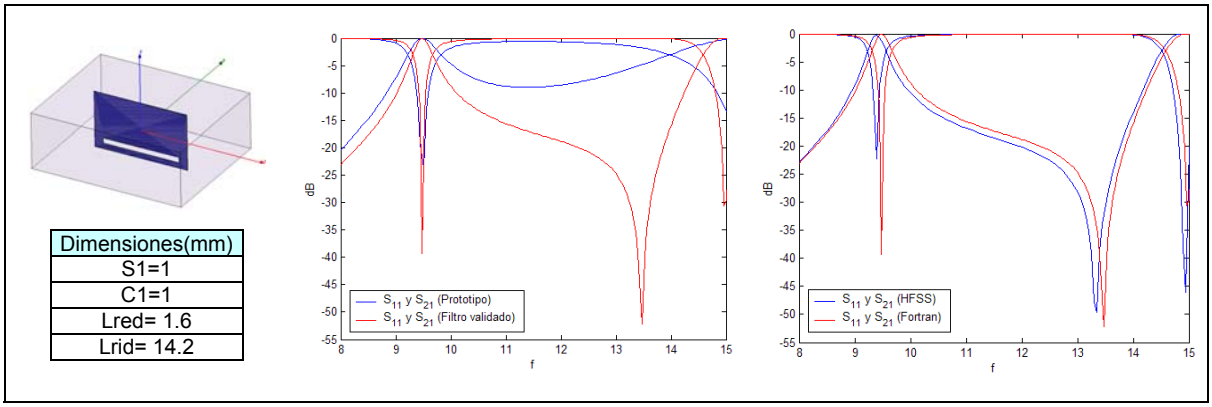


*(a)*

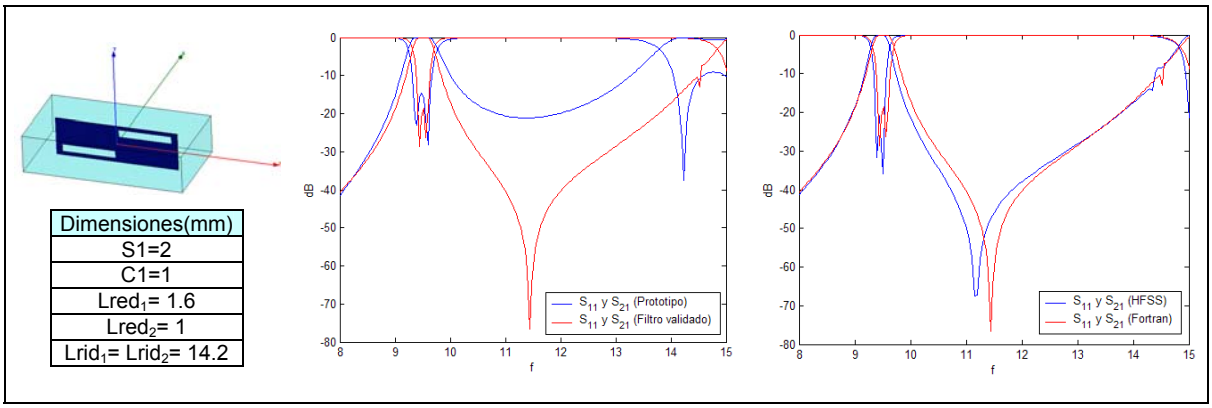


*(b)*

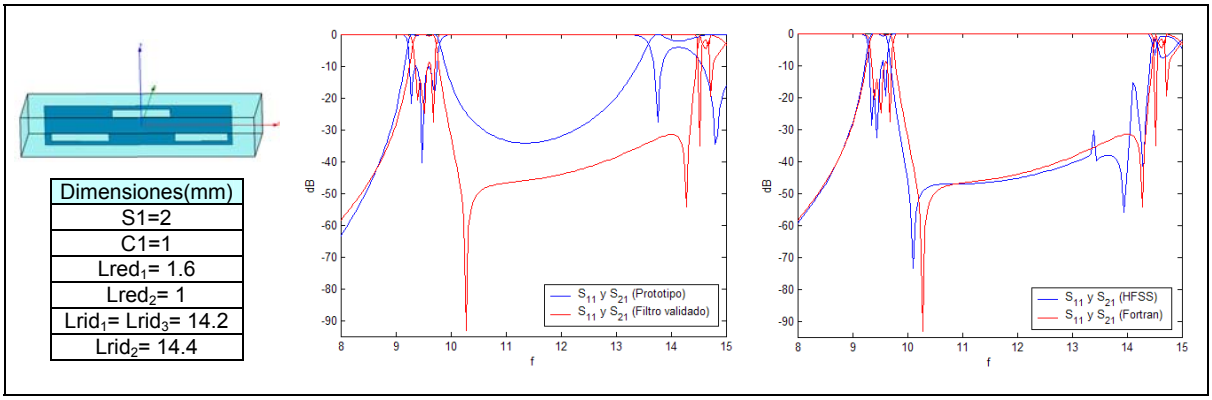


*(c)*

*Figura 2.4-1: Filtros plano-E con uno (a), dos (b) y tres (c) analizados y validados*

Los filtros validados tienen dos ventajas importantes con respecto a los prototipos. Una de ellas es que es más selectivo, debido al alto nivel de atenuación en la banda de rechazo y a la obtención de un cero de transmisión cercano a la banda de paso. La segunda ventaja es que la longitud total del filtro ha sido reducida tal y como se muestra en la *Tabla 2.4-1*.

| (mm) | Filtro Plano-E con inserciones metálicas simples | Filtro Plano-E Con guías de onda ridge | Diferencia |
|---|---|---|---|
| Filtro con un resonador | 20.403 | 17.4 | 3.003 |
| Filtro con dos resonadores | 25.0751 | 16.8 | 8.2751 |
| Filtro con tres resonadores | 66.3 | 48 | 18.3 |

*Tabla 2.4-1: Comparación de las longitudes del prototipo y del filtro analizado*

Además, la *Tabla 2.4-2* presenta la comparación de tiempo necesitado para simular la misma estructura en Fortran y HFSS, y muy buenos resultados son obtenidos. El equipo empleado para ello ha sido un AMD Athlon(tm) 64, 637 MHz, 1GB de RAM. Es importante señalar que a medida que aumenta el número de resonadores HFSS necesita una simulación más precisa y compleja.

| (seg.) | Fortran | HFSS | $Tiempo_{HFSS}/Tiempo_{Fortran}$ |
|---|---|---|---|
| Filtro con un resonador | 15 | 1260 | 84 |
| Filtro con dos resonadores | 24 | 2400 | 100 |
| Filtro con tres resonadores | 40 | 17820 | 445.5 |

*Tabla 2.4-1: Comparación de tiempos simulando el filtro en Fortran y en HFSS*

## 2.5. MEDIDAS DE PROTOTIPOS FABRICADOS

A partir de la validación anterior, se han fabricado tres prototipos presentados en la *Figura 2.5-1*, que permiten la validación experimental de dichos filtros. En dicha figura se muestra una comparación entre la respuesta simulada y medida de cada uno de los filtros.

| Dimensiones (mm) |
|---|
| B=10.05 |
| Lred=1.6 |
| Lrid=14.2 |
| T=0.1 |
| C1=1 |
| S1=2 |

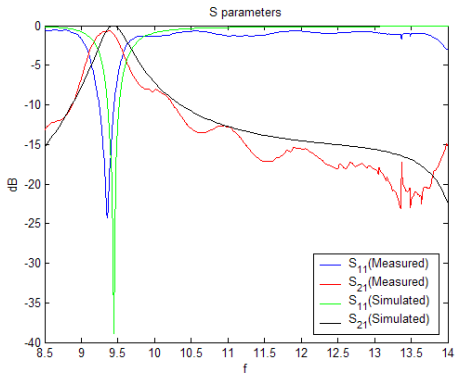


*(a)*

| Dimensiones (mm) |
|---|
| B=10.05 |
| T=0.1 |
| $Lred_1$=1.6 |
| $Lred_2$=1 |
| Lrid=14.2 |
| C1=1 |
| S1=2 |

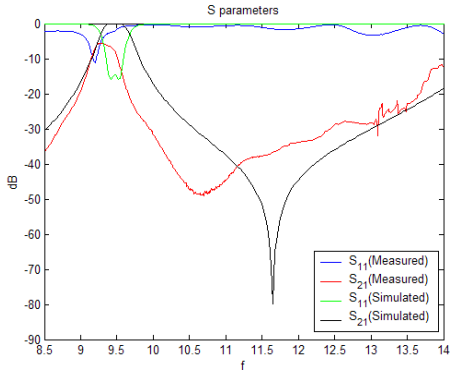


*(b)*

| Dimensiones (mm) |
|---|
| B=10.05 |
| T=0.1 |
| $Lred_1$=1.6 |
| $Lred_2$=1 |
| Lrid=14.2 |
| C1=1 |
| S1=2 |

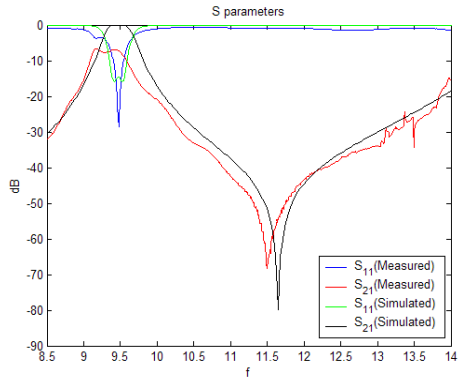


*(c)*

*Figura 2.5-1: Prototipos fabricados y comparación de los resultados medidos y simulados*

Buenos resultados entre la simulación y las medidas han sido obtenidos para el filtro fabricado con un resonador. Las pérdidas en la banda de paso son menores a 1dB, por lo tanto los resultados son aceptables. Por el contrario, los resultados obtenidos para las dos configuraciones fabricadas con dos resonadores no son aceptables debido a que las pérdidas en la banda de paso superan los 5dB. Al igual que una simulación más compleja es requerida cuando el número de resonadores aumenta, la fabricación debe ser más precisa debido a que cualquier mínimo error en el prototipo o mal contacto entre la inserción metálica y la guía dan lugar a grandes pérdidas.

Teniendo en cuenta lo señalado anteriormente, hay que recordar que para futuras fabricaciones es importante mejorar el contacto entre la guía de onda y la inserción metálica, y también la precisión del proceso de fabricación.

Una de las propuestas para mejorar el contacto es utilizar una guía de onda seccionada a lo largo del plano E, presentada en la *Figura 2.5-2 (b),* en lugar de la guía usada seccionada transversalmente al plano E, mostrada en la *Figura 2.5-2 (a).*

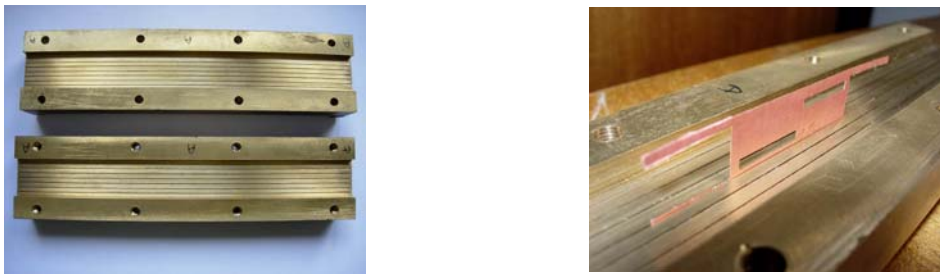

*(a)*

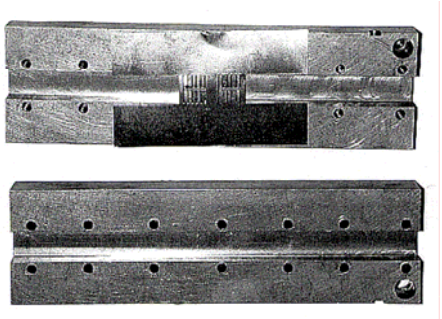

*(b)*

*Figura 2.5-2: Guía onda utilizada (a) y guía de onda propuesta (b)*

# 3. CONCLUSIONES Y LÍNEAS FUTURAS

En este proyecto se ha llevado a cabo el análisis de discontinuidades entre guías de onda mediante el método Mode Matching. Dicho método ha sido empleado para el modelado de filtros plano-E que incorporan secciones de guía de onda ridge actuando como resonadores.

Al mismo tiempo, ha sido desarrollada una herramienta rápida de simulación de dichas configuraciones en Fortran y Matlab, consiguiendo una gran reducción del tiempo de simulación con respecto al programa comercial HFSS.

También han sido validados los resultados obtenidos consiguiendo diversas ventajas frente a estructuras previamente utilizadas. Entre las ventajas más importantes destacan: la reducción de las dimensiones del filtro, respuestas de alta selectividad y aparición de ceros de transmisión en frecuencias finitas cercanas a la banda de paso.

Además han sido fabricados y medidos tres prototipos con uno y dos resonadores, obteniendo buenos resultados para el prototipo con un resonador. Debido a las pérdidas obtenidas en los prototipos con dos resonadores se proponen soluciones para realizar de manera más precisa tanto la fabricación como la medición.

Finalmente, tras haber desarrollado los objetivos de este proyecto y observar los resultados y conclusiones obtenidos, es posible proponer trabajos futuros que continúen explorando las ventajas de la tecnología de los filtros plano-E que incorporan secciones de guías de onda con ridges.

En primer lugar, para llevar a cabo dicha investigación es necesaria la creación de una herramienta de diseño para esta tecnología.

En segundo lugar, uno de los trabajos propuestos más interesante es analizar una estructura nueva presentada en la *Figura 3-1*, completamente compatible con el bajo coste y la fácil fabricación de los filtros plano-E.

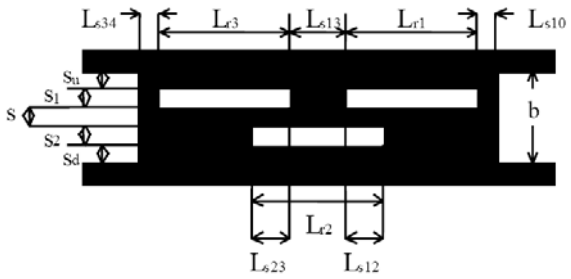


*Figura 3-1: Sección transversal en el plano YZ de la configuración propuesta*

Además, esta estructura introduce acoplo paralelo entre los resonadores. Por tanto, los resonadores se acoplan tanto en serie con en paralelo. Este efecto es importante para la reducción de las dimensiones del filtro. También, dicha configuración permite la aparición de ceros de transmisión en frecuencias finitas debido al acoplamiento cruzado entre los resonadores. Por tanto, para realizar el análisis de la estructura es necesario resolver la discontinuidad creada entre una guía de onda ridge y una guía de onda coaxial ridge siguiendo el método Mode Matching explicado en este proyecto.

**REFERENCIAS**

[1] Konish Y. and Unakada K., *"The Design of a Band-Pass Filter with Inductive Strip-Planar Circuit Mounted in Waveguide"*, IEEE Trans. Microwave Theory and Techniques, MTT-22, pp. 869-873, October 1974

[2] G. Goussetis and D. Budimir, *"E-plane Manifold Multiplexers with Improved Bandwidth"*, 31st European Microwave Conference, London 2001, UK, September 24-27

[3] Deslandes D. and Wu K., *"Integrated Transition of Coplanar to Rectangular Waveguides"*, IEEE MTT-S International Microwave Symposium Digest, pp. 619-622, 2001

[4] Rong Y., Zaki K., Hageman M., Stevens D. and Gipprich J., *"Low Temperature Cofired Ceramics (LTCC) Ridge Waveguide Bandpass Chip Filters"*, IEEE Transactions on Microwave Theory and Techniques, MTT-47, No. 12, pp. 2317-2324, December 1999

[5] Bornemann J., and Arndt F., *"Rigorous Design of Evanscent Mode E-plane Finned Waveguide Bandpass Filters"*, IEEE MTT-S International Microwave Symposium Digest, pp. 603-606, 1989

[6] Konish Y. and Unakada K., *"The Design of a Band-Pass Filter with Inductive Strip-Planar Circuit Mounted in Waveguide"*, IEEE Trans. Microwave Theory and Techniques, MTT-22, pp. 869-873, October 1974

[7] Budimir D., *"Design of E-plane Filters with Improved Stopband Performance"*, PhD thesis, Department of Electronic and Electrical Engineering, University of Leeds, July 1994

[8] MªÁngeles Ruiz Bernal, *"Modal analysis of Ridge Coaxial waveguide using the transverse resonance method and field matching to study microwave filters"*, Final Year Project, May 2006

[9] J. Bomemam, F. Arndt, *"Model S-Matrù- Design of Optiniun Stepped Ridged and Finned Waveguide Transfomers"*, IEEE MTT-35, June 1987, pp. 56 1-567.

[10] DIGITAL Visual FORTRAN

[11] MATLAB, Mathworks Inc.

[12] Agilent High Frequency Structure Simulator (HFSS)

ESCUELA TÉCNICA SUPERIOR DE INGENIERÍA DE TELECOMUNICACIÓN
UNIVERSIDAD POLITÉCNICA DE CARTAGENA


**Proyecto Fin de Carrera**

# PARTE II:

# Mode matching analysis of waveguide discontinuities and filters with asymmetrical ridge waveguide resonators

AUTOR: María Valverde Navarro
DIRECTOR(ES): José Luís Gómez Tornero

Cartagena, Mayo 2006

# CONTENTS

# 1. INTRODUCTION.

## 1.1. MICROWAVE FILTERS

Microwave passive filters are essential components in the implementation of telecommunication systems. Their main purpose is to pass selected signals and attenuate unwanted signals.

Microwave filters are generally made of transmission lines or waveguides. Common transmission lines used to build microwave filters are: stripline, microstrip line, coaxial line, circular waveguide, rectangular waveguide, ridged waveguide and dielectric filled waveguide.

Depending on the electric, mechanical and environmental specifications, some transmission lines offer better performance over the others. It is the microwave designer responsibility to be aware of all the transmission line properties so that the optimum filter performance is obtained.

The research has particularly increased over the last decade with the explosive growth of wireless and satellite telecommunication systems requiring higher performance and more reliable filter designs.

## 1.2. E-PLANE FILTERS

Inductive elements such as posts, transverse strips and transverse diaphragms are extensively employed in industry to produce waveguide bandpass filters for a wide variety of applications. However they are difficult to make at low cost and to put into mass production. To solve this problem, E-plane metal insert filters have been proposed by [1-1].

The standard configuration for E-plane filters is to use a split block waveguide housing and place inductive obstacles, typically all metal septa, in the E-plane of a rectangular waveguide, at spacing close to a half wavelength apart. *Figure 1-1* present this standard configuration.

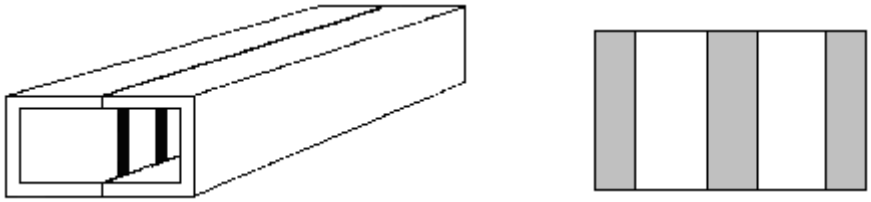

*(a)* *(b)*

*Figure 1-1: E-Plane filter geometry (a) and layout of the metal insert (b)*

Such a configuration has many advantageous characteristics including low cost, no need for tuning and mass productivity. Furthermore, the all-metal E-plane insertions consist in printed circuits that are very easy to fabricate using the photolithographic process.

However despite such favourite characteristics, the attainable rejection bandwidth and level might be too low for some applications such as multiplexers. Harmonic resonance of the resonators of which the filter consist result in a spurious passband of the E-plane filters at a frequency roughly 1.5 time the centre frequency. This effect limits the available bandwidth or requires extra components to suppress signals at the spurious passband of filters.

In addition, Ridge waveguide can be incorporated in the all-metal E-plane split-block-housing technology, as it is shown in *Figure 1-2 (a)*, in its variation with thin ridges printed on an all-metal E-plane insert with no further fabrication complexity. Since the guided wavelength as well as the characteristic impedance in Ridged waveguide propagation varies with the ridges height, therefore, with no further manufacturing complexity, allows altered propagation characteristics along the same waveguide housing. Based on this remark, [1-6] suggested that the use of sections of ridged waveguide as resonators in an all-metal E-plane filter may optimise its stopband performance without increasing its manufacturing complexity. The argument in [1-7] was that all the waveguide sections will be resonant at a single fundamental frequency, but not simultaneously resonant at higher frequencies, provided the ridges' gap differs, due to different guide wavelengths in the different filter sections. Hence the spurious harmonic resonance will appear shifted to higher frequencies and the filter's rejection at the stopband will generally be improved.

Furthermore, one of the objectives of this project is to improve the selectivity of the response of the filter. Therefore, asymmetric Ridge waveguides are incorporated in the all-metal E-plane split-block-housing technology, as it is shown in *Figure 1-2 (a)*, due to such configuration can give rise to the appearance of a transmission zero at finite frequencies close to the passband of the filter and increase with that the selectivity. That is one of the advantages found with respect to the standard configuration presented in *Figure 1-1*.

When the wave can follow two different ways, at the end of the ways the waves can be added in phase or in phase opposition, hence a transmission zero appears when the waves are subtracted because of the phase opposition. As an example *Figure 1-2 (b)* presents the responses of two filters like the ones in *Figure 1-2 (a),* with resonators in opposite

directions, where cross coupling exists between them and a transmission zero appears close to the passband improving the selectivity of the filter.

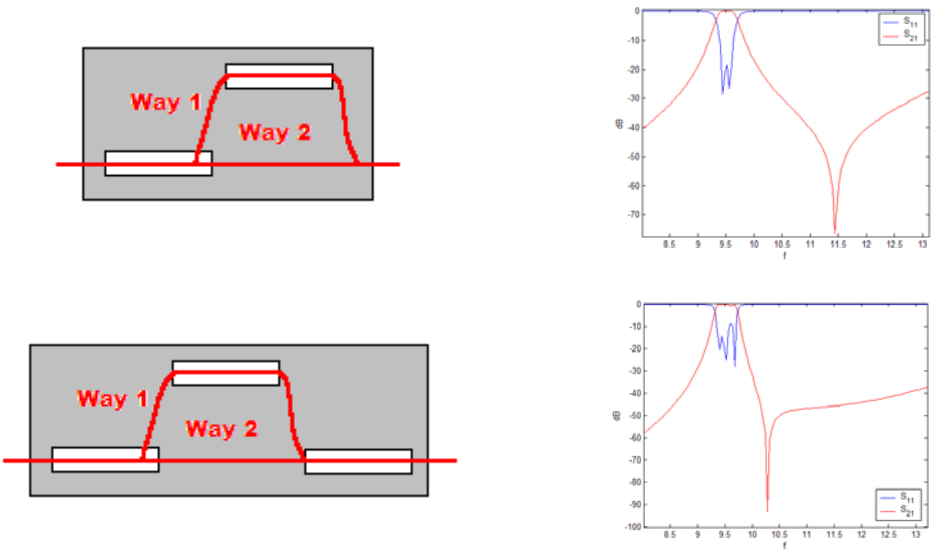


(a) (b)

*Figure 1-2: All metal insert of a E-plane filter with two and three asymmetric Ridge waveguides (a) and the response of these filters (b)*

Moreover, as with all waveguide structures, there always exists an issue of bulkiness. This is important e.g. for space applications, where units of mass on board the satellites are very expensively put into orbit. Various suggestions to miniaturise waveguide components have been reported[1-3], [1-4], [1-5].

One possible solution to achieve miniaturisation is filling the waveguide with dielectric. This reduces the wavelength by a factor inversely proportional to the dielectric permittivity and miniaturisation is achieved by the fact that a constant physical length appears electrically longer. Such contributions are very interesting, since they allow the opportunity to make use of the advantages of the waveguide as transmission line, mainly eliminate losses due to radiation, usually mounted in portable devices. However there is one main drawback of this approach, the fact that the overall loss compared with standard waveguide, is significantly higher. This is due to the dielectric losses. Hence, even though considerable field for the application of waveguide technology in MIC and MMIC structures is opened.

In addition, another solution that will be studied along this work, is the use of Ridge waveguides as an alternative of the standard configuration. As it will be verified, the total

size of the filter is reduced obtaining the same response improving the selectivity and the overall losses are conserved in a low level.

## 1.3. MODELLING OF E-PLANE FILTERS

*Figure 1-3 (a)* shows the layout of a E-plane filter metal insert indicating the different sections that can form a filter. As it is presented, essentially a filter is constituted by couplers and resonators. The all-metal septa operate as couplers, and basically they consist in Reduced waveguides sections. On the other hand we can find different kinds of resonators: simple waveguide and Ridge waveguide sections that operate as simple resonators, and Ridge Coaxial waveguide section that operates as two resonators in parallel. Therefore, we can say that a E-plane filter is formed as a junction of different waveguides, as the ones presented in *Figure 1-3 (b)*.

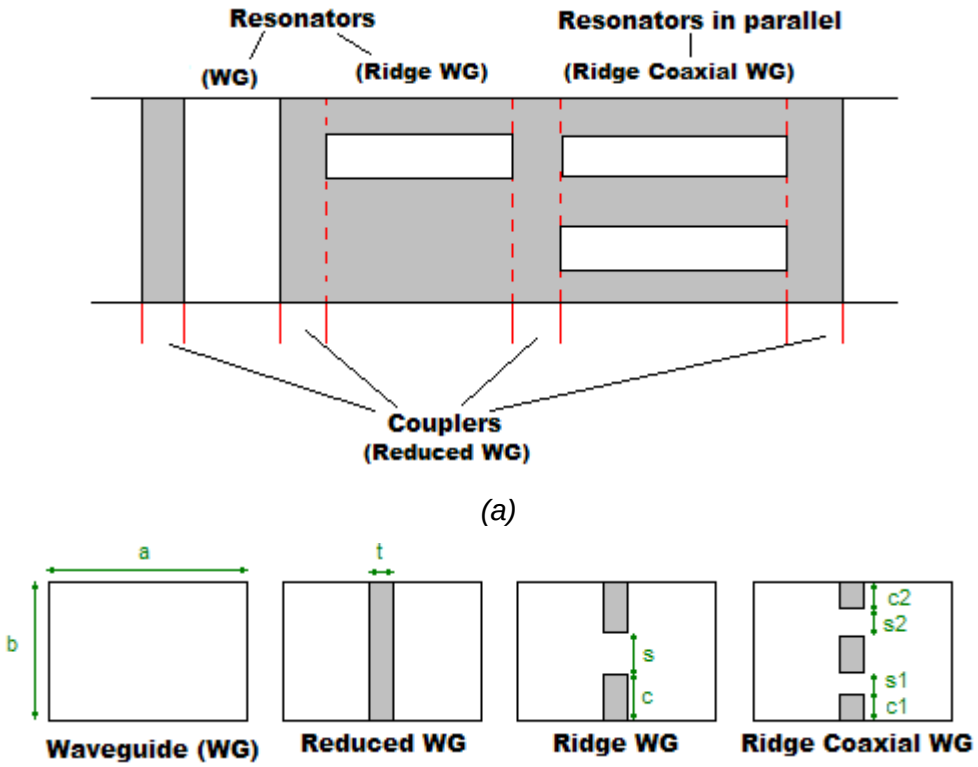


*Figure 1-3: All-metal insert indicating the possible parts of a E-Plane Filter (a), and Cross section of different waveguides (b)*

Therefore, to calculate the final response of the filter it is necessary to solve two different problems.

The first of them is to study the propagation in each waveguide sections, namely calculating the modes which can exist in each sections. In the case of the WG and the Reduced WG, the calculation of the modes is analytical. On the other hand, for waveguides as Ridge WG and Ridge Coaxial WG, the calculation is not analytical. For that reason methods as the Transverse Resonance and Field Matching are required to obtain the modes in these waveguides. The way to solve this problem is explained in [1-8], and also the propagation in a Ridge WG and in a Ridge Coaxial WG is calculated.

The second problem, and one of the main objectives of this project, is the full-wave modelling of an E-plane all metal insert filter with Ridge WG. First of all, it is necessary the modelling of the discontinuities formed between the different sections that constitute the filter. Mainly, the discontinuities that appear in *Figure 1-3 (a)* are: WG-Reduced WG, Ridge WG- Reduced WG and Ridge Coaxial WG- Ridge WG. In [1-9] the first of them was studied and the second was analysed but for a particular case when the resonator is positioned in a symmetric position. For that reason, the discontinuity between a general Ridge WG (symmetric or asymmetric resonator) and Reduced WG is solved in this project for first time. The last discontinuity, Ridge Coaxial WG-Ridge WG, will be interesting for a future work as it is mentioned in chapter nine.

The generalized scattering matrix of the Ridge WG-Reduced WG discontinuity is obtained using Mode Matching Method. Basically, this method analyses the fields at the junction of two waveguides with dissimilar cross-sections. Chapter two present the general formulation of the Mode Matching Method and also its application to characterise the discontinuity under study. Once the generalized scattering matrices of all discontinuities are available, the overall generalized scattering matrix of the filter can be obtained using cascading procedure.

## 1.4. PROPAGATION IN E-PLANE FILTERS

The filters under study in this project are going to operate in the X-Band, therefore the lowest central frequency will be 8 GHz and the highest will be 12 GHz. Moreover, they are excited with the first TE mode of a rectangular waveguide, the $TE_{10}$ mode. The field distribution of this mode is presented in *Figure 1-4*.

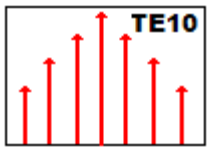


*Figure 1-4: $TE_{10}$ in a rectangular waveguide*

Attending to the cutoff frequencies of the modes in each section of the filter it is possible to know which modes are propagated. If the cutoff frequency of the mode, $f_c$, is lower than the central operation frequency of the filter, $f_o$, the mode is propagated.

| Propagation condition | $fc < fo$ |
|---|---|

Furthermore, the cutoff wavenumber, $k_c = \frac{2 \cdot \pi \cdot f_c}{c_o}$, is directly related to $f_c$ and it is determined by the boundary conditions along x and y axis. It turns out that $k_c$ is only allowed to have a set of discrete values, each of which corresponds to a cross-sectional field distribution pattern that propagates along z according to $e^{(j\omega t - \gamma z)}$ where:

$$\gamma = \sqrt{k_o^{\,2} - k_c^{\,2}}$$

A mode will propagate when $k_c < k_o$, or, in other words, when $\gamma$ is real. When $k_c > k_o$, $\gamma$ is purely imaginary, therefore the mode will not propagate. These last modes receive the name of evanescent modes and are characterized by an exponential attenuation and lack of a phase shift.

*Table 1-1* presents the cutoff frequencies for the two first modes in different sections, as WG, Reduced WG, Ridge WG and Ridge Coaxial WG.

Apart from the case of the Reduced WG, the cutoff frequencies for the first modes in each section are lower than the possible central frequencies at the X band. Therefore, the first mode satisfy the propagation condition and will propagate. As a remark, if the Reduced WG is seen as a WG with half width, the first mode of the Reduced WG will have a cutoff frequency higher than the cutoff frequency of the WG (since $f_c = \frac{c_o}{2}\sqrt{\left(\frac{m}{a}\right)^2 + \left(\frac{n}{b}\right)^2}$ and $a^{WG} \approx 2 \cdot a^{RedWG}$). This effect is appreciated in *Table 1-1*, where $f_c^{WG}$=6,561679615 GHz and $f_c^{RedWG}$=13,18101898 GHz.

In the case of the second mode of the sections, the cutoff frequencies are higher than the possible central frequencies at the X band. For that reason the second mode and higher modes will not propagate.

| | fc 1st TE mode (GHz) | fc 2nd TE mode (GHz) |
|---|---|---|
| WG | 6,561679615 | 16,1562629 |
| Reduced WG | 13,18101898 | 14,7637797 |
| Ridge WG | 4,53617877 | 14,0478872 |
| Ridge Coaxial WG | 6,143415621 | 15,982071 |

*Table 1-1: Cutoff frequencies for the first and the second modes of different waveguides*

Dimensions of the WG in mm: a=22.86, b=10.16

Dimensions of the Reduced WG in mm: a=22.86, b=10.16, t=0.1

Dimensions of the Ridge WG in mm: a=22.86, b=10.16, t=0.1, s=2, c=1

Dimensions of the Ridge Coaxial WG in mm: a=22.86, b=10.16, t=0.1, s1=s2=2, c1=c2=1

*Figure 1-5* shows an example of E-plane filter with different waveguide sections to explain the propagation of the modes through the filter. When the $TE_{10}$ mode travels through the waveguide and arrives to the Reduced WG, is transformed into evanescent modes. These modes are excited with an amplitude that is reduced exponentially along the Reduced waveguide section until arrive to the next waveguide section. In some occasions, when the Reduced waveguide section is too long the evanescent modes vanish before arrive to the next waveguide section, so no propagation will take place.

When the evanescent modes see the discontinuity with the Ridge waveguide, they are transformed into the first TE mode of this waveguide. If the next section is a Ridge Coaxial waveguide, the propagated modes in this section are the TEM and the first TE mode. The TEM mode is the fundamental quasi-static mode in the Ridge Coaxial WG, having zero cutoff frequency. The total energy propagated in the Ridge Coaxial WG will be a combination of both modes, the TEM and the $TE_1$, above the cutoff.

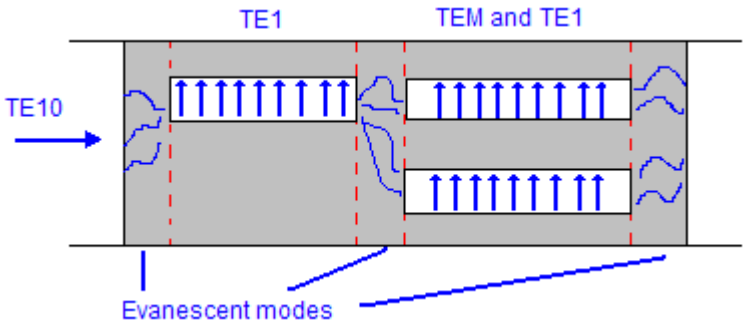


*Figure 1-5: Propagation of modes in a E-plane filter excited with the $TE_{10}$ of a waveguide*

## 1.5. OBJECTIVES

The aims and objectives of this work are therefore to explore the possibilities of improvement of the E-plane metal insert filters characteristics incorporating asymmetric Ridge waveguide. The main goals are to increase the selectivity and reduce the dimensions of the filter conserving the advantages that this filters provide, as low cost and mass producible filters.

In order to reach the point where investigation is feasible, a fast and accurate simulation tool for the structures under investigation is needed.

Hence a major initial objective of this work is to formulate in matrix eigenvalue equations the two problems that were commented in section 1.3. The first problem, propagation in a Ridge WG, was solve in [1-8]. The second one is going to be solved in this project and it consist in the application of the Mode Matching (MM) method for E-plane configurations, in particular to characterize the discontinuity between Ridge WG and Reduced WG and in a higher stage to define the overall scattering matrix that generates the response of the filter.

The stopband performance improvement, obtaining also a transmission zero at finite frequencies, and the increase of the selectivity of filters are then investigated for various geometries, incorporating Ridge WG. The latter usually involves a thorough study of the improvement versus all the parameters that can possibly affect it and then try to relate the latter regressively with the affecting parameters.

Having developed the above simulation tool, investigation for the first aim of the work, namely the exploration of opportunities of response improvement of E-plane filters using ridge waveguide, can directly start.

In addition, as it was said before, there always exists an issue of bulkiness, in special for space applications, for that reason the second main aim is to reduce the total size of the filter keeping the response improvement and conserving the overall losses in a low level.

## 1.6. OUTLINE OF THIS PROJECT

This project presents the work carried out from October (2005) to May (2006) with aims and objectives as described in section 1.5.

Chapter two presents the MM method for the field analysis at the junction of two waveguides with dissimilar cross-sections. The waveguide discontinuity that is studied in this chapter is the Ridge Waveguide-Reduced Waveguide. Furthermore, it is shown how to obtain a Generalised Scattering Matrix (GSM) for the waveguide step from the MM analysis. This chapter also explains the decomposition of a microwave bandpass filter in terms of its GSMs. The GSM method is presented to compute the overall GSM of the microwave filter. The combination of the two methods, MM-GSM, gives the complete field analysis of a rectangular-ridged waveguide bandpass filter.

Chapters three and four comment the simulation tool created in Fortran and Matlab to make the study of these structures faster and more comfortable.

From chapter five to seven, E-plane filters with different number of resonators are analysed, emphasizing the characteristics of the asymmetric ridge waveguide resonators over the symmetric ridge waveguide resonators, the main of which is a transmission zero at the stopband. Furthermore, a prototype model, as the type in *Figure 1-1*, is used as starting point for the validation of E-plane filters with passband between 9.25 and 9.75 GHz. Moreover the commercial program HFSS for a final validation of the analysed filters.

Three prototypes were fabricated by the photolithographic process. The comparison between measured and simulated results is discussed in chapter eight.

Chapter nine introduces future works. It recommends further work as design tools for this kind of configurations, and introduces a novel structure of a filter using Ridge Coaxial waveguide. The main objective of this novel filter is to reduce the dimensions of the filter, due to the resonators can be superimposed. Furthermore, in this chapter the analysis of the MM method for the field analysis at the junction between a Ridge Coaxial WG and a Ridge WG is made.

Finally, chapter ten summarizes the work that was done and expound the obtained conclusions.

## 1.7. REFERENCES

[1-1] Konish Y. and Unakada K., *"The Design of a Band-Pass Filter with Inductive Strip-Planar Circuit Mounted in Waveguide"*, IEEE Trans. Microwave Theory and Techniques, MTT-22, pp. 869-873, October 1974

[1-2] G. Goussetis and D. Budimir, *"E-plane Manifold Multiplexers with Improved Bandwidth"*, 31st European Microwave Conference, London 2001, UK, September 24-27

[1-3] Deslandes D. and Wu K., *"Integrated Transition of Coplanar to Rectangular Waveguides"*, IEEE MTT-S International Microwave Symposium Digest, pp. 619-622, 2001

[1-4] Rong Y., Zaki K., Hageman M., Stevens D. and Gipprich J., *"Low Temperature Cofired Ceramics (LTCC) Ridge Waveguide Bandpass Chip Filters"*, IEEE Transactions on Microwave Theory and Techniques, MTT-47, No. 12, pp. 2317-2324, December 1999

[1-5] Bornemann J., and Arndt F., *"Rigorous Design of Evanscent Mode E-plane Finned Waveguide Bandpass Filters"*, IEEE MTT-S International Microwave Symposium Digest, pp. 603-606, 1989

[1-6] Konish Y. and Unakada K., *"The Design of a Band-Pass Filter with Inductive Strip-Planar Circuit Mounted in Waveguide"*, IEEE Trans. Microwave Theory and Techniques, MTT-22, pp. 869-873, October 1974

[1-7] Budimir D., *"Design of E-plane Filters with Improved Stopband Performance"*, PhD thesis, Department of Electronic and Electrical Engineering, University of Leeds, July 1994

[1-8] MªÁngeles Ruiz Bernal, *"Modal analysis of Ridge Coaxial waveguide using the transverse resonance method and field matching to study microwave filters"*, Final Year Project, May 2006

[1-9] George Goussetis, *"Waveguide bandpass with improved performance"*, Ph.D. 2002.

# 2. ELECTROMAGNETIC MODELLING. MODE MATCHING

## 2.1. INTRODUCTION

The Mode Matching method is often used to solve boundary-value problems involving waveguides discontinuities. It is preferably used if the structures involved have fixed-boundary cross-sections and discontinuities in the propagation direction. Usually these geometries can be identified as junctions of two or more regions, each belonging to a separable coordinate system. We can therefore express the field in each region as a weighted sum of orthonormal modes, usually in the form of Fourier series. Matching the tangential electric and magnetic field at the discontinuity surface, and making use of the orthogonality properties of modes, we finally derive the generalized scattering matrix.

In this chapter, the general formulation of mode matching method is presented, assuming known field distribution at both sides of the waveguide. In addition, the Generalized Scattering Matrix (GSM) at the junction of two dissimilar waveguides is extracted. The scattering matrix obtained is said generalized because it measures the fundamental mode and the higher-order modes scattering parameters. Therefore, a microwave circuit composed of various waveguide sections can be decomposed in terms of its GSMs. Then, the overall GSM of the circuit can be computed by the GSM method.

Furthermore, a particular junction between Asymmetric Ridge waveguide and Reduced waveguide is analysed in this chapter.

## 2.2. METHODS TO CALCULATE THE SCATTERING PARAMETERS OF WAVEGUIDE DISCONTINUITIES.

Many numerical methods have been introduced in the past two decades to describe the scattering phenomena of waves inside microwave passive components.

These numerical methods are often classified as space domain, modal domain or time domain method depending on the parameter that is being evaluated numerically (and usually truncated) when solving the field equations. Methods like Finite-Difference Method (FDM) [2-1] and Finite-Element Method (FEM) [2-2] are examples of space discretization methods. Mode-Matching Method (MMM) [2-3] and Method of Moments (MOM) [2-4] are based on modal discretization, and Finite-Difference Time Domain (FDTD) [2-5] and Transmission Line Method (TLM) [2-6] belong to time and space discretization. A brief summary of each method is given in [2-7] and [2-8].

A good comparison between the different methods is usually done in terms of its computing requirements as shown by *Table 2-1*.

| Method | Storage | CPU | Versatility | Pre-processing |
|---|---|---|---|---|
| FDM | L | L | ++ | Nil |
| FEM | L | L | +++ | + |
| TLM | L | L | ++ | + |
| MMM | S/M | S/M | + | ++ |

*Table 2-1: Comparison of Numerical Methods*

Note: L=large, M=medium, S=small, +++=very good, ++=good, +=poor

In general, *Table 2-1* shows that space and time discretization methods require more memory storage and computer processing time than modal discretization methods.

However, space and time discretization methods are more versatile in the sense that they can analyse complex geometrical structures. Therefore, as a rule of thumb, it is usually preferred to use modal discretization methods over time and space discretization methods when the structure involved is of simple geometrical form because less memory and computing is required to converge to the solution.

In addition, a part from the previous advantages, MM method is the most efficient for the accurate prediction of the EM performance of E-plane structures. Furthermore it is a very efficient method for structures consisting of cascaded homogeneous sections of waveguides.

## 2.3. MODE MATCHING FOR SURFACE DISCONTINUITIES.

As it was presented before, the MM method is a popular numerical method for the field analysis between two dissimilar waveguide discontinuities. The method consists of first finding the modes in each waveguide, as it was made in [2-9]. The fields in the waveguides are then expanded as the sum of all mode functions with unknown forward and backward amplitude coefficients. By matching the tangential electromagnetic fields at the junction of the two waveguides and isolating for the unknown forward and backward coefficients, the GSM of the waveguide step was derived. If all the modes are used, the MM analysis would compute the exact GSM to the problem. Since it is impossible to use an infinite number of terms in the computation of the GSM waveguide step, the result is an approximation to the exact solution. However, it starts to converge to the exact solution after a few modes only.

The formulas that will be derived in this section are based on [2-10] and are valid for waveguide steps with any cross-section geometry.

The first step in the MM method consists decomposing the complex structure into two waveguide rectangular sections, *WG-I* and *WG-II,* as it is shown in *Figure 2-1*.

The total electric and magnetic fields inside each waveguide section can be expressed by the superposition of the TE and TM wave components:

$$E = E_{TE} + E_{TM} = \nabla \times A_h + \frac{1}{j\omega\varepsilon} \nabla \times \nabla \times A_e \qquad (2.3\text{-}1)$$

$$H = H_{TM} + H_{TE} = \nabla \times A_e - \frac{1}{j\omega\mu} \nabla \times \nabla \times A_h \qquad (2.3\text{-}2)$$

The Hertzian vector potentials are often used in electromagnetic boundary-value problems to represent the electric and magnetic fields. The advantage of using these vector potentials is that it simplifies the mathematical solution. Electric and magnetic vector potentials components, $A_h$, and $A_e$, are defined by the superposition of all the TE and TM modes by:

$$A_h = \sum_{q=1}^{\infty} \sqrt{Z_{hq}} \cdot T_{hq}(x,y) \cdot \left[ F_{hq} e^{-j \cdot K_{zhq} \cdot z} + B_{hq} e^{+j \cdot K_{zhq} \cdot z} \right] \cdot \hat{z} \qquad (2.3\text{-}3)$$

$$A_e = \sum_{p=1}^{\infty} \sqrt{Y_{ep}} \cdot T_{ep}(x,y) \cdot \left[ F_{ep} e^{-j \cdot K_{zep} \cdot z} - B_{ep} e^{+j \cdot K_{zep} \cdot z} \right] \cdot \hat{z} \qquad (2.3\text{-}4)$$

where Z and Y are the waveguide impedance and admittance of TE and TM modes respectively and are given by the expressions:

$$Z_{hq} = \frac{\omega\mu}{K_{hq}} = \frac{1}{Y_{hq}} \qquad Y_{ep} = \frac{\omega\mu}{K_{ep}} = \frac{1}{Z_{ep}} \qquad (2.3\text{-}5)$$

and the wavenumbers are related according to

$$k_o^2 = \left(k_z^i\right)^2 + \left(k_c^i\right)^2 \qquad (2.3\text{-}6)$$

$k_c^i$ being the cutoff frequency of the i-th mode.

Forward propagating waves ( $F_{hq}e^{-j\cdot K_{zhq}\cdot z}$ ) and backward propagating waves ( $B_{hq}e^{j\cdot K_{zhq}\cdot z}$ ) appear in both sides of the discontinuity between *WG-I* and *WG-II* . At this point we should mention that for simplicity, the common surface consists the complete cross section of the smaller region. With no further loss of generality we assume this region to be region *WG-II*.

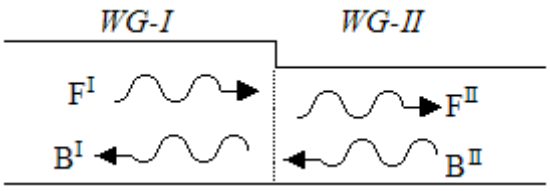


*Figure 2-1: Surface discontinuity*

The generalized scattering matrix aims to solve for the scattered waves at the discontinuity when the incident waves are known:

$$\begin{bmatrix} B^I \\ F^{II} \end{bmatrix} = \begin{bmatrix} S_{11} & S_{12} \\ S_{21} & S_{22} \end{bmatrix} \cdot \begin{bmatrix} F^I \\ B^{II} \end{bmatrix} \qquad (2.3\text{-}7)$$

In order for the S-parameters of the generalized scattering matrix to have amplitude between 0 and 1, so that we will be able to use them globally and without further study, the power carried by each mode with constant amplitude at any side of the discontinuity should have constant value. For simplicity we set the power of any a forward/backward propagating mode with amplitude F/B equal to $1\sqrt{W}$ to be 1W.

We can assume the discontinuity plane at z=0. Therefore the continuity property of electric fields can now take the following formulation, with no loss of generality, by matching the transverse electric field of *WG-I* on the left side with the transverse electric field of *WG-II* on the right side at z = 0.

$$\begin{aligned} & E_t^{TE,I} + E_t^{TM,I} = E_t^{TE,II} + E_t^{TM,II} \Rightarrow \\ & \sum_{q=1}^{\infty} \sqrt{Z_{hq}^I} \left(\nabla T_{hq}^I \times \hat{z}\right) \cdot \left(F_{hq}^I + B_{hq}^I\right) - \sum_{r=1}^{\infty} \sqrt{Z_{er}^I} \nabla T_{er}^I \cdot \left(F_{er}^I + B_{er}^I\right) = \\ & \sum_{s=1}^{\infty} \sqrt{Z_{hs}^{II}} \left(\nabla T_{hs}^{II} \times \hat{z}\right) \cdot \left(F_{hs}^{II} + B_{hs}^{II}\right) - \sum_{t=1}^{\infty} \sqrt{Z_{et}^{II}} \nabla T_{et}^{II} \cdot \left(F_{et}^{II} + B_{et}^{II}\right) \end{aligned} \qquad (2.3\text{-}8)$$

Doing the same procedure for the tangential magnetic fields $H_t$, we get:

$$H_t^{TE,I} + H_t^{TM,I} = H_t^{TE,II} + H_t^{TM,II} \Rightarrow$$
$$\sum_{q=1}^{\infty} \sqrt{Y_{hq}^I}\nabla T_{hq}^I \cdot \left(F_{hq}^I - B_{hq}^I\right) + \sum_{r=1}^{\infty} \sqrt{Y_{er}^I}\left(\nabla T_{er}^I \times \hat{z}\right)\cdot\left(F_{er}^I - B_{er}^I\right) =$$
$$\sum_{s=1}^{\infty} \sqrt{Y_{hs}^{II}}\nabla T_{hs}^{II} \cdot \left(F_{hs}^{II} - B_{hs}^{II}\right) + \sum_{t=1}^{\infty} \sqrt{Y_{et}^{II}}\left(\nabla T_{et}^{II} \times \hat{z}\right)\cdot\left(F_{et}^{II} + B_{et}^{II}\right) \quad (2.3\text{-}9)$$

In order to solve for the F and B parameters, we need to eliminate the x- and y-dependence implied in the cross section functions *T*. We must make sure that the tangential electric field of the larger region is zero at metallic boundaries, as it was made in the field matching procedure in [2-9]. We therefore successively multiply (2.3-8) with $\nabla T_{hq}^I \times \hat{z}$ and $-\nabla T_{er}^I$ then integrate over the cross-section surface of *WG-I*. We use the relations:

$$\iint_S \left(\nabla T_{h,ei}^I \times \hat{z}\right)\cdot\left(\nabla T_{h,ej}^I \times \hat{z}\right)\cdot dS = \iint_S \nabla T_{h,ei}^I \cdot \nabla T_{h,ej}^I \cdot dS = \delta_{ij} \quad (2.3\text{-}10)$$

which is the mathematical expression of the fact that both the sets of TE and TM modes are orthogonal and:

$$\iint_S \left(\nabla T_{er}^I \times \hat{z}\right)\cdot \nabla T_{hq}^I \cdot dS = \iint_S \nabla T_{er}^I \cdot \left(\nabla T_{hq}^I \times \hat{z}\right)\cdot dS = 0 \quad (2.3\text{-}11)$$

which is the mathematical expression of the fact that TE and TM modes in a hollow waveguide are uncoupled. These identities are easily verified upon substitution of the transverse dependence functions.

Upon rearrangement of the expressions in matrix form, we obtain:

$$diag\left\{\sqrt{Z_{hq}^I}\right\}\cdot\left(F_h^I + B_h^I\right) = J_{hh}\cdot diag\left\{\sqrt{Z_{hs}^{II}}\right\}\cdot\left(F_h^{II} + B_h^{II}\right) + J_{he}\cdot diag\left\{\sqrt{Z_{et}^{II}}\right\}\cdot\left(F_e^{II} + B_e^{II}\right) \quad (2.3\text{-}12)$$

$$diag\left\{\sqrt{Z_{er}^I}\right\}\cdot\left(F_e^I + B_e^I\right) = J_{eh}\cdot diag\left\{\sqrt{Z_{hs}^{II}}\right\}\cdot\left(F_h^{II} + B_h^{II}\right) + J_{ee}\cdot diag\left\{\sqrt{Z_{et}^{II}}\right\}\cdot\left(F_e^{II} + B_e^{II}\right) \quad (2.3\text{-}13)$$

Similar procedure we follow in order to eliminate the x- and y- dependence from $H_t$. However now, since we are dealing with magnetic fields, there is no zero condition for tangential components at metallic boundaries. Hence now we successively multiply (2.3-9) with $\nabla T_{hs}^{II}$ and $\nabla T_{et}^{II} \times \hat{z}$ then integrate over the smaller cross-section, *WG-II.* We use the relations described in equations (2.3-10) and (2.3-11) which are valid still in case of *WG-II*.

Upon rearrangement in a matrix form, we finally obtain:

$$J_{hh}^{T}\cdot diag\left\{\sqrt{Y_{hq}^{I}}\right\}\cdot\left(F_{h}^{I}-B_{h}^{I}\right)+J_{eh}^{T}\cdot diag\left\{\sqrt{Y_{er}^{I}}\right\}\cdot\left(F_{e}^{I}-B_{e}^{I}\right)=diag\left\{\sqrt{Y_{hs}^{II}}\right\}\cdot\left(F_{h}^{II}-B_{h}^{II}\right) \quad (2.3\text{-}14)$$

$$J_{he}^{T}\cdot diag\left\{\sqrt{Y_{hq}^{I}}\right\}\cdot\left(F_{h}^{I}-B_{h}^{I}\right)+J_{ee}^{T}\cdot diag\left\{\sqrt{Y_{er}^{I}}\right\}\cdot\left(F_{e}^{I}-B_{e}^{I}\right)=diag\left\{\sqrt{Y_{et}^{II}}\right\}\cdot\left(F_{e}^{II}-B_{e}^{II}\right) \quad (2.3\text{-}15)$$

The matrices J, called the coupling matrices, are given at the following expressions:

$$\left(J_{hh}\right)_{qs}=\iint_{SII}(\nabla T_{hq}^{I}\times\hat{z})\cdot(\nabla T_{hs}^{II}\times\hat{z})dS \quad (2.3\text{-}16)$$

$$\left(J_{eh}\right)_{rs}=\iint_{SII}(-\nabla T_{er}^{I})\cdot(\nabla T_{hs}^{II}\times\hat{z})dS \quad (2.3\text{-}17)$$

$$\left(J_{he}\right)_{qt}=\iint_{SII}(\nabla T_{hq}^{I}\times\hat{z})\cdot(-\nabla T_{et}^{II})dS \quad (2.3\text{-}18)$$

$$\left(J_{ee}\right)_{rt}=\iint_{SII}(-\nabla T_{er}^{I})\cdot(-\nabla T_{et}^{II})dS \quad (2.3\text{-}19)$$

The integral of equation (2.3-18) is identically zero, thus suggesting that TE modes of region *WG-I* are not couple with TM modes of region *WG-II*. Upon multiplication (2.3-12), (2.3-13), (2.3-14) and (2.3-15) with, $diag\left\{\sqrt{Y_{hq}^{I}}\right\}$, $diag\left\{\sqrt{Y_{er}^{I}}\right\}$, $diag\left\{\sqrt{Y_{hs}^{II}}\right\}$, $diag\left\{\sqrt{Y_{ey}^{II}}\right\}$ respectively, we can write in a matrix form:

$$\begin{bmatrix}F_{h}^{I}+B_{h}^{I}\\F_{e}^{I}+B_{e}^{I}\end{bmatrix}=M\cdot\begin{bmatrix}F_{h}^{II}+B_{h}^{II}\\F_{e}^{II}+B_{e}^{II}\end{bmatrix}\qquad\begin{bmatrix}F_{h}^{II}-B_{h}^{II}\\F_{e}^{II}-B_{e}^{II}\end{bmatrix}=M^{T}\cdot\begin{bmatrix}F_{h}^{I}-B_{h}^{I}\\F_{e}^{I}-B_{e}^{I}\end{bmatrix} \quad (2.3\text{-}20)$$

where

$$M=\begin{bmatrix}diag\left\{\sqrt{Y_{hq}^{I}}\right\}\cdot J_{hh}\cdot diag\left\{\sqrt{Z_{hs}^{II}}\right\} & diag\left\{\sqrt{Y_{hq}^{I}}\right\}\cdot J_{he}\cdot diag\left\{\sqrt{Z_{et}^{II}}\right\}\\ diag\left\{\sqrt{Y_{er}^{I}}\right\}\cdot J_{eh}\cdot diag\left\{\sqrt{Z_{hs}^{II}}\right\} & diag\left\{\sqrt{Y_{er}^{I}}\right\}\cdot J_{ee}\cdot diag\left\{\sqrt{Z_{et}^{II}}\right\}\end{bmatrix} \quad (2.3\text{-}21)$$

Rearranging forward and backward waves in equation (2.3-21) , we can derive the scattering matrix

$$\begin{bmatrix}\begin{bmatrix}B_{h}^{I}\\B_{e}^{I}\end{bmatrix}\\\begin{bmatrix}F_{h}^{II}\\F_{e}^{II}\end{bmatrix}\end{bmatrix}=\begin{bmatrix}S_{11} & S_{12}\\S_{21} & S_{22}\end{bmatrix}\cdot\begin{bmatrix}\begin{bmatrix}F_{h}^{I}\\F_{e}^{I}\end{bmatrix}\\\begin{bmatrix}B_{h}^{II}\\B_{e}^{II}\end{bmatrix}\end{bmatrix} \quad (2.3\text{-}22)$$

where

$$S_{11} = -W \cdot \left(U - M \cdot M^T\right)$$
$$S_{12} = 2 \cdot W \cdot M$$
$$S_{21} = M^T \cdot \left[U + W \cdot \left(U - M \cdot M^T\right)\right]$$
$$S_{22} = U - 2 \cdot M^T \cdot W \cdot M \qquad (2.3\text{-}23)$$

where U is the unity matrix and, W is given by

$$W = (U + MM^T)^{-1} \qquad (2.3\text{-}24)$$

Hence we have obtained the scattering matrix for a surface discontinuity. This procedure is applicable to all discontinuities that we will discuss further on

## 2.4. DISCONTINUITY OF FINITE LENGTH

The above analysis was valid for a surface discontinuity plane between two waveguides. It yields the GSM for incident and reflected waves on a particular surface discontinuity. In practice however, microwave components (filters, couplers etc.), have a finite length. In the structures investigated in this work, filters consist of a cascade of finite length homogeneous waveguide sections. In order to obtain a tool for simulating such finite length structures, a mean of combining the finite length of homogeneous waveguide with the scattering matrix of the surface discontinuity is required. This section will therefore deal with modelling the cascade of surface discontinuities, for which the generalised scattering matrix as well as the propagation characteristics are known. This method is commonly referred to as mode matching method [2-7] or as generalised scattering matrix technique [2-8].

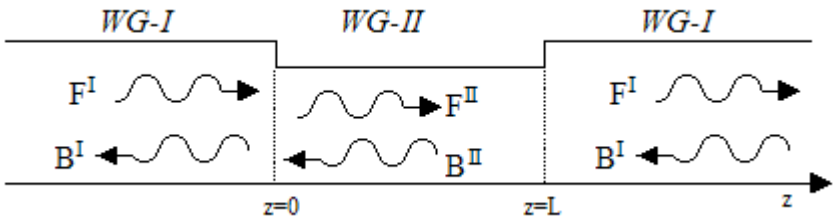


*Figure 2-2: Discontinuity of finite lengtht*

Assume we want to characterize the finite-length discontinuity of the above *Figure 2-2*. In order to achieve that, we distinguish three regions; surface discontinuity at z= 0,

propagation along *WG-II* and surface discontinuity at z= L. Knowing the behaviour of the field at these three regions, we can superimpose in order to derive the total S-matrix.

Referring to *Figure 2-2*, the scattering matrix of the surface discontinuity at z= 0 is already obtained from the previous analysis. Using the same result, it is easy to obtain the discontinuity at z= L. The previous analysis for the discontinuity plane was carried assuming z = 0. However, this does not affect the generality of the result; hence this result can be used also at the discontinuity. However, at the surface z = L the order of the regions is interchanged. This is equivalent to swapping the vectors B and F in (2.3-22). It is obvious to see that the new scattering matrix is directly obtained upon interchange of the rows on the left- and right-hand side vectors:

$$\begin{bmatrix} \begin{bmatrix} B_{h\,L}^{II} \\ B_{e\,L}^{II} \end{bmatrix} \\ \begin{bmatrix} F_{hL}^{I} \\ F_{eL}^{I} \end{bmatrix} \end{bmatrix} = \begin{bmatrix} S_{22} & S_{21} \\ S_{12} & S_{11} \end{bmatrix} \cdot \begin{bmatrix} \begin{bmatrix} F_{h\,L}^{II} \\ F_{e\,L}^{II} \end{bmatrix} \\ \begin{bmatrix} B_{hL}^{I} \\ B_{eL}^{I} \end{bmatrix} \end{bmatrix} \qquad (2.4\text{-}1)$$

Obviously the $S_{ij}$ sub-matrices are given by the same equations as for the surface discontinuity at z= 0.

In order to find the total S-matrix, we also need to characterize the effect of field propagation along the finite length *L* of *WG-II*. The potential non-stability of the first approach derives from the exponential terms with positive real arguments that appear in the transmission line of a homogeneous waveguide section of length *L*:

$$\begin{bmatrix} F \\ B \end{bmatrix} = \begin{bmatrix} \mathrm{diag}\left\{\exp\left(-jk_z L\right)\right\} & 0 \\ 0 & \mathrm{diag}\left\{\exp\left(+jk_z L\right)\right\} \end{bmatrix} \cdot \begin{bmatrix} F^{L} \\ B^{L} \end{bmatrix} \qquad (2.4\text{-}2)$$

Instead, the scattering matrix for this section would be:

$$\begin{bmatrix} \begin{bmatrix} B_{h}^{II} \\ B_{e}^{II} \end{bmatrix} \\ \begin{bmatrix} F_{h\,L}^{II} \\ F_{e\,L}^{II} \end{bmatrix} \end{bmatrix} = \begin{bmatrix} 0 & \begin{bmatrix} D_{h}^{II} & D_{e}^{II} \end{bmatrix} \\ \begin{bmatrix} D_{h}^{II} & D_{e}^{II} \end{bmatrix} & 0 \end{bmatrix} \cdot \begin{bmatrix} \begin{bmatrix} F_{h}^{II} \\ F_{e}^{II} \end{bmatrix} \\ \begin{bmatrix} B_{h\,L}^{II} \\ B_{e\,L}^{II} \end{bmatrix} \end{bmatrix} \qquad (2.4\text{-}3)$$

where

$$D_{h}^{II} = \mathrm{diag}\left\{\exp\left(-jk_{zh}^{II} \cdot L\right)\right\} \qquad D_{e}^{II} = \mathrm{diag}\left\{\exp\left(-jk_{ze}^{II} \cdot L\right)\right\} \qquad (2.4\text{-}4)$$

We now have to superimpose the already obtained partial scattering matrices, in order to obtain the total scattering matrix. For two cascaded discontinuities with scattering matrices $S^F$ and $S^L$ we can rearrange the following equations in order to eliminate the $_{MED}$ indexed fields.

$$\begin{bmatrix} B_{IN} \\ F_{MED} \end{bmatrix} = \begin{bmatrix} S^F_{11} & S^F_{12} \\ S^F_{21} & S^F_{22} \end{bmatrix} \cdot \begin{bmatrix} F_{IN} \\ B_{MED} \end{bmatrix} \qquad \begin{bmatrix} B_{MED} \\ F_{OUT} \end{bmatrix} = \begin{bmatrix} S^L_{11} & S^L_{12} \\ S^L_{21} & S^L_{22} \end{bmatrix} \cdot \begin{bmatrix} F_{MED} \\ B_{OUT} \end{bmatrix}$$

$$\begin{bmatrix} B_{IN} \\ F_{OUT} \end{bmatrix} = \begin{bmatrix} S^F_{11} + S^F_{12} S^L_{11} V S^F_{12} & S^F_{12}\left(I + S^L_{11} V S^F_{22}\right) S^L_{12} \\ S^L_{21} V S^F_{21} & S^L_{22} + S^L_{21} V S^F_{22} S^L_{12} \end{bmatrix} \cdot \begin{bmatrix} F_{IN} \\ B_{OUT} \end{bmatrix} \qquad (2.4\text{-}5)$$

where

$$V = \left(I - S^F_{22} S^L_{11}\right)^{-1} \qquad (2.4\text{-}6)$$

Application of this procedure twice, will finally produce the total scattering matrix for a finite length discontinuity.

For two two-port networks, the GSMs, $S^F$ and $S^L$ shown in *Figure 2-3*, can be cascaded to obtain the equivalent GSM, $S^T$.

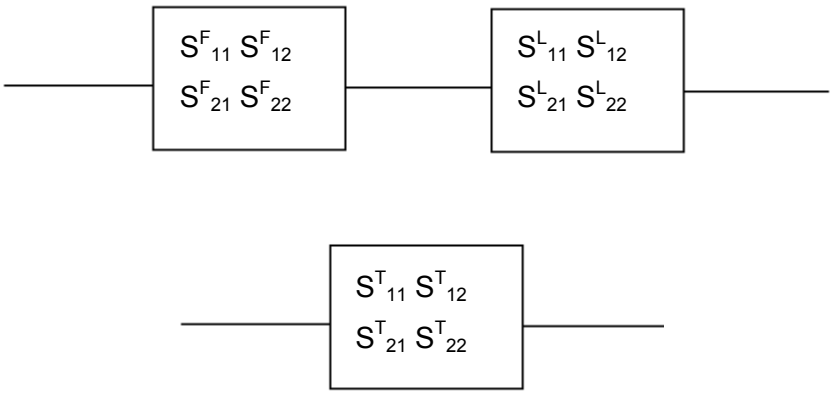


*Figure 2-3: Cascading two-port GSM*

## 2.5. GENERAL RIDGE WAVEGUIDE –REDUCED WAVEGUIDE.

The discontinuity between General (Symmetric and Asymmetric) Ridge waveguide and Reduced waveguide is analysed by the MM method, taking as a reference [2-10].

*Figure 2-4* shows the cross sections of the structures at both sides of the discontinuity that is going to be analysed.

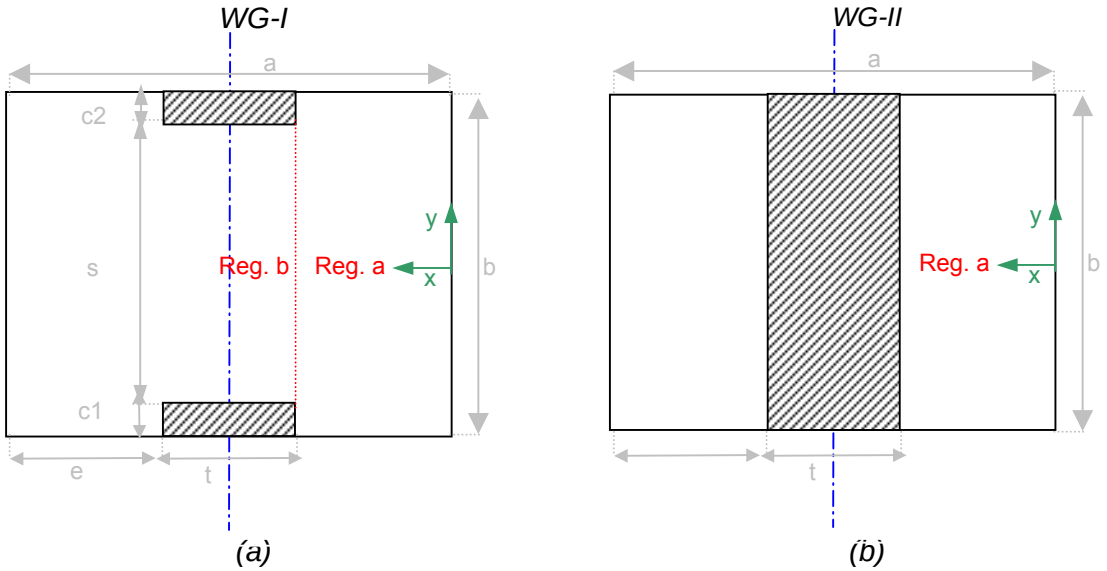


*Figure 2-4: Cross section of Ridge Waveguide (a) and Reduced Waveguide (b)*

Firstly the expressions for the vector potential relative to TE and TM modes for each structures have to be known.

The first structure, Ridge waveguide (*WG-I*), can be divided in two simple regions, *'a'* and *'b'*. The field distribution for TE and TM modes, the cutoff wavenumbers, *K*, and the amplitude coefficients, *A* and *D*, in each regions were obtained in [2-9]. The expressions for the field distribution for TE and TM modes are:

TE modes:

$$T_{hq}^{Ia}(x,y) = \sum_{m=0}^{Ma} A_{qm}^{a} \cos\left(K_{xqm}^{a} x\right) \frac{\cos\left(\frac{m\pi}{b}\left(y+\frac{b}{2}\right)\right)}{\sqrt{1+\delta_{om}}} \qquad (2.5\text{-}1)$$

$$T_{hq}^{Ib}(x,y) = \sum_{m=0}^{Mb} A_{qm}^{b} \frac{1}{K_{xqm}^{b}} \sin\left(K_{xqm}^{b}\cdot\left(x-\frac{a}{2}\right)\right) \frac{\cos\left(\frac{m\pi}{s}\left(y+\frac{b}{2}-c\right)\right)}{\sqrt{1+\delta_{om}}} \qquad (2.5\text{-}2)$$

TM modes:

$$T_{er}^{Ia}(x,y)=\sum_{m=1}^{Ma} D_{rm}^{\ a}\,\frac{1}{K_{xrm}^{a}}\sin\left(K_{xrm}^{a}x\right)\cdot\sin\left(\frac{m\cdot\pi}{b}\left(y+\frac{b}{2}\right)\right) \qquad (2.5\text{-}3)$$

$$T_{er}^{Ib}(x,y)=\sum_{m=1}^{Mb} D_{rm}^{\ b}\cos\left(K_{xrm}^{b}\cdot(x-\frac{a}{2})\right)\cdot\sin\left(\frac{m\cdot\pi}{s}\left(y+\frac{b}{2}-c\right)\right) \qquad (2.5\text{-}4)$$

In the case of a Reduced waveguide (*WG-II*), that only has region *'a'*, using the Hertzian potential analysis, it is relatively easy to see that the transverse dependence of the nm-mode of magnetic and electric type of vector potential, relative to $TE_{nm}$ and $TM_{nm}$ modes respectively, have a general solution:

TE modes:
$$T_{hnm}^{Ia}=A_{nm}\cdot\frac{\cos\left(\frac{n\pi}{e}x\right)}{\sqrt{1+\delta_n}}\cdot\frac{\cos\left(\frac{m\pi}{b}\left(y+\frac{b}{2}\right)\right)}{\sqrt{1+\delta_{0m}}} \qquad (2.5\text{-}5)$$

TM modes:
$$T_{enm}^{Ia}=D_{nm}\cdot\sin\left(\frac{n\pi}{e}x\right)\cdot\sin\left(\frac{m\pi}{b}\left(y+\frac{b}{2}\right)\right) \qquad (2.5\text{-}6)$$

We can easily find the values of the *A* and *D* coefficients using the following expression:

$$A_{nm}=D_{nm}=\frac{2}{\sqrt{e\cdot b\cdot\left[\left(\frac{n\cdot\pi}{e}\right)^2+\left(\frac{m\cdot\pi}{b}\right)^2\right]}} \qquad (2.5\text{-}7)$$

Secondly, we have to solve the coupling matrices, J, for the respective discontinuity. The next expression define the $\boldsymbol{J_{hh}}$:

$$\left(J_{hh}\right)_{qs}=\int_0^e\int_{-\frac{b}{2}}^{\frac{b}{2}}(\nabla T_{hq}^{Ia}\times\hat{z})\cdot(\nabla T_{hs}^{IIa}\times\hat{z})\,dxdy \qquad (2.5\text{-}8)$$

The solution of this integral can be separated in different cases depending on the value of n and m:

- n=0: $$J_{hh}=A^{I}A^{II}\cdot(m\cdot\pi)^2\cdot\frac{\sin(k^{I}e)}{b\cdot2\cdot\sqrt{2}\cdot k^{I}}$$
- m=0: $$J_{hh}=A^{I}A^{II}\cdot(n\cdot\pi)^2\cdot k^{I}\cdot\frac{b}{2}\cdot\frac{\cos(n\cdot\pi)\cdot\sin(k^{I}e)}{(k^{I}e)^2-(n\cdot\pi)^2}$$
- Other case: $$J_{hh}=A^{I}A^{II}\cdot\pi^2\cdot\frac{k^{I}}{2\cdot b}\cdot\frac{\cos(n\cdot\pi)\cdot\sin(k^{I}e)}{(k^{I}e)^2-(n\cdot\pi)^2}\cdot\left((me)^2+(n\cdot b)^2\right)$$

The following expression define the $\boldsymbol{J_{eh}}$:

$$\left(J_{eh}\right)_{rs} = \int_{0}^{e}\int_{-\frac{b}{2}}^{\frac{b}{2}} (-\nabla T_{er}^{Ia})\cdot(\nabla T_{hs}^{IIa} \times \hat{z})dxdy \qquad (2.5\text{-}9)$$

The solution of this integral can be separated in different cases depending on the value of n and m:

- n=0: $J_{eh} = A^{I}A^{II}\cdot m\cdot\pi\cdot\dfrac{\sin(k^{I}e)}{2\cdot\sqrt{2}\cdot k^{I}}$
- m=0: $J_{eh} = 0$
- Other case: $J_{eh} = A^{I}A^{II}\cdot\pi\cdot m\cdot\dfrac{\cos(n\cdot\pi)\cdot\sin(k^{I}e)}{2\cdot k^{I}}$

As the previous cases the next expression define the $\boldsymbol{J_{ee}}$:

$$\left(J_{ee}\right)_{rt} = \int_{0}^{e}\int_{-\frac{b}{2}}^{\frac{b}{2}} (\nabla T_{er}^{Ia})\cdot(\nabla T_{et}^{IIa})dxdy \qquad (2.5\text{-}10)$$

In this case the solution of this integral is for m≥1:

$$J_{ee} = A^{I}A^{II}\cdot\pi\cdot\frac{n\cdot e}{2\cdot b}\cdot\frac{\cos(n\cdot\pi)\cdot\sin(k^{I}e)}{(k^{I}e)^{2}-(n\cdot\pi)^{2}}\cdot\left((m\cdot\pi)^{2}+(k^{I}\cdot b)^{2}\right)$$

## 2.6. REFERENCES

[2-1] J. B. Davies, C.A. Muilwyk, *"Numerical Solution of Uniform Hollow Waveguides with Boundaries of Arbitrary Shapes*", Proc. IEE, vol. 1 13, Feb. 1966

[2-2] P .P. Silvester, R.L. Ferrari, "*Finite Elements for Electrical Engineers"*, Cambridge University Press, New York, 1983

[2-3] A. Wexler, *"Solution to Waveguide Discontinuities by Modal Analysis*", *IEEE* MTT-15, Sep. 1967, pp. 508-517

[2-4] Roger F. Harrington, *"Field Computation* by *Moment Methods*", Macmillan, New York, 1968

[2-5] K.S. Yee, *"Numerical Solution of Initial Boundary Value Problems Involving Maxwell's Equations in Isotropic Media",* IEEE Trans. Antennas Propagation, vol. 14, May 1966, pp. 302-307

[2-6] P.B- Johns, R.L. Beurle, *"Numerical Solution of Two-dimensional Scattering Problems Using Transmission-line Matrix"*, Proc. Inst. Electr. Eng., vol. 118, Sep. 1971, pp. 1203-1208

[2-7] R. Sorentino, *"Numerical Methods for Passive Microwave and Millimeter-Wave Structures"*, IEEE Press, N.Y., 1989, Part 1

[2-8] T. Itoh, *"Numerical Techniques for Microwave and Millimeter- Wave Passive Structures"*, John Wiley & Sons, N.Y., 1989

[2-9] MªÁngeles Ruiz Bernal, *"Modal analysis of Ridge Coaxial waveguide using the transverse resonance method and field matching to study microwave filters"*, Final Year Project, May 2006

[2-10] J. Bomemam, F. Arndt, *"Model S-Matrù- Design of Optiniun Stepped Ridged and Finned Waveguide Transfomers"*, IEEE MTT-35, June 1987, pp. 56 1-567.

[2-10] George Goussetis, *"Waveguide bandpass with improved performance"*, Ph.D. 2002.

# 3. IMPLEMENTATION OF THE FILTERS IN FORTRAN

## 3.1. INTRODUCTION

Modelling tools are essential for the analysis of microwave components and subsystems.

Important properties for an electromagnetic modelling tool are the *accuracy* with respect to the actual experimental measurement and the *computational efficienc*y. Computational efficiency refers to both the memory and time requirements of the program. Memory requirements should be such that the execution of the program is feasible without significantly slowing it down. The time required for execution is particularly important when the model is used recurrently. Accuracy is important in order to avoid manual tuning of the structure after fabrication. Usually accuracy and computational efficiency are contradictive qualities. A compromise between the two factors is therefore commonly made, while flexibility for the user to decide whether one factor should be suppressed for the benefit of the other is an advantage.

Throughout this work, numerical electromagnetic modelling has extensively been used. In many cases, commercial general purpose software packages, as HFSS [3-1], have been used due to it can simulate the electromagnetic scattering at random shaped objects. However, these are time and memory consuming, and often do not offer the required accuracy. Their use has been mostly restricted to initial investigation or verification. For the major part of the work therefore, specific modelling tools for particular structures have been developed and employed. In section 3.2 this tool is explained.

The user is then asked to specify the values of the variables in order to get simulated results for the particular structure. These models are efficiently fast and accurate for the particular structures. Their major drawback, compared to general purpose commercial packages is that they apply only to a limited family of structures.

## 3.2. IMPLEMENTATION

The mathematical formulation presented in chapter 2 has been implemented as computer algorithm and FORTRAN [3-2] has been used for this purpose. The program was written in FORTRAN to speed its execution time. Latter, in chapter 4, we will explain how MATLAB [3-3] is used as a tool to represent the final response of the filters in an interface easy to use by the customer

The structures involved in this work are E-plane filters with thin all-metal insert, consisting usually of a cascade of waveguide sections of different cross-sections including ridge waveguide. *Figure 3-1* shows an example of E-Plane filter with two resonators where all the discontinuities or waveguide sections are marked. In addition, this figure tries to explain the procedure of the function *"GeneralFilter"* to calculate the overall S-matrix of the filter to represent the final response of it. To calculate this total S-matrix we have to complete several steps.

First of all, the field distribution (cutoff wavenumbers, amplitude coefficients) of each waveguide section has to be known. This step was carried out in [1-8].

Secondly, the generalized scattering matrix of each discontinuity (WG-Reduced WG, Ridge WG-Reduced WG) has to be solved following the procedure explain in section 2.3. The next functions are used to achieve this task.

| | |
|---|---|
| MMATR_WG_RED | This subroutine generates the M matrix needed for the S-matrix at the WG- Reduced WG discontinuity. |
| MMATR_RID_RED | This subroutine generates the M matrix needed for the S-matrix at the Ridge WG- Reduced WG discontinuity. |
| SSURFACE | This subroutine will return the multi-port S-matrix for a surface discontinuity |

In practice, filters consist of a cascade of finite length homogeneous waveguide sections. To solve the discontinuity of finite length we have to follow the instructions in section 2.4, and calculate the D-matrix. In addition another function is needed to make the cascade of the S and D matrix as it is exposed in the next table.

| | |
|---|---|
| DMATR | This subroutine receives as an input the Kc values for a waveguide of finite length L (mm) and returns an array vector D containing the S-parameter for each mode. |
| CASCSMATDFL | This subroutine calculates the overall discontinuity of a surface discontinuity with scattering sub-matrices S11,S12,S21,S22 and a Finite length with scattering array D. |

The last main function is the following and it makes the cascade of two generalized scattering matrices. Finally, using that function, the overall generalized scattering matrix of the filter will be obtained.

| | |
|---|---|
| CASCSCATMAT | This subroutine gives the result of cascaded scattering matrices. |

| | |
|---|---|
| 1 | [S]=cascsmatdfl( [S], [D]) |
| 2 | [G]=cascscatmat( [S], [F]*) |
| 3 | [G]=cascsmatdfl( [G], [D]) |
| 4 | [S]=cascscatmat( [G], [F]) |
| 5 | [T]=cascscatmat( [S], [V]*) |

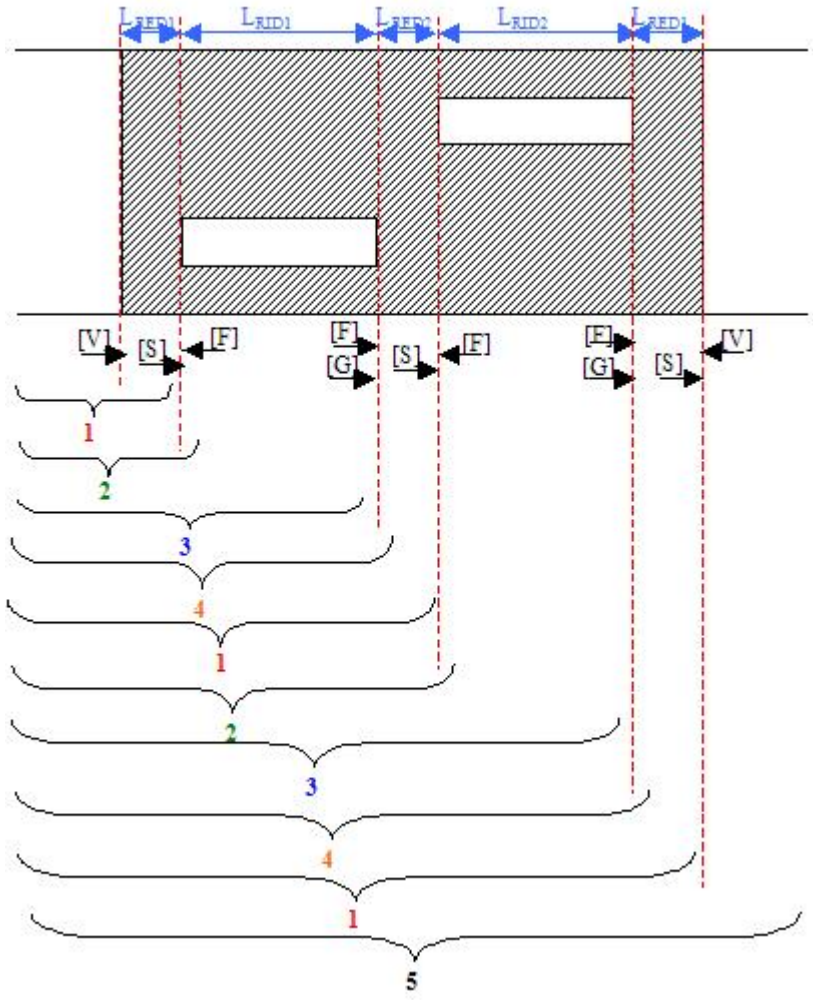


*Figure 3-1: E-plane filter with two resonators*

It is important to make one remark about the generalized scattering matrix in a discontinuity. If the generalized scattering matrix is solved from WG1 to WG2 there is a relation to calculate the generalized scattering matrix in the opposite direction:

From WG1 to WG2: $S = \begin{bmatrix} S_{11} & S_{12} \\ S_{21} & S_{22} \end{bmatrix}$ → From WG2 to WG1: $S^* = \begin{bmatrix} S_{22} & S_{21} \\ S_{12} & S_{11} \end{bmatrix}$

In *Figure 3-2*, a diagram explaining the performance of the *"GeneralFilter"* function is presented.

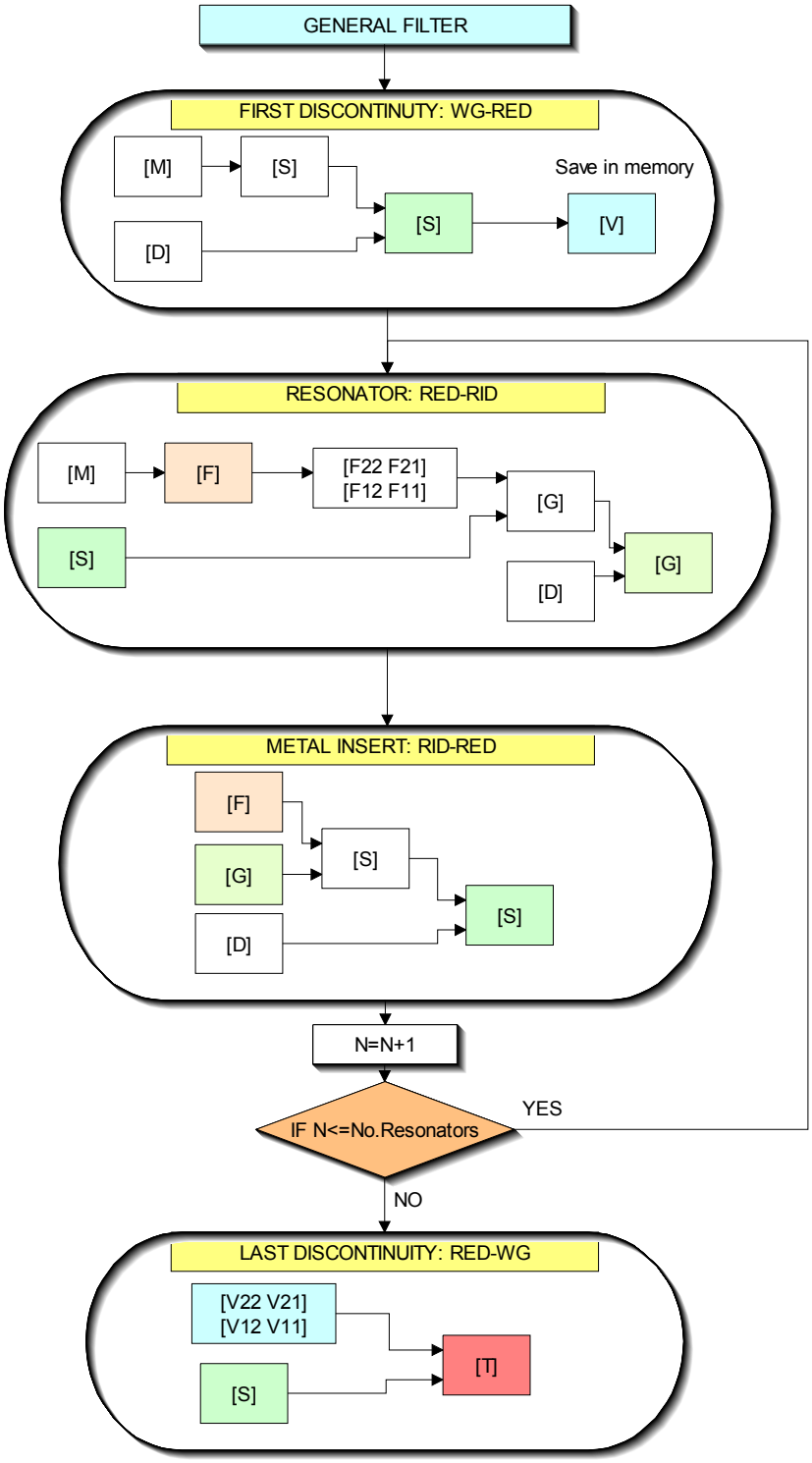


*Figure 3-2: GeneralFilter diagram*

### 3.3. CONVERGENCE STUDY

A convergence analysis, generally in numerical analysis applications, is the one that investigates how an algorithm converges to a nominal value with increasing number of calculations or terms. In this section, the convergence of the response of the filter with increasing the number of TE and TM modes is presented. This analysis is made just for structures with asymmetric ridge waveguide, due to the main objective is to use them to obtain improved responses with better selectivity and transmission zeros. Results obtained by this analysis will be useful in later stages of the work, where more complex structures will be simulated. At that stage it will be useful to know how many TE and TM modes in each section is required in order to obtain accurate results, without overloading the simulation with terms that contribute to a negligible extend. Avoidance of redundancy is particularly essential in optimisation procedures, where the computational cost of each simulation is crucial for the efficiency.

*Figures 3-3, 3-4 and 3-5* presents the convergence to the response of the filter for the configuration described in *Table 3-1* with increasing the number of TE and TM modes. The number of TE and TM modes will be the same in each section of the filter due to the complexity of this study, but it will be possible to obtain different number of TE modes than TM modes.

| | |
|---|---|
| A=22.86 | 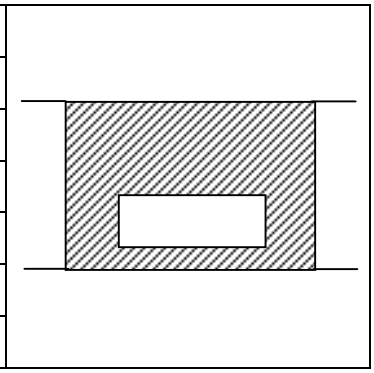 |
| B=10.16 | |
| Lred=2 | |
| Lrid=15 | |
| T=0.1 | |
| C1=1 | |
| S1=2 | |

*Table 3-1: Dimensions in mm of the E-Plane filter with one resonator*

As a first step to study the convergence, several simulations have been done for different number of TE and TM modes. *Figure 3-3 (a)* shows a zoom at the passband. As we can see in this figure similar responses have been obtained when the number of TE modes are 15, 20 or 25. Furthermore, *Figure 3-3 (b)* presents the responses of the filter just for these values and good results are obtained when the number of TE modes are 20 or 25.

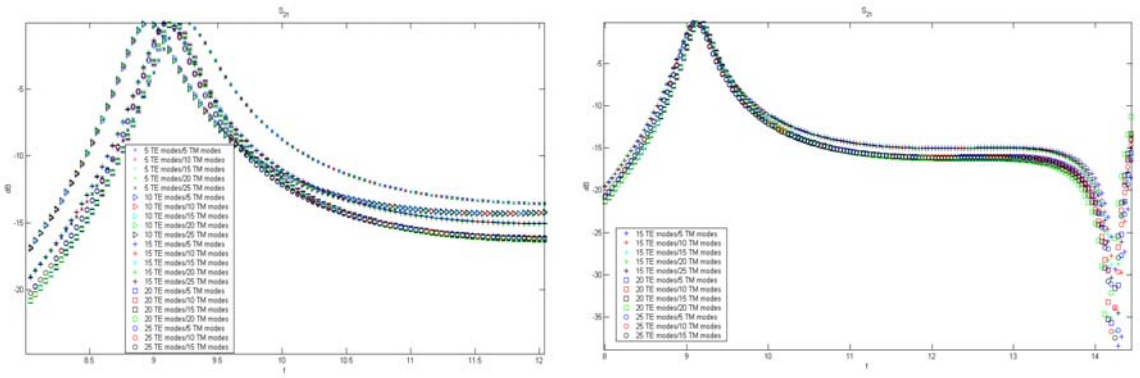

*(a)* *(b)*

*Figure 3-3: $S_{21}$ for different values of the TE and TM modes*

In the previous figure it is not clear the dependence of the number of TM modes, due to that in *Figure 3-4* the responses for 20 and 25 TE modes are shown in separated graphs. Similar responses are obtained for 10 or 15 TM modes.

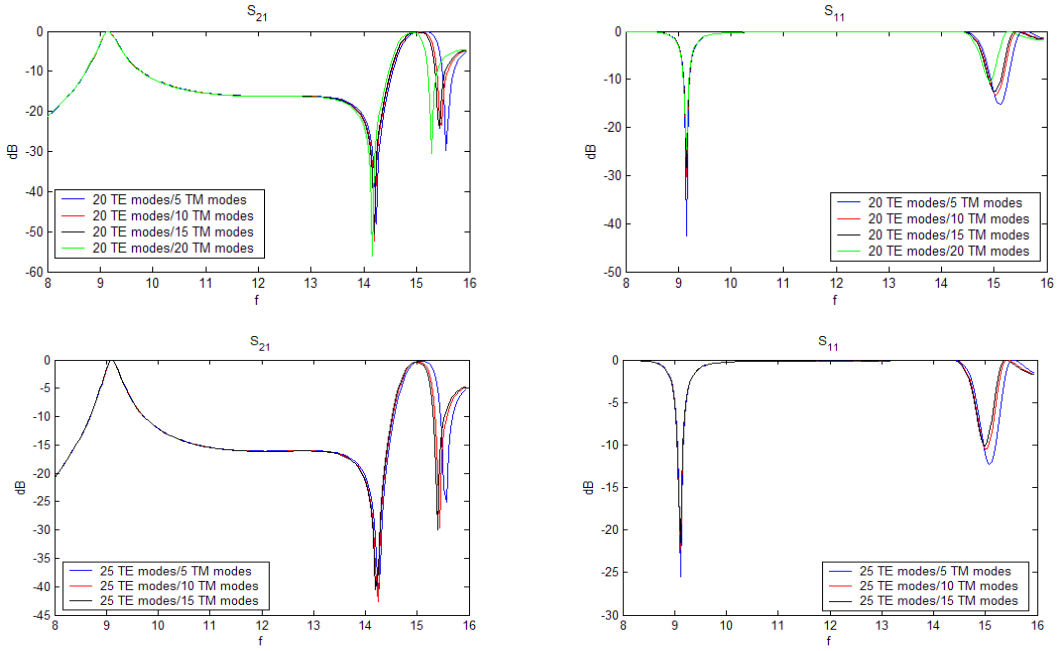


*Figure 3-4: $S_{21}$ and $S_{11}$ for different values of the TE and TM modes*

Finally, as *Figure 3-5* shows, the variation is minimum between TE= 20 or 25 and TM=10 or 15. To sum up good results are observed for 20 TE modes and 15 TM modes.

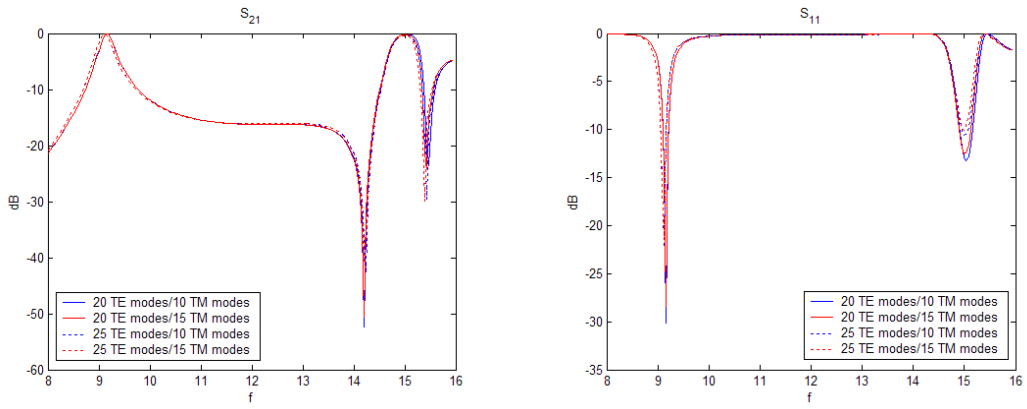


*Figure 3-5: $S_{21}$ and $S_{11}$ for different values of the TE and TM modes*

Furthermore, to validate the previous conclusions it is simulated another filter with two resonators as it is indicated in *Table 3-2*.

| | |
|---|---|
| A=22.86 | 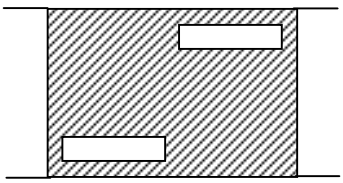 |
| B=10.16 | |
| $Lred_1$= $Lred_2$=2 | |
| $Lrid_1$=$Lrid_2$=15 | |
| T=0.1 | |
| $C1_1$=1( $C1_2$=B-S1-$C1_1$) | |
| S1=2 | |

*Table 3-2: Dimensions in mm of the E-Plane filter with two resonators*

*Figure 3-6* presents the responses for this filter using different values of TE and TM modes. Good results are obtained also for the same values chosen in the previous case with one resonator. For that reason we are going to indicate these values for further analysis.

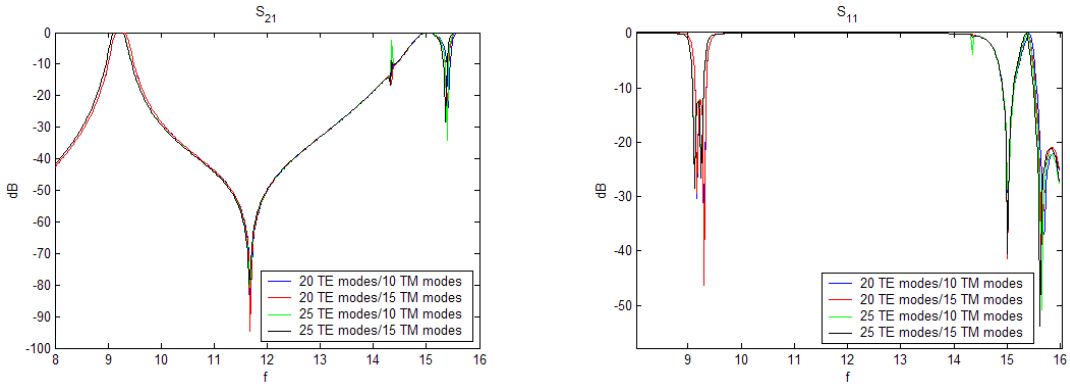


*Figure 3-6: $S_{21}$ and $S_{11}$ of the filter with two resonator for different values of the TE and TM modes*

## 3.4. REFERENCES

[3-1] Agilent High Frequency Structure Simulator (HFSS)

[3-2] DIGITAL Visual FORTRAN

[3-3] MATLAB, Mathworks Inc.

# 4. SIMULATION IN MATLAB

FORTRAN have been used to solve the mathematical formulation presented in chapter 2. As it was explain in chapter 3, the program was written in FORTRAN to speed its execution time. This chapter shows how MATLAB is used as a tool to represent the final response of the filters in an interface easy to use by the customer.

There is a communication between MATLAB and FORTRAN to reproduce the final response of the filter. The procedure that is used is explain in *Figure 4-1*.

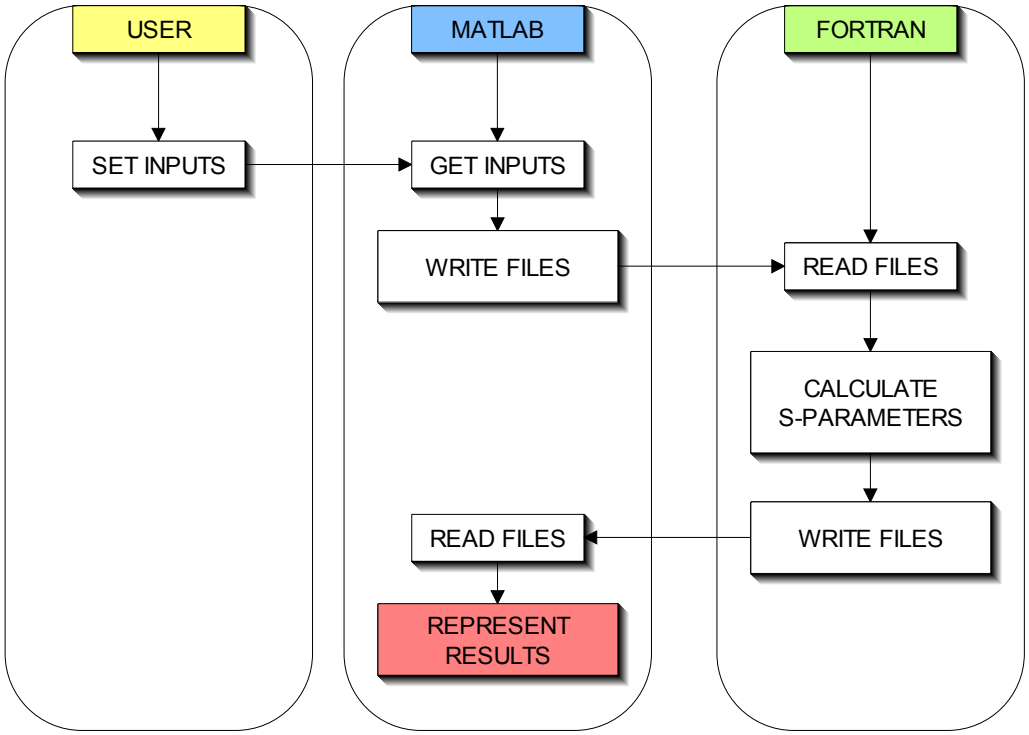


*Figure 4-1: Diagram of the communication between MATLAB and FORTRAN*

In *Figure 4-2* the created interface is presented. The E-Plane filters that can be simulated with this interface can have as much as five resonators in different positions each resonator. The main advantage is that this interface is easy to use and provides a fast tool to simulate the type of structures under study in this project.

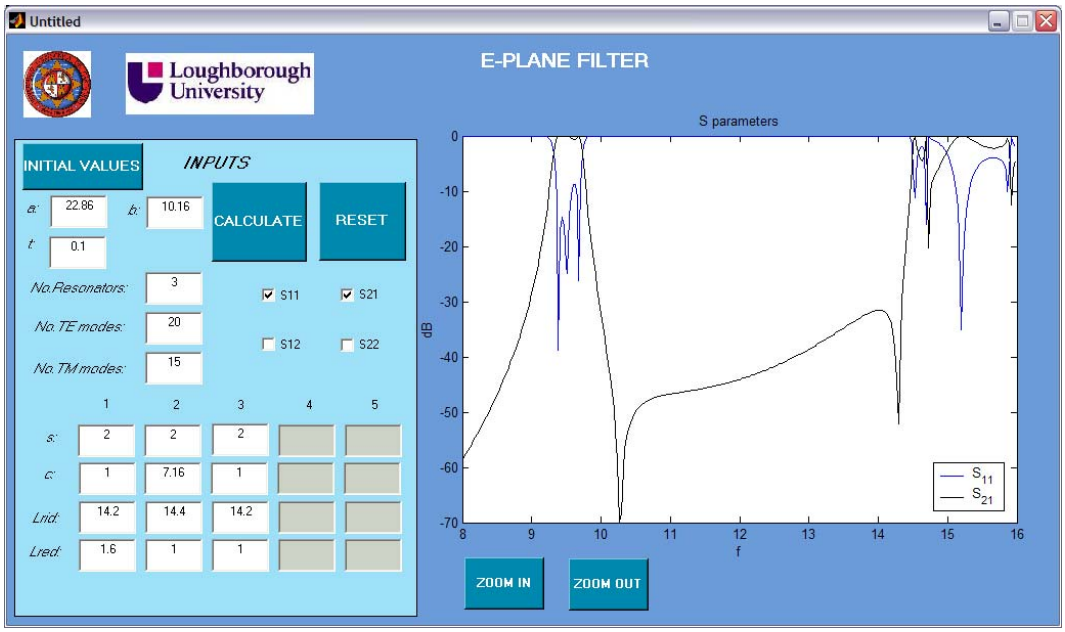


*Figure 4-2: Interface to simulate E-Plane filters*

First of all, the user has to introduce the dimensions of the guide and the E-Plane filter, indicating the number of resonators. Moreover there is the possibility to set the values of the number of TE and TM modes, that is useful to realize a convergence study.

As an example to help the user to utilize the program, the button “Initial Values” generates an E-Plane filter with three resonators in an asymmetric position. When this button is pressed the program shows a figure with the metal insert of this filter to make easier the understanding of the parameters that the user has to indicate. *Figures 4-2* and *4-3* shows the interface when this button has been pressed and the figure with the metal insert of the filter with three resonators respectively.

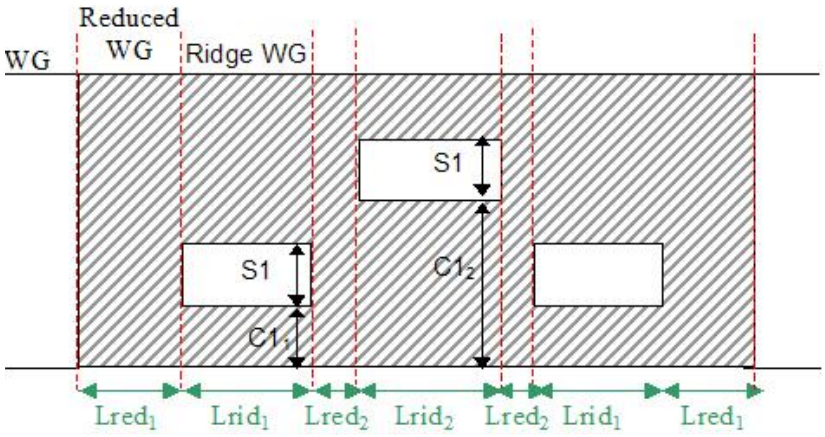


*Figure 4-2: E-plane metal insert with three resonators*

# 5. ANALYSIS OF FILTERS WITH ONE RESONATOR

In this chapter the variation of the response of a E-Plane filter with one resonator is studied. Changing all the parameters that are shown in *Figure 5-1* a complete analysis of this configuration can be obtained.

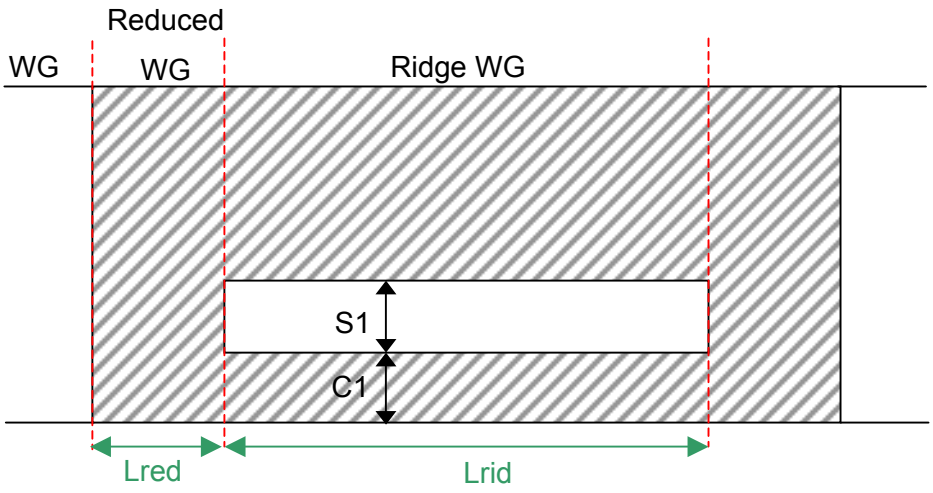


*Figure 5-1: Cross section in the Y-Z plane of a E-Plane Filter with one resonator*

Sections 5.1 and 5.2 present the variation of the filter response for a symmetric and asymmetric position of the resonator respectively.

The comparison between the symmetric and the asymmetric case is made in section 5.3. In addition the peculiar effect to obtain a transmission zero, namely in the asymmetric case, in configurations with one resonator where there is not cross coupling is explained.

Furthermore, the quality factor (Q) will be studied in section 5.4. This study is useful if a specific value of quality factor is required in a future design of the filter.

Finally, in section 5.5, a filter with a passband in 9.25-9.75 GHz is validated using, in a first instant, the response of a prototype with all metal septa, and in a further stage the response of the same filter simulated with a commercial software, HFSS.

From this moment all the parameters will be done in milimeters (mm).

## 5.1. SYMMETRIC POSITION OF THE RESONATOR

### 5.1.1. VARIATION OF THE HEIGHT OF THE RESONATOR (S1,C1)

*Table 5-1* shows the dimensions of the filter under study. The parameters that stand out in blue are the ones that experience changes.

| | |
|---|---|
| A=22.86 | 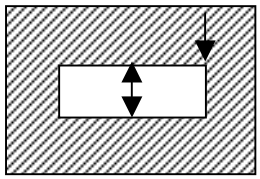 |
| B=10.16 | |
| Lred=2 | |
| Lrid=15 | |
| T=0.1 | |
| C1=0-5 | |
| S1=0.16-10.16 | |

*Table 5-1: Dimensions of the E-Plane filter with one resonator*

*Figure 5-2* shows the S parameters for different values of the height of the resonator which is placed in a symmetric position. When the height decreases the selectivity of the filter increases. If the height is very thin an unexpected transmission zero at a finite frequency appears.

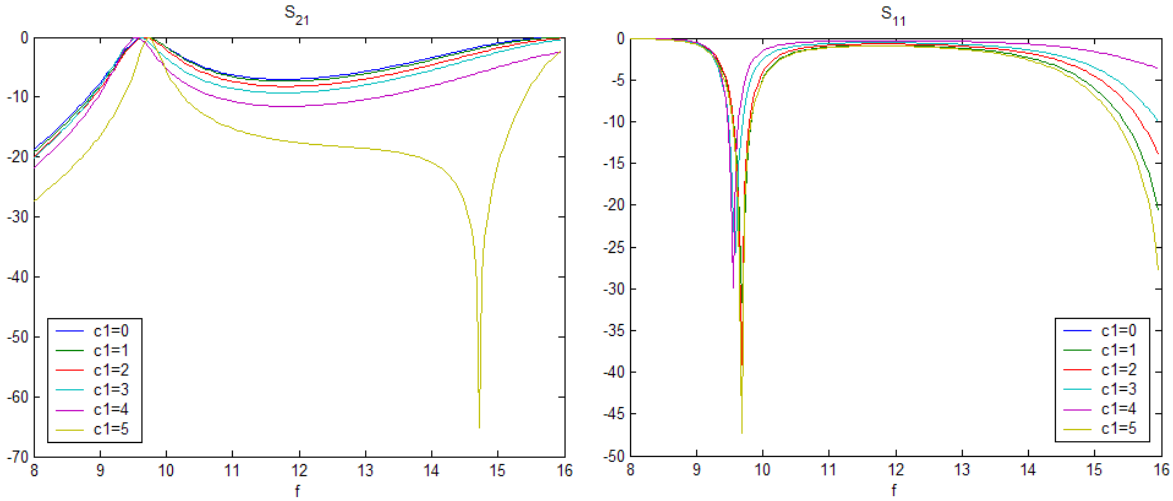


*(a)* *(b)*

*Figure 5-2: $S_{21}$ (a) and $S_{11}$ (b) for different values of c1 in a symmetric case*

### 5.1.2. VARIATION OF THE LENGTH OF THE RESONATOR ($L_{RID}$)

As in the previous section, *Table 5-2* shows the dimensions of the filter under study.

| | |
|---|---|
| A=22.86 | 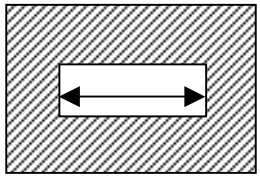 |
| B=10.16 | |
| Lred=2 | |
| Lrid=13-17 | |
| T=0.1 | |
| C1=4.08 | |
| S1=2 | |

*Table 5-2: Dimensions of the E-Plane filter with one resonator*

*Figure 5-3* shows the S parameters for different values of the length of the resonator. There is a relationship between the length of the resonator and the wavelength. The length of the resonator(Lrid) must be around $\lambda_{g\_rid}$ /2. Hence, when Lrid increases, the central frequency decreases and the response is more selective.

The length of the resonator is very important to design the passband of the filter.

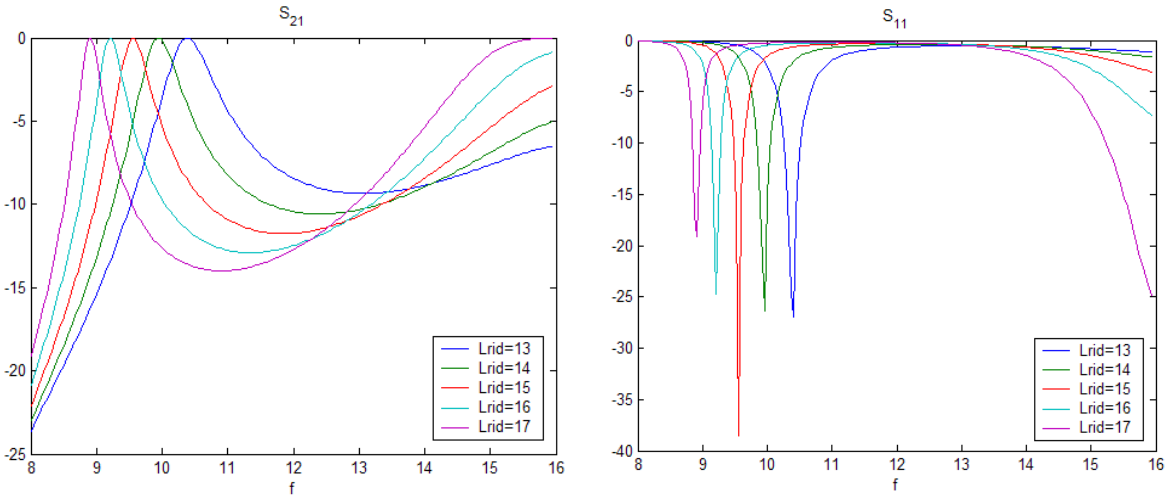


*(a)* *(b)*

*Figure 5-3: $S_{21}$ (a) and $S_{11}$ (b) for different values of Lrid in a symmetric case*

### 5.1.3. VARIATION OF THE LENGTH OF THE METAL INSERT ($L_{RED}$)

*Table 5-3* presents the dimensions of the filter under study.

| | |
|---|---|
| A=22.86 | 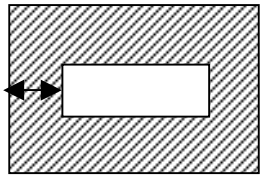 |
| B=10.16 | |
| Lred=1-6 | |
| Lrid=15 | |
| T=0.1 | |
| C1=4.08 | |
| S1=2 | |

*Table 5-3: Dimensions of the E-Plane filter with one resonator*

*Figure 5-4* shows the S parameters for different values of the length of the metal inserts (Lred). When Lred increases, the selectivity is improved because the discontinuity is more reflective, hence the coupling is weaker.

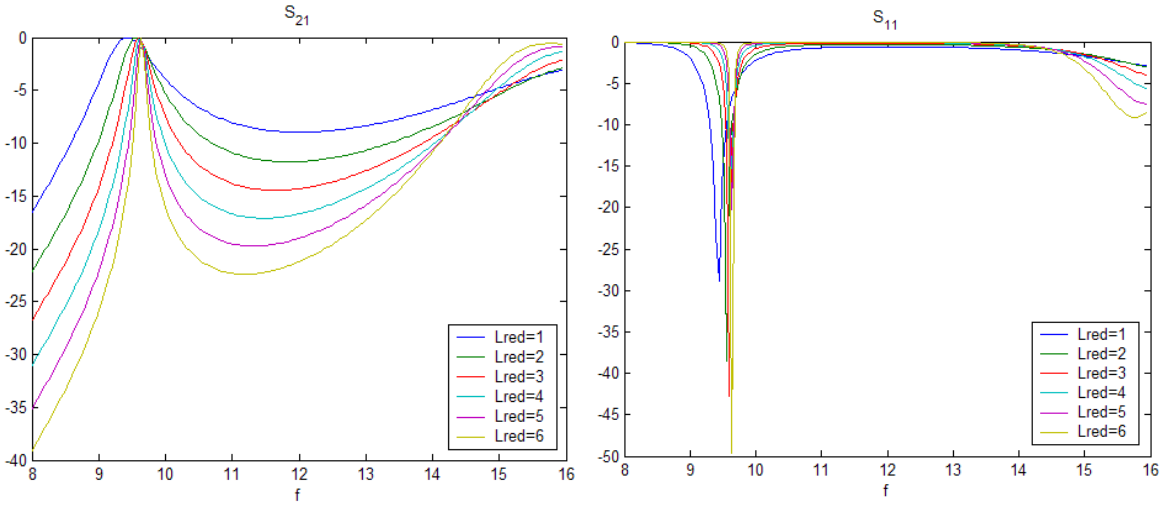


*(a)* *(b)*

*Figure 5-4: $S_{21}$ (a) and $S_{11}$ (b) for different values of Lred in a symmetric case*

## 5.2. ASYMMETRIC POSITION OF THE RESONATOR

### 5.2.1. VARIATION OF THE POSITION OF THE RESONATOR (C1) WITH A FIXED HEIGHT

*Table 5-4* shows the dimensions of the filter under study, where the height of the resonator is fixed.

| | |
|---|---|
| A=22.86 | 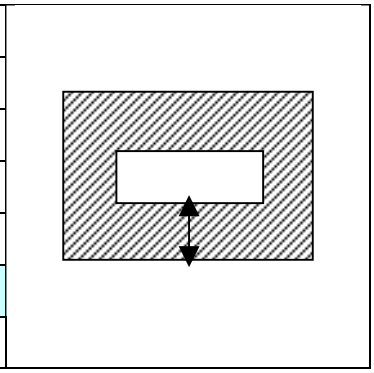 |
| B=10.16 | |
| Lred=2 | |
| Lrid=15 | |
| T=0.1 | |
| C1=0-4 | |
| S1=2 | |

*Table 5-4: Dimensions of the E-Plane filter with one resonator*

*Figure 5-5* represents the S parameters for different values of the position of the resonator. When the resonator is far for the central position, the response is more selective and the central frequency is lower. In addition a transmission zero is obtained at finite frequencies except when the resonator is placed in a symmetric position.

The position of the resonator is very important to design the passband of the filter and to obtain a selectivity improvement.

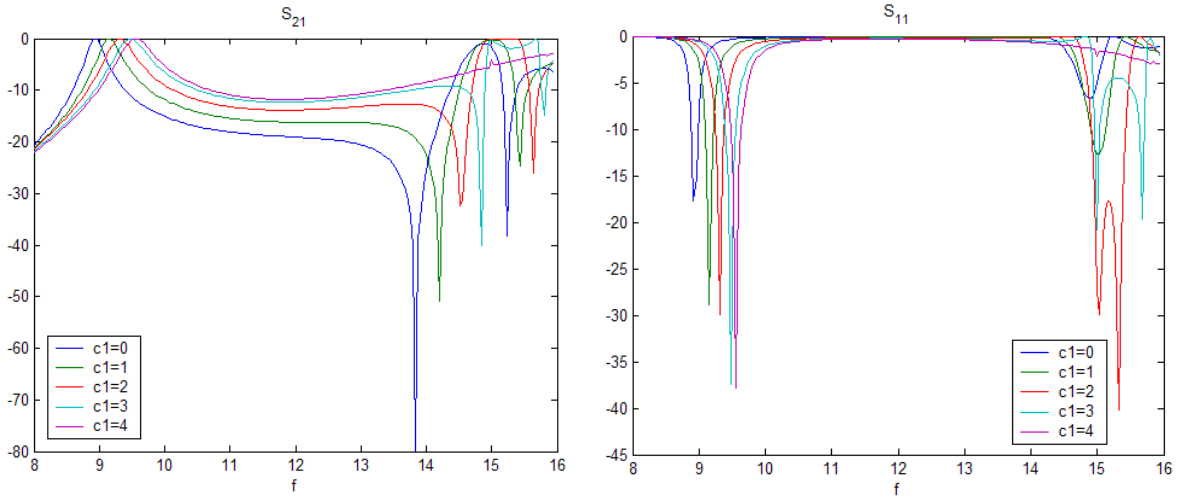


*(a)* *(b)*

*Figure 5-5: $S_{21}$ (a) and $S_{11}$ (b) for different values of c1 in an asymmetric case*

### 5.2.2. VARIATION OF THE HEIGHT OF THE RESONATOR (S1) WITH A FIXED POSITION

In this case, *Table 5-5* shows the dimensions of the filter under study, where the position of the resonator is fixed, very close to the bottom wall of the waveguide.

| | |
|---|---|
| A=22.86 | 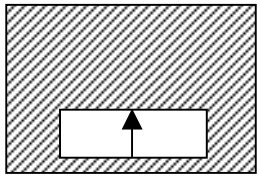 |
| B=10.16 | |
| Lred=2 | |
| Lrid=15 | |
| T=0.1 | |
| C1=1 | |
| S1=1-9 | |

*Table 5-5: Dimensions of the E-Plane filter with one resonator*

*Figure 5-6* illustrates the S parameters for different values of the height of the resonator in an asymmetric position. When the height is small, the response is more selective, the central frequency is lower and we can obtain a transmission zero. Furthermore, when the height of the resonator is bigger the selectivity is lower due to the coupling is higher. In this case the transmission zero is not obtained.

We can say that the height of the resonator is important to improve the selectivity.

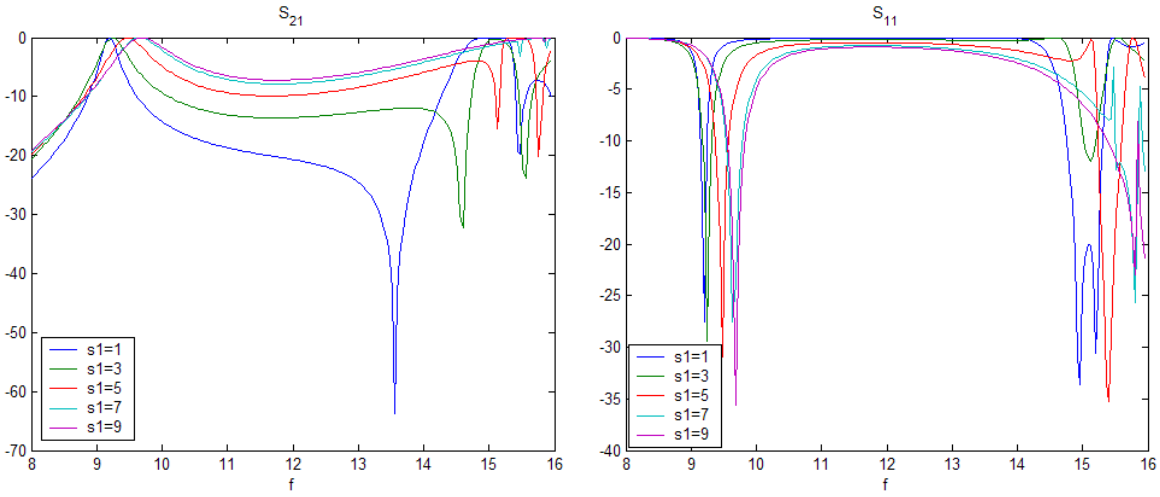


*(a)* *(b)*

*Figure 5-6: $S_{21}$ (a) and $S_{11}$ (b) for different values of c1 in an asymmetric case*

## 5.3. COMAPRISON BETWEEN SYMMETRIC AND ASYMMETRIC POSITION OF THE RESONATOR

In the asymmetric case the studies changing the length of the metal insert, Lred, and the length of the resonator, Lrid, have not been represented because the same behaviour was found for both cases. Moreover, as a remark, it can be said that the selectivity is improved when Lrid and Lred increase. In addition, Lrid is the parameter that can define the passband in a first moment due to it is directly related with the frequency.

Another important parameter is the height of the resonator, s1. In general, to obtain a better stopband performance narrower height of the resonator is required. For the symmetric case a transmission zero is only obtained when the value of s1 is very low. As it is shown in *Figure 5-5*, for a fix value of s1= 2 mm, a transmission zero appears in all the cases menus when the resonator is almost in a symmetric position. Therefore a transmission zero is easily obtained when the resonator is placed in an asymmetric position.

These transmission zeros are unexpected for configurations with one resonator. Therefore it is not known the reason of its appearance. It would be necessary a deeper study about the impedance and the field distribution of the waveguide sections.

The frequency where the transmission zero is found is important too, because it can affect to the selectivity of the filter response. To get a improved selectivity the transmission zero has to be close to the passband. As it can be observed in *Figures 5-5* and *5-6*, when the value of s1 is low and the resonator is placed close to the up or bottom walls of the guide the transmission zeros have frequencies closer to the passband and also the losses at the stopband are higher, as a result the selectivity has been improved.

## 5.4. QUALITY FACTOR

The Q factor or quality factor is a measure of the "quality" of a resonant system. Resonant systems respond to frequencies close to their natural frequency much more strongly than they respond to other frequencies. The Q factor indicates the amount of resistance to resonance in a system. Systems with a high Q factor resonate with a greater amplitude, at the resonant frequency, than systems with a low Q factor.

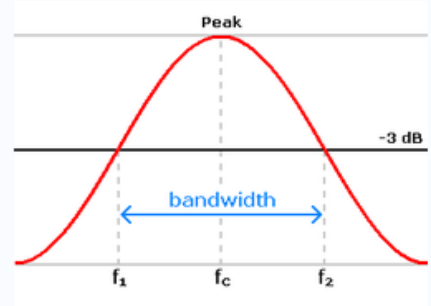


*Figure 5-7: Definition of Bandwidth*

The Q factor is defined as the resonant frequency (central frequency) $f_0$ or $f_c$ divided by the bandwidth Δf or BW:

$$Q = \frac{f_C}{f_2 - f_1} = \frac{f_C}{BW_{-3dB}}$$

Bandwidth BW or $\Delta f = f_2 - f_1$, where $f_2$ is the upper and $f_1$ the lower cutoff frequency. On a graph of response versus frequency like *Figure 5-7*, the bandwidth is defined as the 3 dB change in level on either side of the center frequency.

The value of the quality factor has been studied for a filter with one resonator changing its position and the length of the metal insert. The used dimensions are given in *Table 5-6*.

| | |
|---|---|
| A=22.86 | 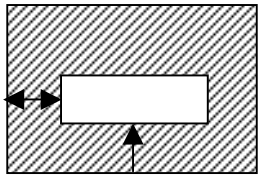 |
| B=10.16 | |
| Lred=2-7 | |
| Lrid=15.56 | |
| T=0.1 | |
| C1=0-4 | |
| S1=2.16 | |

*Table 5-6: Dimensions of the E-Plane filter with one resonator*

The results are presented in *Figure 5-8*. The quality factor increases when the resonator is placed in a position close to the up or bottom walls of the guide, and also when the length of the metal insert is big. That is coherent with the conclusions in section 5.3, where it was said that when the length of the metal insert increases and the resonator is placed in an asymmetric position close to the walls of the waveguide, the selectivity is improved, therefore the bandwidth is smaller and the quality factor is higher. This effect can be observed easily in *Figure 5-8 (c)*.

The knowledge about the behaviour of the Q factor with respect to the parameters of the structure is important in a future stage when a filter with specific characteristics has to be designed.

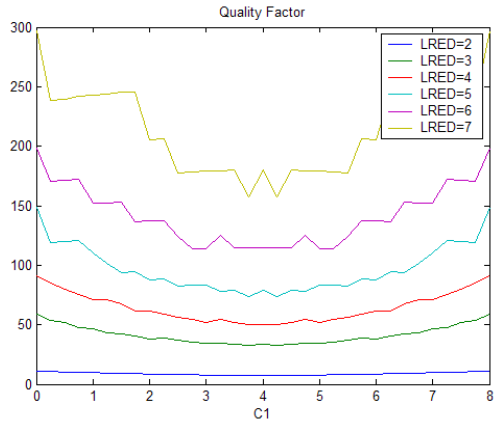


*(a)*

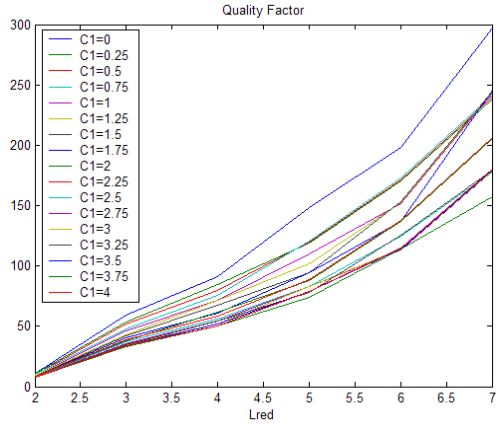


*(b)*

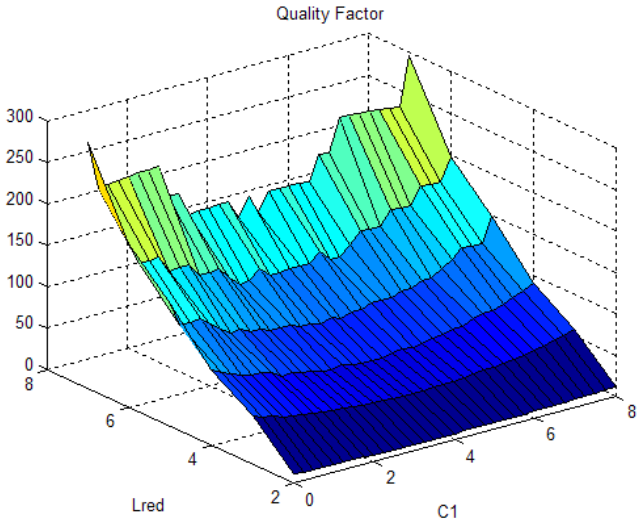


*(c)*

*Figure 5-8: Quality factor vs. Lred and c1, 2D (a) and (b), and 3D (c)*

## 5.5. VALIDATION OF A FILTER: 9.25-9.75 GHZ PASSBAND

To validate the filter we are going to compare the response of the filter with the response of the prototype in [2-10]. We have to find the parameters of the filter that make the response more similar to the response of the prototype. The values of A, B and T for the designed filter will be the same than for the prototype.

One of the objectives is to reduce the length of the total filter, and other objective is to improve the selectivity.

*Table 5-7* gives the parameters and the response of the prototype.

| PROTOTYPE |
|---|
| A=20.86 |
| B=10.16 |
| T=0.1 |
| Ripple=0.5 |
| Lred=2.18800010322593 |
| L=16.0271294973159 |

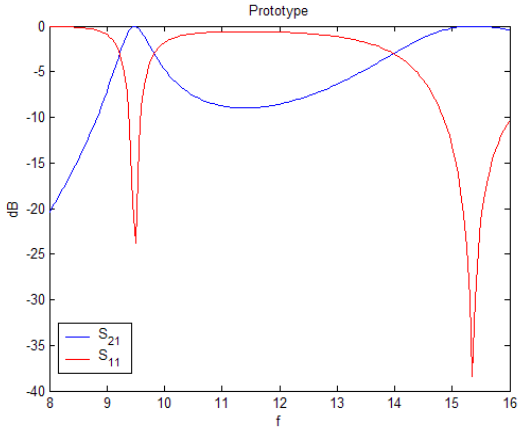


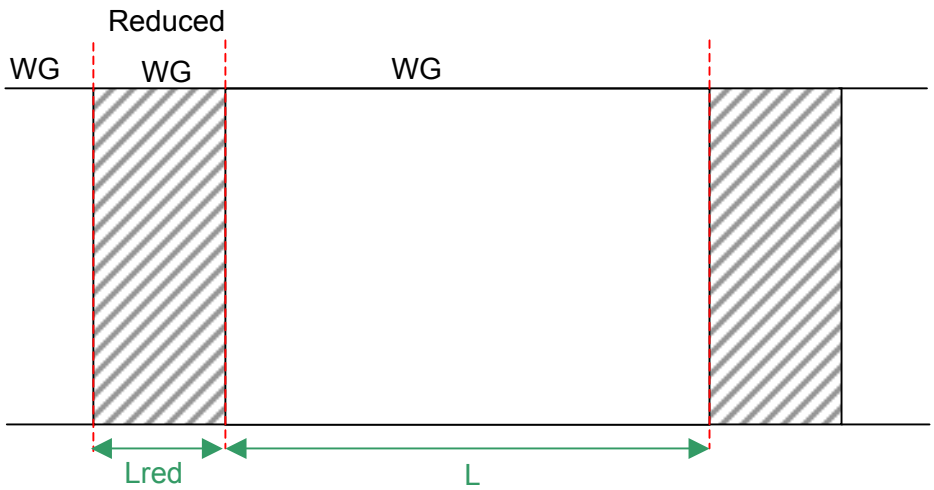


*Table 5-7: Dimensions and response of the prototype with one resonator*

The length of the resonator(Lrid) must be around less than $\lambda_{g\_rid}$ /2. Therefore, $\lambda_{g\_rid}$ is calculated as it is defined in the book: "Microstrip Filters for RF/Microwave Application", Jia-Shen G. Hong, M.J. Lancaster. It is explained in the following code:

```
F1=9.25;
F2=9.75;

Kc=0.137427496487782; %Kc first TE mode for the waveguide
Fc=Kc*3/(0.02*pi);

Krid=8.224469046195766E-002; %Kc first TE mode for the Ridge waveguide

L0=300/F1;
Lg1=L0/sqrt(1-(Fc/F1)^2);
L0=300/F2;
Lg2=L0/sqrt(1-(Fc/F2)^2);

Lg=(Lg1+Lg2)/2;
Fo=sqrt(Fc^2+(300/Lg)^2);
Ko=0.02*pi*Fo/3;

Lgrid=2*pi/sqrt(Ko^2-Krid^2);

Lrid=Lgrid/2
```

This formulation takes into account the effect of the couples. For that reason, the reduction of the length of the resonator comes as a result of the coupling.

The result is Lrid $\leq \lambda_{g\_rid}/2$= 17.3746 mm.

*Figure 5-9* shows the responses of the prototype and the filters for different values of Lrid(mm) for fix values of s1, c1 and Lred.

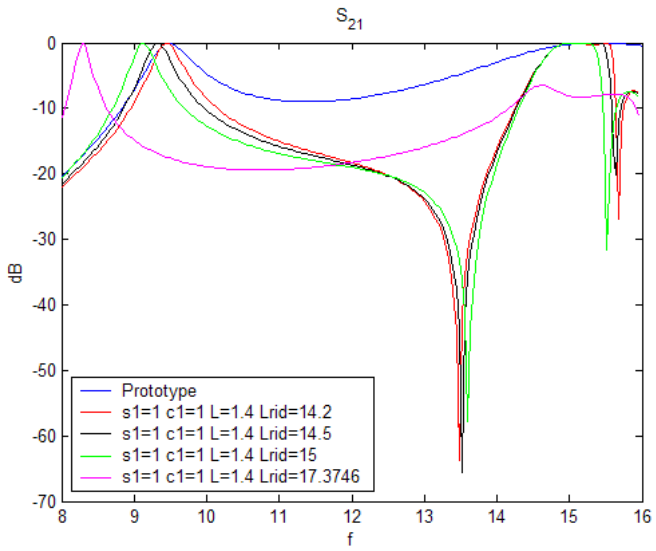


*Figure 5-9: $S_{21}$ for different values of Lrid*

As we can see, for Lrid= 17.3746 mm the filter has a different passband than the prototype, so we have to look for another value of Lrid that make the response similar to the prototype. If we want to increase the central frequency of the passband, we have to decrease the wave length, so Lrid must be smaller.

In *Figure 5-9* good results have been obtained for Lrid=14.2 mm

If we compare with the prototype, we are reducing the length of the filter. On the other hand we have to study how the response changes with the rest of the parameters (s1, c1 and Lred).

Firstly, *Figure 5-10* presents how the response changes for different values of Lred. We can say that if Lred increases the response is more selective, but the passband is shifted to the right or increases in frequency.

As we can see in *Figure 5-10 (b)* one of the best values is Lred=1.6, because the response is more selective and similar to the prototype.

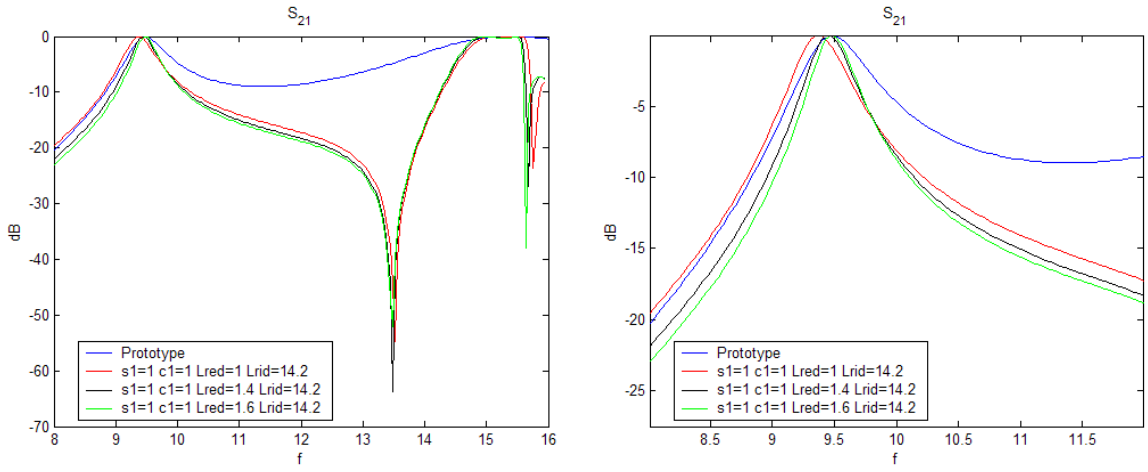


*(a)* *(b)*

*Figure 5-10: $S_{21}$ for different values of Lred (a), and a zoom of it in the passband (b)*

The response for different values of S1 is shown in *Figure 5-11*. We can notice that if S1 decreases the response is more selective, but the passband is shifted to the right or increases in frequency.

For the moment we are going to choose the value S1=1 because the passband is similar to the prototype.

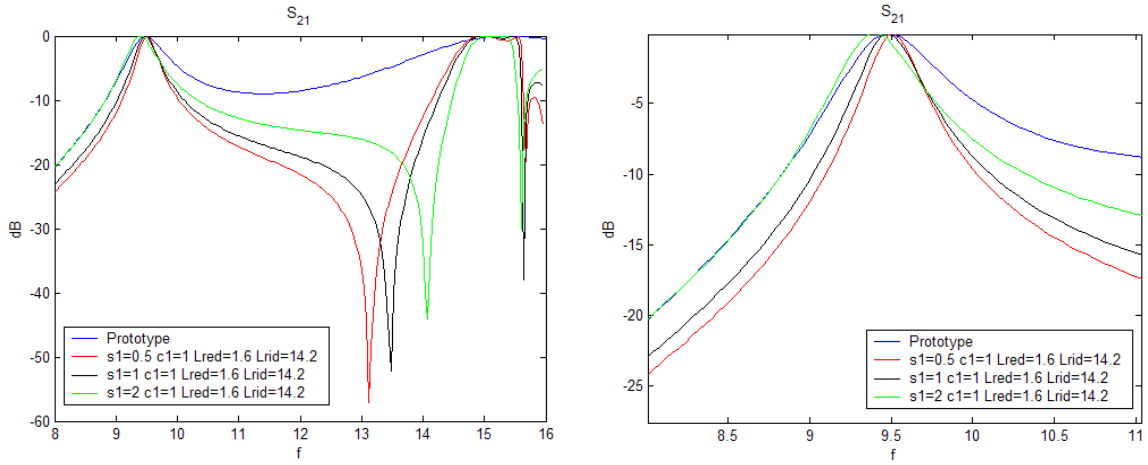


*(a)* *(b)*

*Figure 5-11: $S_{21}$ for different values of S1 (a), and a zoom of it in the passband(b)*

*Figure 5-12* shows the response for different values of C1. We can appreciate that if C1 increases the response is less selective and the passband increases in frequency.

For the moment we are going to choose the value C1=1 because the passband is similar to the prototype and it has good selectivity also with a transmission zero at finite frequencies, although it is not positioned very close to the passband.

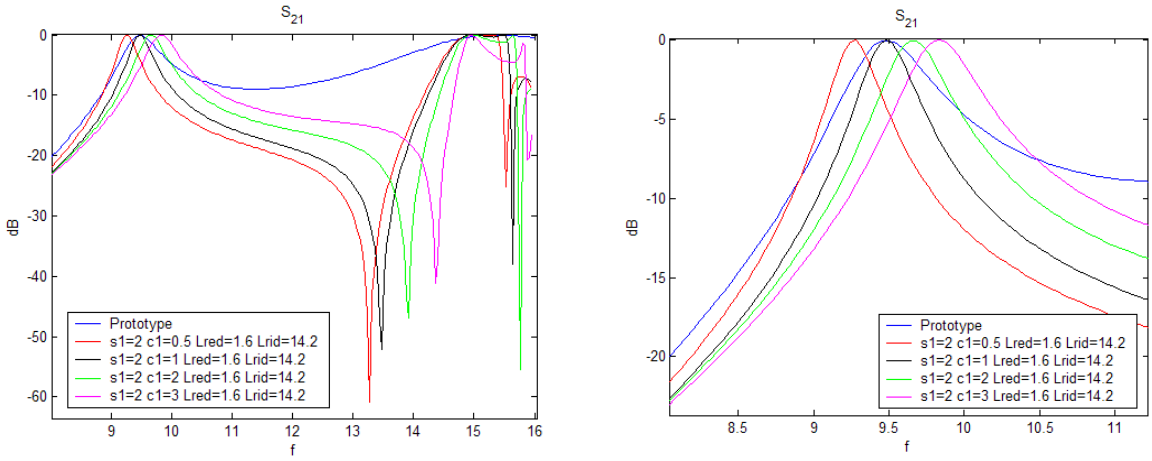


*(a)* *(b)*

*Figure 5-12: $S_{21}$ for different values of C1 (a), and a zoom of it in the passband(b)*

As a conclusion, the dimensions of the filter that has been made are given in *Table 5-8*.

| RWG FILTER | PROTOTYPE |
|---|---|
| S1=1 | |
| C1=1 | |
| Lred= 1.6 | Lred= 2.18800010322593 |
| Lrid= 14.2 | Lrid= 16.0271294973159 |

*Table 5-8: Dimensions of the filter and the prototype with one resonator*

Before analyse the final response of the filter some remarks have to be done about all the parameters that have been studied.

- Lrid: when the central frequency increases Lrid is smaller
- Lred: when it increases the selectivity is improved because the discontinuity is more reflective and the coupling is weaker. Moreover, if Lred increases the central frequency is higher.
- S1: when it decreases the selectivity is improved and the central frequency increases.
- C1: when it increases, the selectivity is lower and the central frequency increases.

Using the parameters of the *Table 5-8* , good agreement between the response of the prototype and the filter has been achieved. *Figure 5-13* verifies how the selectivity has been improved.

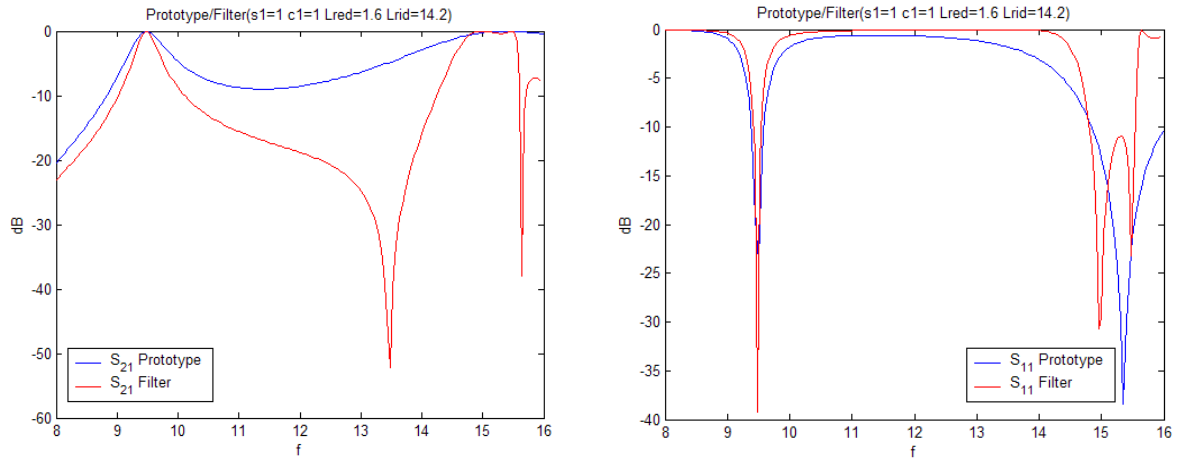


*(a)* *(b)*

*Figure 5-13: $S_{21}$ (a) and $S_{11}$ (b) for the prototype and the final filter*

Another advantage is that the total length of the filter has been reduced around 3mm with respect to the prototype.

| |
|---|
| Prototype length= 20.403 mm |
| RWG filter length= 17.4 mm |

*Figure 5-14* present the comparison of the response of the same filter simulated in HFSS and Fortran. Good agreement between the two simulations has been observed.

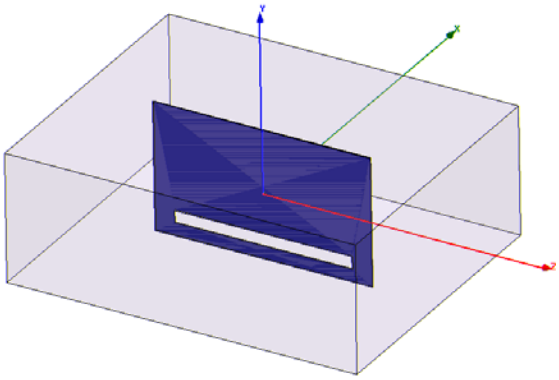

*(a)*

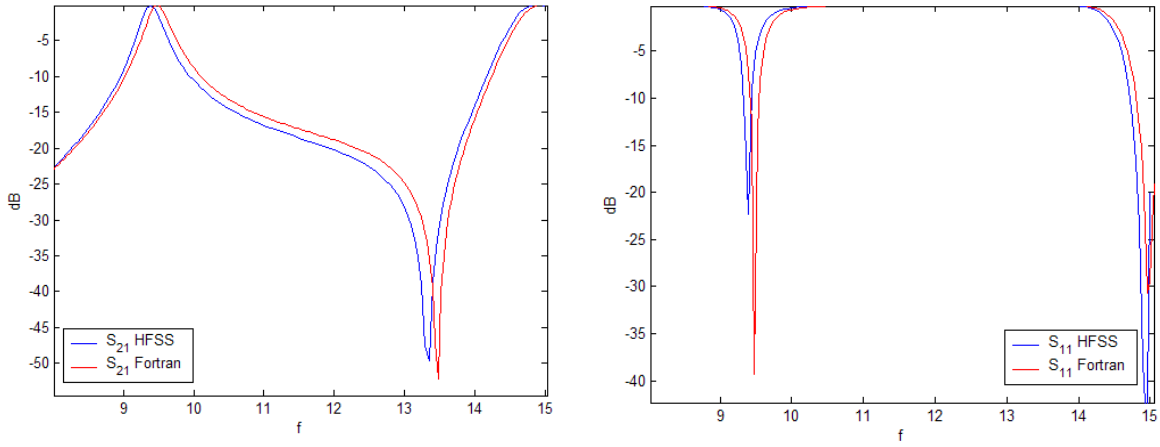


*(b)* *(c)*

*Figure 5-14: Sketch of the filter (a) and comparison of $S_{21}$ (b) and $S_{11}$ (c) obtained with HFSS and Fortran*

The minimum deviations observed in *Figure 5-14* can be due to that HFSS needs more steps to converge to a more accurate response.

*Table 5-9* gives the comparison of the time needed to simulate the same filter in Fortran and HFSS on an AMD Athlon(tm) 64, 637 MHz, 1GB RAM. The results are exceptionally good. .That remembers that it is important to develop a tool to analyse a specific type of structures that is going to be used recurrently.

| Fortran | HFSS |
|---|---|
| 15 sec. | 1260 sec. (21 min.) |

*Table 5-9: Time comparison*

# 6. ANALYSIS OF FILTERS WITH TWO RESONATORS

In this chapter the variation of the response of a E-Plane filter with two resonators is studied. A full analysis of this configurations will be obtained varying the parameters that are shown in *Figure 6-1*.

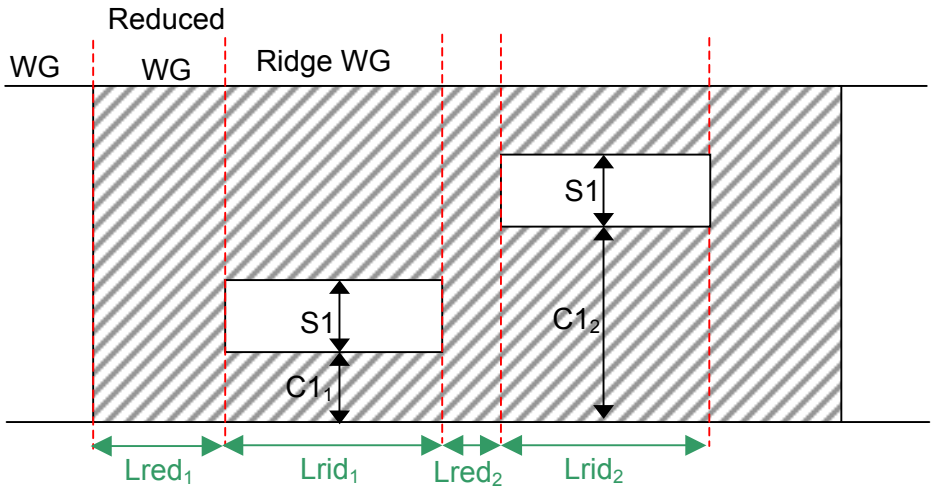


*Figure 6-1: Cross section in the Y-Z plane of a E-Plane Filter with two resonators*

It is important to remark that the topologies analysed in this project are synchronous. *Figure 6-2* introduces a basic definition of synchronous and asynchronous topologies. As it is presented, in a synchronous structure, the wave that travel through the waveguide crosses the same path in both directions (the way from Port 1 to Port 2 is equal to the way from Port 2 to Port 1). Contrary, in an asynchronous structure, the wave crosses different ways depend on the direction (the way from Port 1 to Port 2 is different to the way from Port 2 to Port 1).

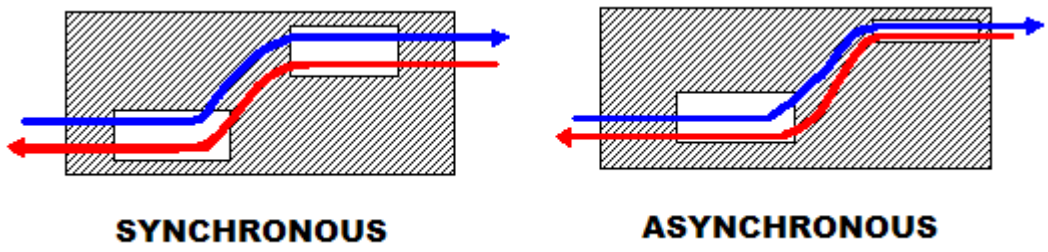


*Figure 6-2: Synchronous and asynchronous topologies*

Sections 6.1 and 6.2 present the variation of the filter response for a symmetric and asymmetric position of the resonators.

Moreover, section 6.3 tries to sum up the conclusions of the studies of the previous sections.

The coupling coefficient is analysed in section 6.4. This study is useful if a specific value of coupling coefficient is required in a later stage as in the design of the filter.

Finally, in section 6.4, a filter with a passband in 9.25-9.75 GHz is validated using, in a first instant, the response of a prototype with all metal septa, and in a further stage the response of the same filter simulated with a commercial software, HFSS.

## 6.1. SYMMETRIC POSITION OF THE RESONATORS

### 6.1.1. VARIATION OF THE HEIGHT OF THE RESONATORS (S1,C1)

*Table 6-1* shows the dimensions of the filter under study. As in chapter 5, the parameters that stand out in blue are the ones that experience changes.

| | |
|---|---|
| A=22.86 | 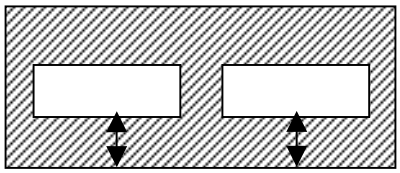 |
| B=10.16 | |
| Lred1=2 | |
| Lred2=2 | |
| Lrid1=Lrid2=15 | |
| T=0.1 | |
| $C1_1$= $C1_2$=0-5 | |
| S1=0.16-10.16 | |

*Table 6-1: Dimensions of the E-Plane filter with two resonators*

*Figure 6-3* presents the S parameters for different values of the height of the resonators in a symmetric position. When the height decreases, the selectivity of the filter is improved. If the height is very thin we obtain a very high level of attenuation at the stopband. As a difference in the case with one resonator, a transmission zero is not obtained in this case with two resonators in a symmetric position.

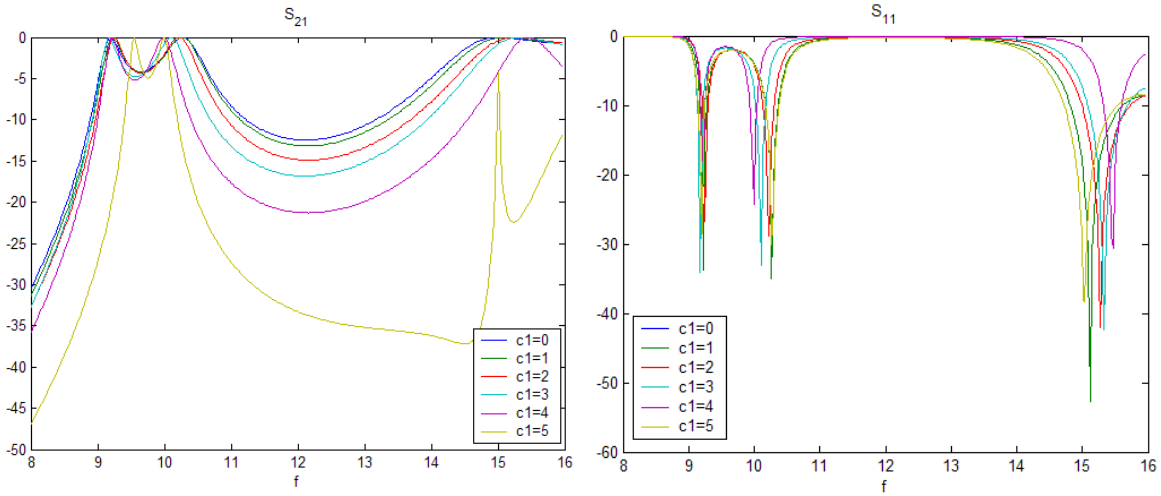


*(a)* *(b)*

*Figure 6-3: $S_{21}$ (a) and $S_{11}$ (b) for different values of c1 in a symmetric case*

### 6.1.2. VARIATION OF THE LENGTH OF THE RESONATORS (LRID1, LRID2)

As in the previous section *Table 6-2* gives the dimensions of the filter under study.

| | |
|---|---|
| A=22.86 | 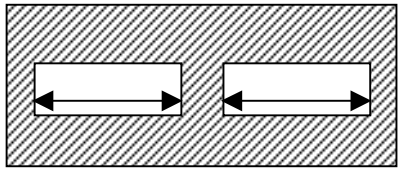 |
| B=10.16 | |
| Lred1=2 | |
| Lred2=2 | |
| Lrid1=Lrid2=13-17 | |
| T=0.1 | |
| C1=4.08 | |
| S1=2 | |

*Table 6-2: Dimensions of the E-Plane filter with two resonators*

*Figure 6-4* shows the S parameters for different values of the length of the resonators. Hence, when Lrid increases, the central frequency decreases and the selectivity is improved.

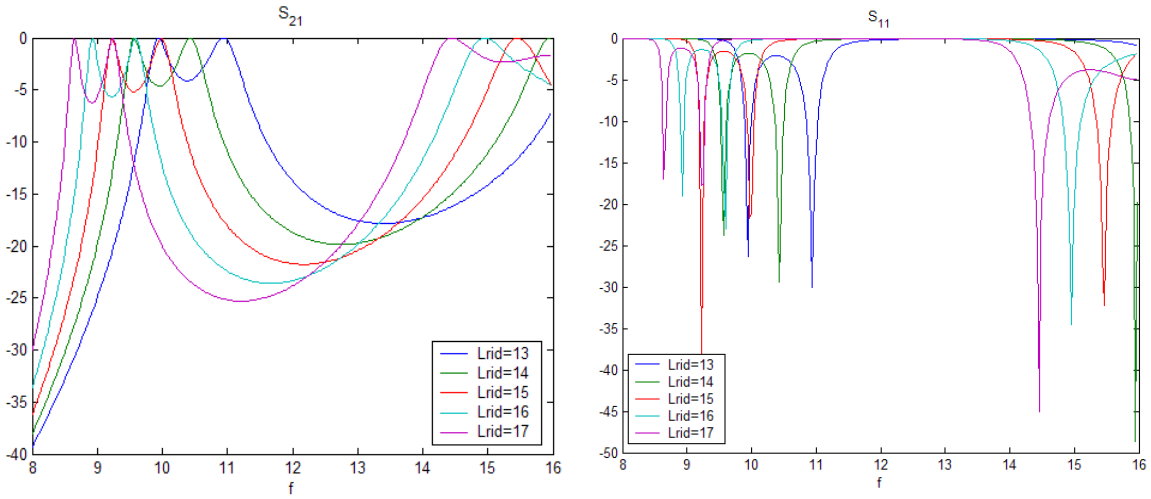


*(a)* *(b)*

*Figure 6-4: $S_{21}$ (a) and $S_{11}$ (b) for different values of Lrid in a symmetric case*

### 6.1.3. VARIATION OF THE LENGTH OF THE FIRST METAL INSERTS (LRED1)

*Table 6-3* presents the dimensions of the filter under study.

| | |
|---|---|
| A=22.86 | 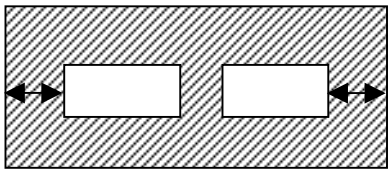 |
| B=10.16 | |
| Lred1=1-6 | |
| Lred2=2 | |
| Lrid1=Lrid2=15 | |
| T=0.1 | |
| C1=4.08 | |
| S1=2 | |

*Table 6-3: Dimensions of the E-Plane filter with two resonators*

*Figure 6-5* shows the S parameters for different values of the length of the external metal inserts. When Lred1 increases, the selectivity is improved because the coupling is weaker.

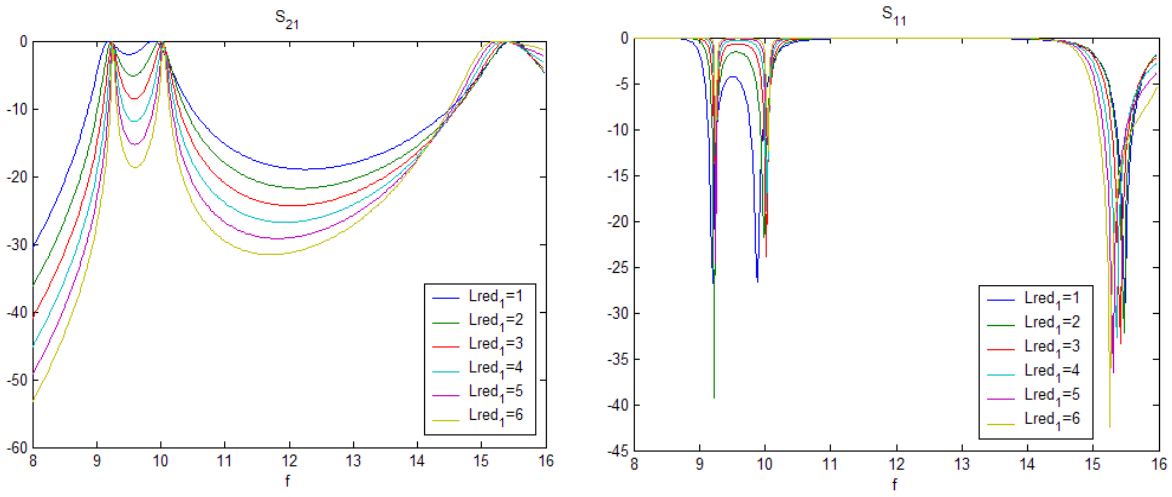


*(a)* *(b)*

*Figure 6-5: $S_{21}$ (a) and $S_{11}$ (b) for different values of Lred1 in a symmetric case*

### 6.1.4. VARIATION OF THE LENGTH OF THE SECOND METAL INSERT (LRED2)

The dimensions of the filter under study are given in *Table6-4*.

| | |
|---|---|
| A=22.86 | 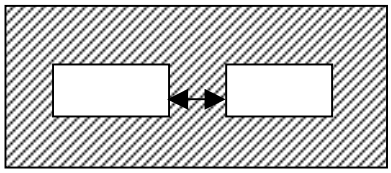 |
| B=10.16 | |
| Lred1=2 | |
| Lred2=1-6 | |
| Lrid1=Lrid2=15 | |
| T=0.1 | |
| C1=4.08 | |
| S1=2 | |

*Table 6-4: Dimensions of the E-Plane filter with two resonators*

*Figure 6-6* presents the S parameters for different values of the length of the internal metal insert. When Lred2 increases, the response is more selective because the discontinuity is more reflective and the coupling between the resonators is weaker.

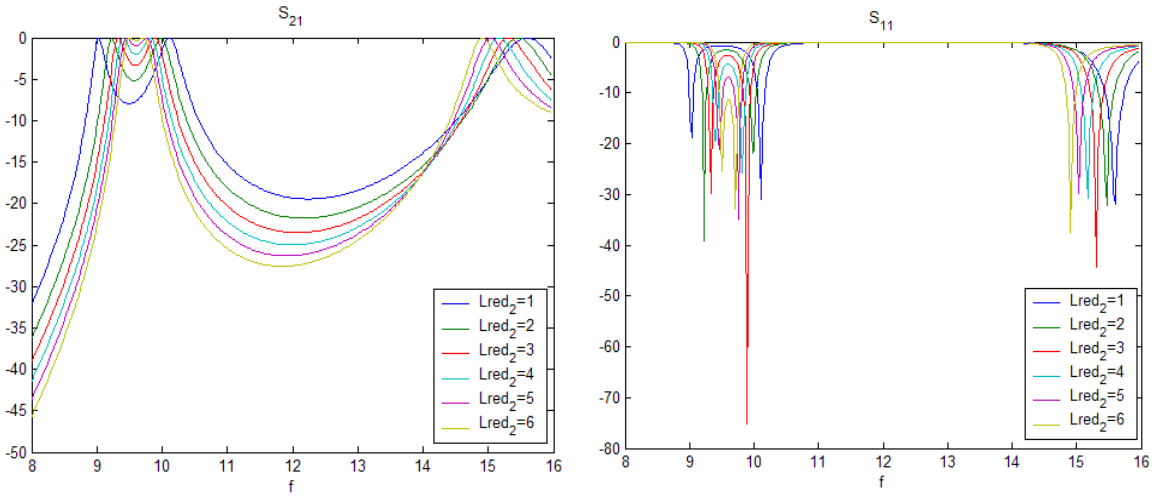


*(a)* *(b)*

*Figure 6-6: $S_{21}$ (a) and $S_{11}$ (b) for different values of $Lred_2$ in a symmetric case*

## 6.2. ASYMMETRIC POSITION OF THE RESONATORS

### 6.2.1. VARIATION OF THE POSITION OF THE RESONATORS ($C1_1$=$C1_2$) WITH A FIXED HEIGHT

*Table 6-5* gives the dimensions of the filter under study, where the height of the resonators is fixed to 2 mm.

| | |
|---|---|
| A=22.86 | 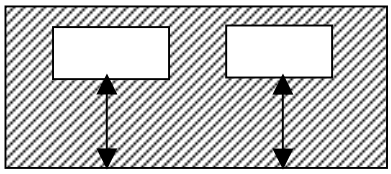 |
| B=10.16 | |
| $Lred_1$=2 | |
| $Lred_2$=2 | |
| $Lrid_1$=$Lrid_2$=15 | |
| T=0.1 | |
| $C1_1$= $C1_2$=0-4 | |
| S1=2 | |

*Table 6-5: Dimensions of the E-Plane filter with two resonators*

*Figure 6-7* shows the S parameters for different values of the position of the resonators, keeping the same value for both resonators. When the resonators are far for the central position, the central frequency is lower and the level of attenuation is higher at the stopband.

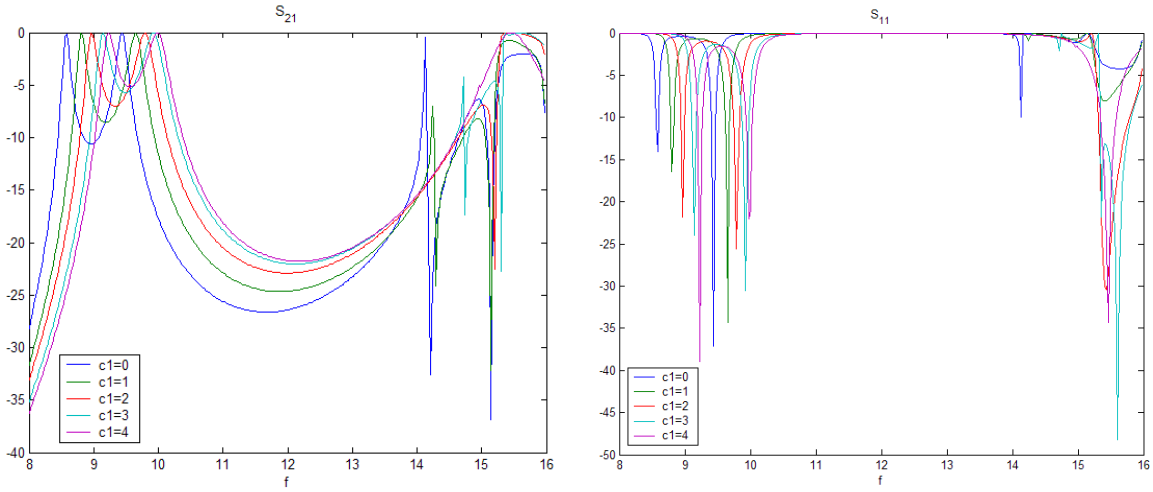


*(a)* *(b)*

*Figure 6-7: $S_{21}$ (a) and $S_{11}$ (b) for different values of c1 in an asymmetric case*

### 6.2.2. VARIATION OF THE POSITION OF THE RESONATORS ($C1_1 \neq C1_2$) WITH A FIXED HEIGHT

As in the previous section *Table 6-6* introduces the dimensions of the filter under study, where the height of the resonator is fixed to 2 mm. The difference is that in this case the values of the position of the resonators change in an opposite way.

| |
|---|
| A=22.86 |
| B=10.16 |
| $Lred_1$=2 |
| $Lred_2$=2 |
| $Lrid_1$=$Lrid_2$=15 |
| T=0.1 |
| $C1_1$=0-4 |
| $C1_2$=B-$C1_1$-S1 |
| S1=2 |

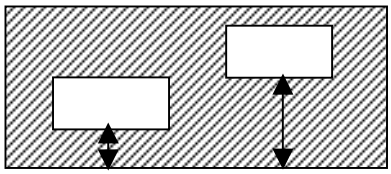

*Table 6-6: Dimensions of the E-Plane filter with two resonators*

When the resonators are far for the central position, the selectivity is improved and the central frequency is lower, as it is shown in *Figure 6-8*. The main difference with respect to the previous section is that in this case a transmission zero appears at finite frequencies. In addition, when the resonators are close to the up and bottom walls of the guide, the transmission zero goes closer to the passband obtaining a better response due to it is more selective.

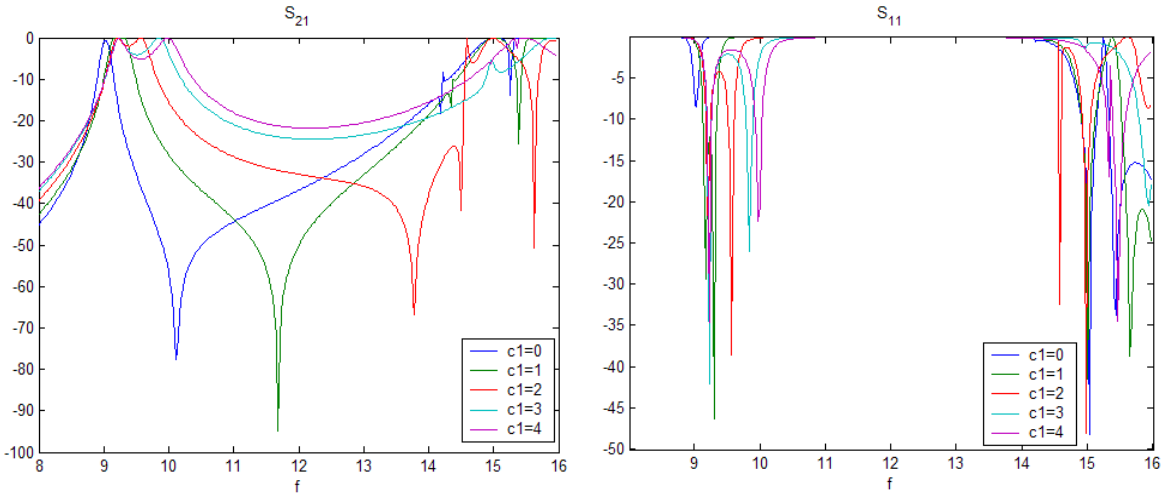


*(a)* *(b)*

*Figure 6-8: $S_{21}$ (a) and $S_{11}$ (b) for different values of c1 in an asymmetric case*

### 6.2.3. VARIATION OF THE HEIGHT OF THE RESONATORS (S1) WITH A FIXED POSITION ($C1_1$=$C1_2$)

The dimensions of the filter are shown in *Table 6-7*.

| | |
|---|---|
| A=22.86 | 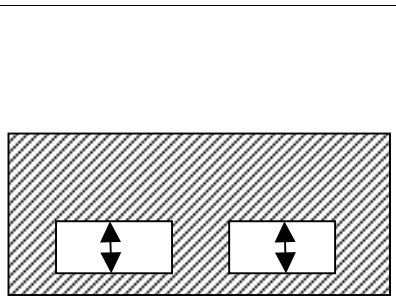 |
| B=10.16 | |
| $Lred_1$=2 | |
| $Lred_2$=2 | |
| $Lrid_1$=$Lrid_2$=15 | |
| T=0.1 | |
| $C1_1$= $C1_2$=1 | |
| S1=1-9 | |

*Table 6-7: Dimensions of the E-Plane filter with two resonators*

*Figure 6-9* shows the S parameters for different values of the height of the resonators when they are in the same asymmetric position. When the value of the height is small, the selectivity is improved, the central frequency is lower and a high level of attenuation at the stopband is obtained. As in section 6.2.1 a transmission zero is not obtained because the resonator are positioned in the same level.

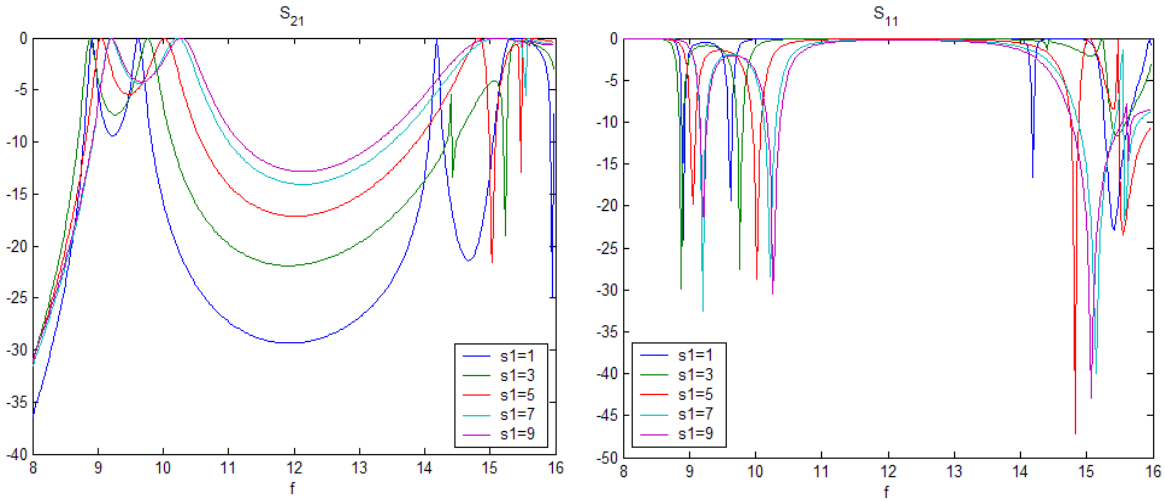


*(a)* *(b)*

*Figure 6-9: $S_{21}$ (a) and $S_{11}$ (b) for different values of the height of the resonators in an asymmetric case*

### 6.2.4. VARIATION OF THE HEIGHT OF THE RESONATORS (S1) WITH A FIXED POSITION ($C1_1 \neq C1_2$)

*Table 6-8* gives the dimensions of the filter under study, where the resonators are placed in the opposite asymmetric position.

| |
|---|
| A=22.86 |
| B=10.16 |
| $Lred_1$=2 |
| $Lred_2$=2 |
| $Lrid_1=Lrid_2$=15 |
| T=0.1 |
| $C1_1$= 1 |
| $C1_2$=B- $C1_1$-S1 |
| S1=1-9 |

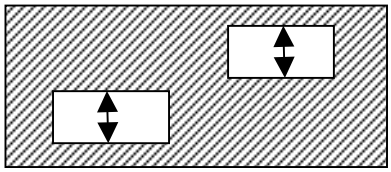

*Table 6-8: Dimensions of the E-Plane filter with two resonators*

The S parameters for different values of the height of the resonators are shown in *Figure 6-10*. When the value of the height is small (the distance between the resonator is higher), similar conclusions than in section 6.2.2 can be made. The selectivity is improved, the central frequency is lower and we can obtain a transmission zero at lower frequencies.

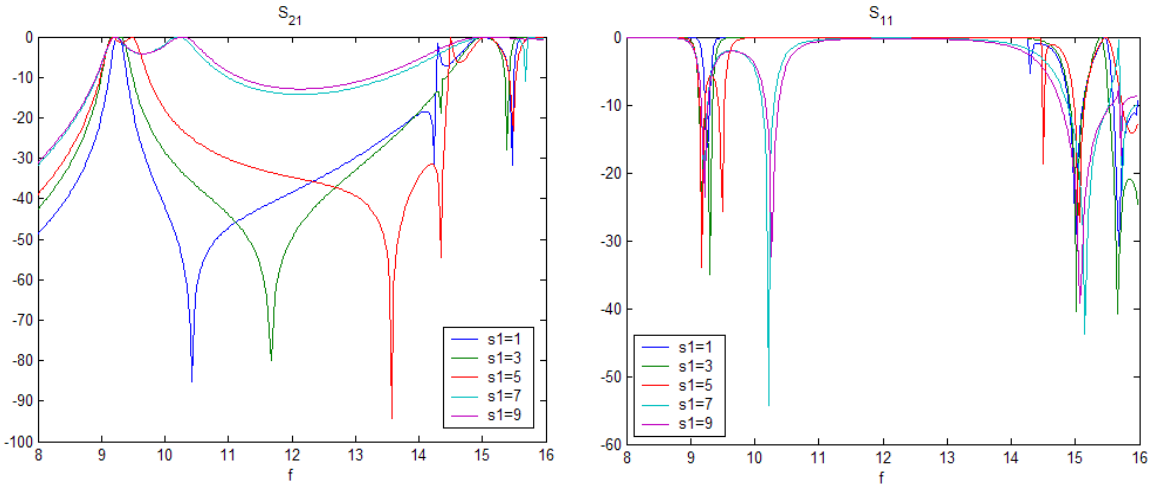


*(a)* *(b)*

*Figure 6-10: $S_{21}$ (a) and $S_{11}$ (b) for different values of the height of the resonators in an asymmetric case*

### 6.2.5. VARIATION OF THE LENGTH OF THE SECOND METAL INSERT (LRED2) WHEN $C1_1$=$C1_2$

As in other sections *Table 6-9* shows the dimensions of the filter under study, where the two resonator are in the same position with a fixed height equal to 2 mm.

| | |
|---|---|
| A=22.86 | 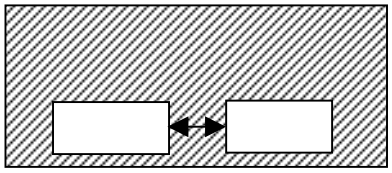 |
| B=10.16 | |
| $Lred_1$=2 | |
| $Lred_2$=1-6 | |
| $Lrid_1$=$Lrid_2$=15 | |
| T=0.1 | |
| $C1_1$= $C1_2$= 1 | |
| S1=2 | |

*Table 6-9: Dimensions of the E-Plane filter with two resonators*

*Figure 6-11* presents the S parameters for different values of the central metal insert when the resonators are in the same asymmetric position. The main difference is that the bandwidth is smaller when $Lred_2$ increases due to the coupling is weaker, keeping the same central frequency and the attenuation at the stopband increases, therefore, the selectivity is improved.

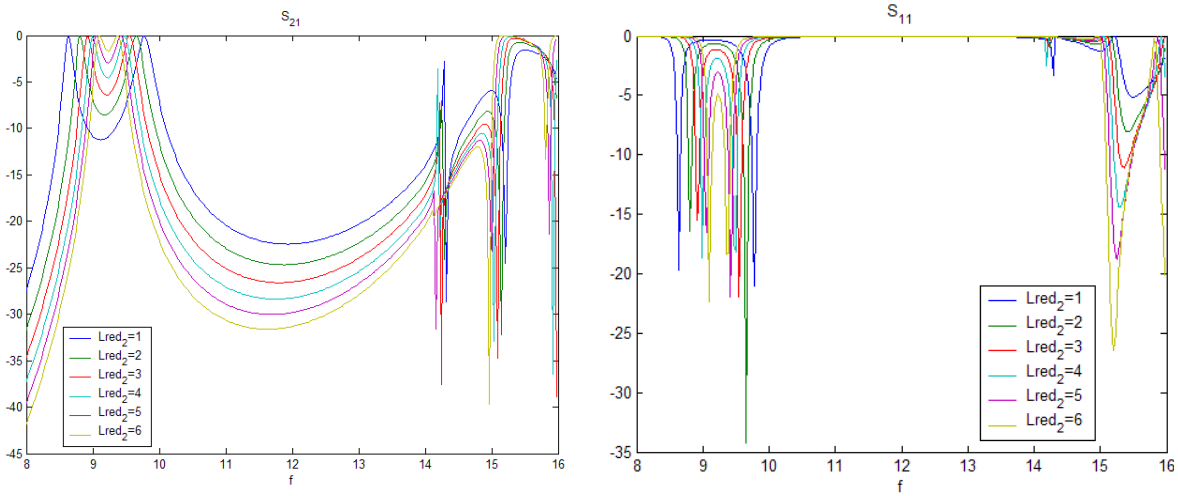


*(a)* *(b)*

*Figure 6-11: $S_{21}$ (a) and $S_{11}$ (b) for different values of the central metal insert*

### 6.2.6. VARIATION OF THE LENGTH OF THE SECOND METAL INSERT (LRED2) WHEN $C1_1 \neq C1_2$

*Table 6-10* gives the dimensions of the filter under study, where the resonators are placed in the opposite asymmetric position with a fixed height equal to 2 mm.

| | |
|---|---|
| A=22.86 | 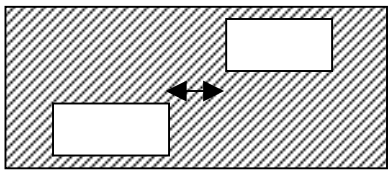 |
| B=10.16 | |
| $Lred_1$=2 | |
| $Lred_2$=1-6 | |
| $Lrid_1$=$Lrid_2$=15 | |
| T=0.1 | |
| $C1_1$= 1 | |
| $C1_2$= 7.16 | |
| S1=2 | |

*Table 6-10: Dimensions of the E-Plane filter with two resonators*

The S parameters for different values of the central metal insert when the resonators are in the opposite asymmetric position are represented in *Figure 6-12*. The differences in the passband are not very relevant. The only thing that can be stand out is that the transmission zero is moved to lower frequencies when the central metal insert is thinner. Precisely, this effect is the one that we are interested in, because we are looking for a selective response with a transmission zero close to the passband.

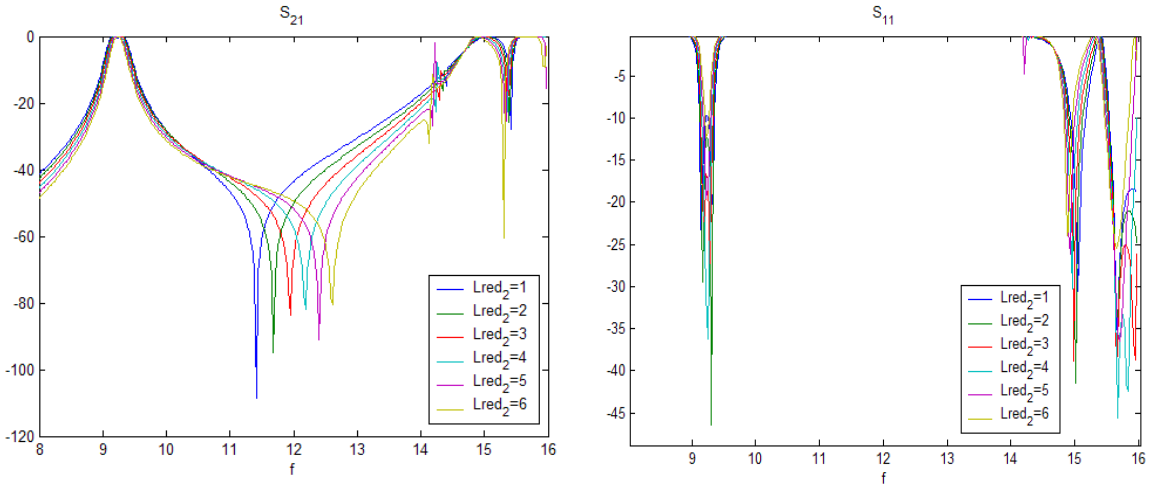


*(a)* *(b)*

*Figure 6-12: $S_{21}$ (a) and $S_{11}$ (b) for different values of the central metal insert*

## 6.3. CONCLUSIONS

First of all, as it was explained in section 5.3, in the asymmetric case the studies changing the length of the first metal inserts and the length of the resonators have not been represented because similar behaviour was found for both cases.

Secondly, looking all the results obtained for the moment, the changes that the response of the filter suffers with respect all the parameters are known at this time. Moreover it can be said that we have now tools to obtain the kind of response that is needed.

In this project, one of the objectives is to obtain a response with a transmission zero close to the passband to improve the selectivity. For this reason, after fixing the passband changing the value of the length of the resonators, the rest of the parameters can be chosen to get the required response.

After analyse sections 6.2.2, 6.2.4 and 6.2.6, this type of response was found and some remarks can be made:

- The resonators must be placed in opposite positions close to the up and bottom walls of the guide.
- The height of the resonators should be thin
- The length of the central metal insert must be short.

Following these points we will be able to obtain a filter with a high selectivity and with a transmission zero close to the passband due to the coupling is weaker between the resonators.

## 6.4. COUPLING COEFFICIENT

The K coefficient between two resonators at synchronous topologies is defined as:

$$K = \frac{\left(f_2^{\,2} - f_1^{\,2}\right)}{\left(f_2^{\,2} + f_1^{\,2}\right)}$$

Where $f_1$ and $f_2$ are the resonance frequencies of each resonators as it is shown in *Figure 6-13*.

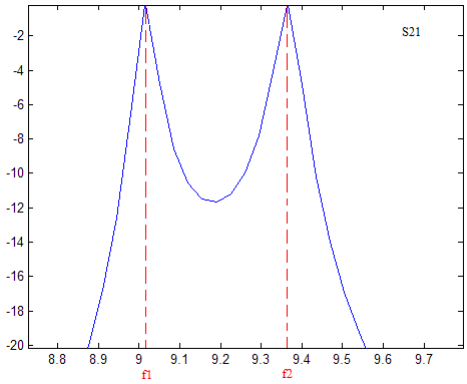


*Figure 6-13: Resonance frequiencies*

The value of the coupling coefficient has been studied for a filter with two resonators changing their positions and the length of the second metal insert. The used dimensions are given in *Table 6-11*.

| | |
|---|---|
| A=22.86 | 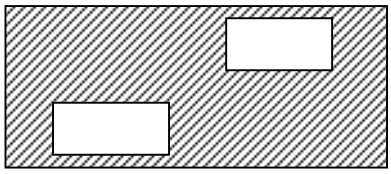 |
| B=10.16 | |
| $Lred_1$=5 | |
| $Lred_2$=1-5 | |
| $Lrid_1$=$Lrid_2$=15.56 | |
| T=0.1 | |
| $C1_1$= 0-4 | |
| $C1_2$= 4-8 | |
| S1=2.16 | |

*Table 6-11: Dimensions of the E-Plane filter with two resonators*

The results are presented in *Figure 6-14*. The K coefficient increases when the resonators are close each other, and also when the length of the second metal insert is small. This effect can be observed easily in *Figure 6-14 (c)*.

It is interesting to remark that to carry out the objective of the selectivity improvement the resonators has to be in opposite positions to make the coupling weaker, as it was said before. Moreover, another main objective is to reduce the size of the filter and if we look in *Figure 6-14 (b)* the dependence of K with respect to $Lred_2$ is very small when the resonators are in opposite positions close to the up and bottom walls of the guide. For that reason we can choose a small value for $Lred_2$ and make shorter the filter with that.

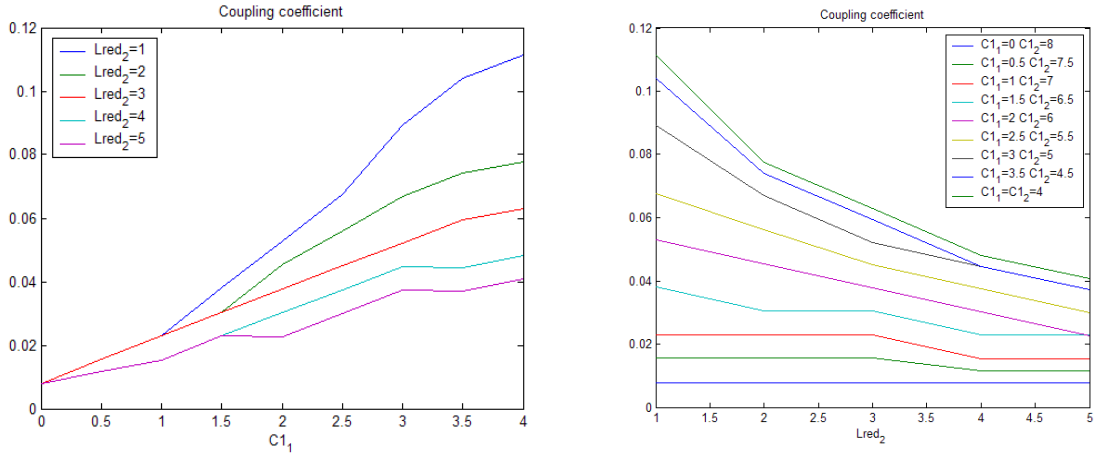


*(a)* *(b)*

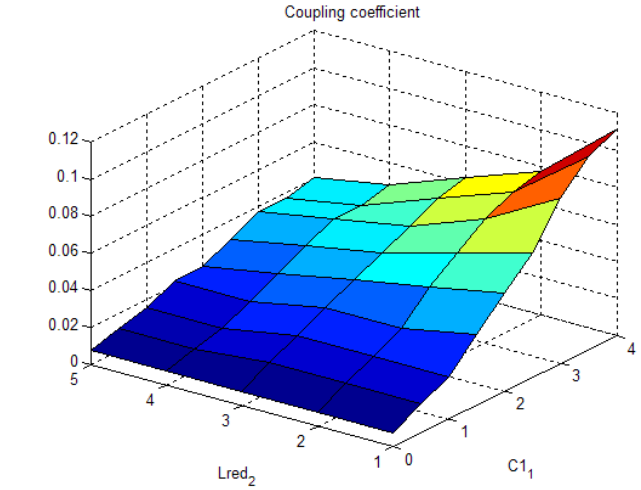


*(c)*

*Figure 6-14: Coupling coefficient vs. $Lred_2$ and c1, 2D (a) and (b), and 3D (c)*

*Figure 6-15* presents the contour lines for the coupling coefficient versus the positions of the resonators and the length of the second metal insert. In this figure, the specific value of K coefficient is exposed for certain values of the parameters $C1_1$, $C1_2$ and $Lred_2$.

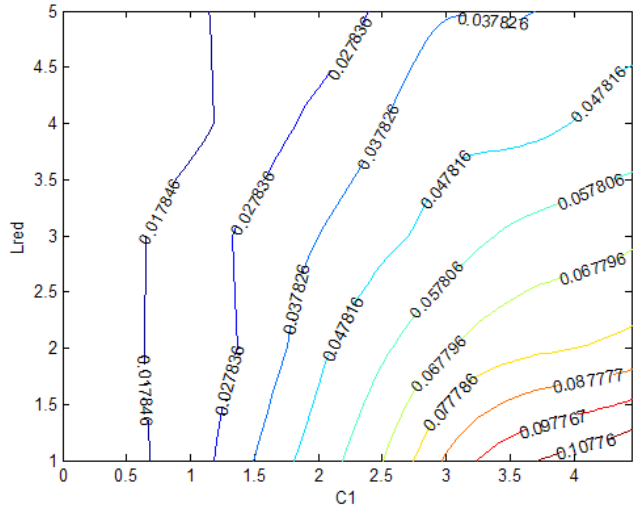


*Figure 6-15: Coupling coefficient contour lines vs. $Lred_2$ and c1*

The knowledge about the behaviour of the K coefficient with respect to the parameters of the structure is important in a future stage when a filter with specific characteristics, as a special coupling coefficient, has to be designed.

## 6.5. VALIDATION OF A FILTER: 9.25-9.75 GHZ PASSBAND

*Table 6-12* shows the parameters and the response of the prototype in [2-10].

| PROTOTYPE |
|---|
| A=20.86 |
| B=10.16 |
| T=0.1 |
| Ripple=0.5 |
| $Lred_1$=2.18800010322593 |
| $Lred_2$=6.85999984666705 |
| $L_1$=$L_2$=16.0271294973159 |

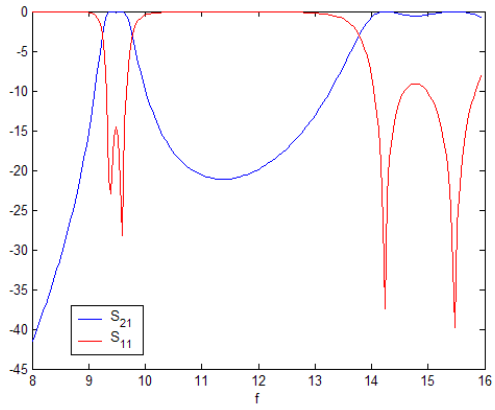


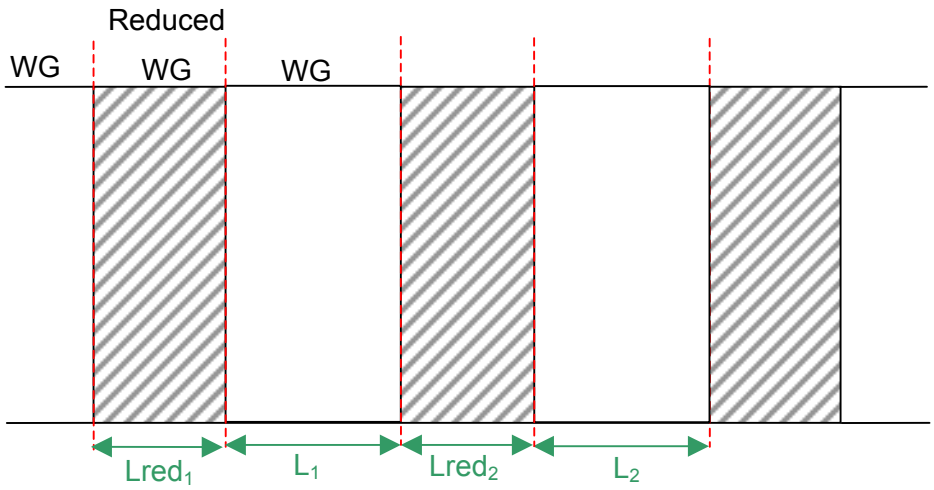


*Table 6-12: Dimensions of the prototype with two resonator*

The values of A, B and T for the filter will be the same than for the prototype.

To validate this filter we are going to keep the values for $Lred_1$=1.6, Lrid ($L_1$ and $L_2$)=14.2, $C1_1$=1 ($C1_2$=8.16) and S1=1 used in one resonator filter, but now we have to choose the value for $Lred_2$ to get a similar response to the prototype.

*Figure 6-16* shows the response for different values of $Lred_2$. Good results have been obtained when $Lred_2$ decreases due to the selectivity is improved because of the

transmission zero is obtained close to the passband, although the bandwidth is a little bit wider. The selected value is $Lred_2$=1.

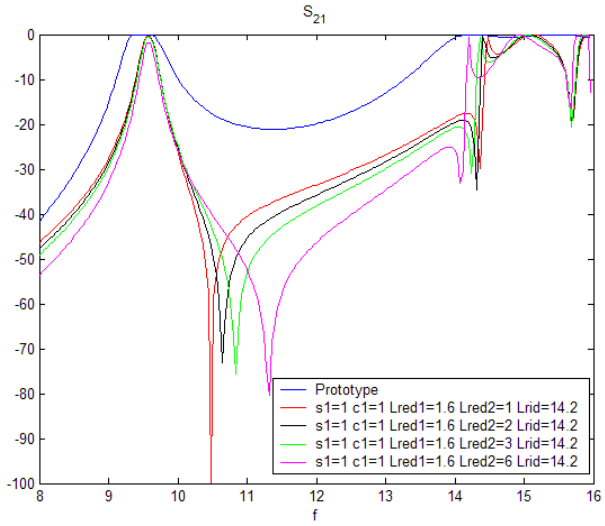


*Figure 6-16: $S_{21}$ for the prototype and different values of Lred2*

As it is presented in *Figure 6-16* the response is not very similar to the prototype, so we are going to modify the rest of the parameters to obtain a similar response.

In *Figure 6-17* is shown the response of the filter for different values of S1. We can notice that if S1 increases the response is less selective , increasing the bandwidth. Due to that, for S1=2 a more similar response is obtained.

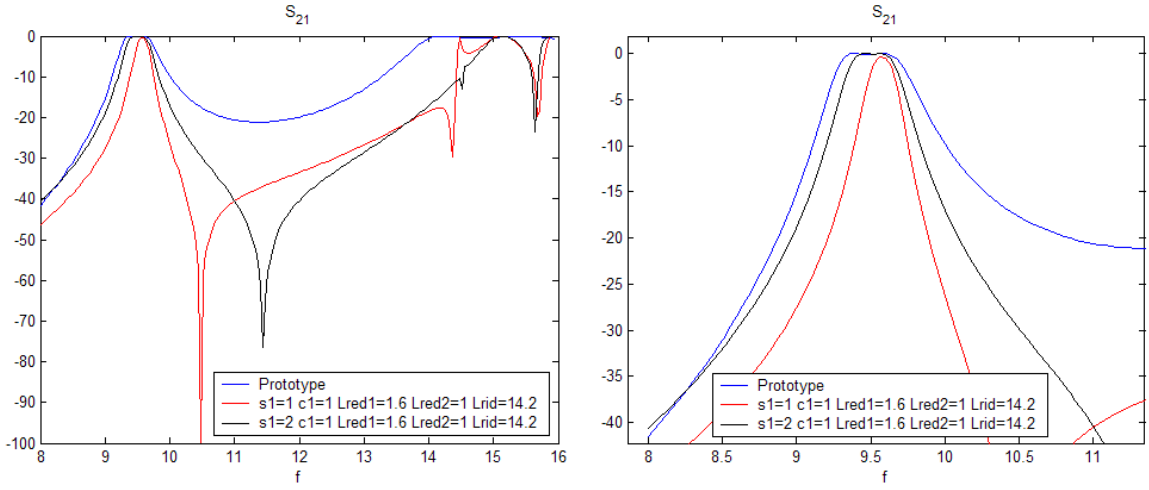


*(a)* *(b)*

*Figure 6-17: $S_{21}$ for different values of S1 (a), and a zoom of it in the passband(b)*

*Figure 6-18* shows the response for different values of C1. When C1 increases the bandwidth is bigger and the selectivity decreases. As it is shown, the best value of C1 is 1mm, because the response is selective and similar to the prototype.

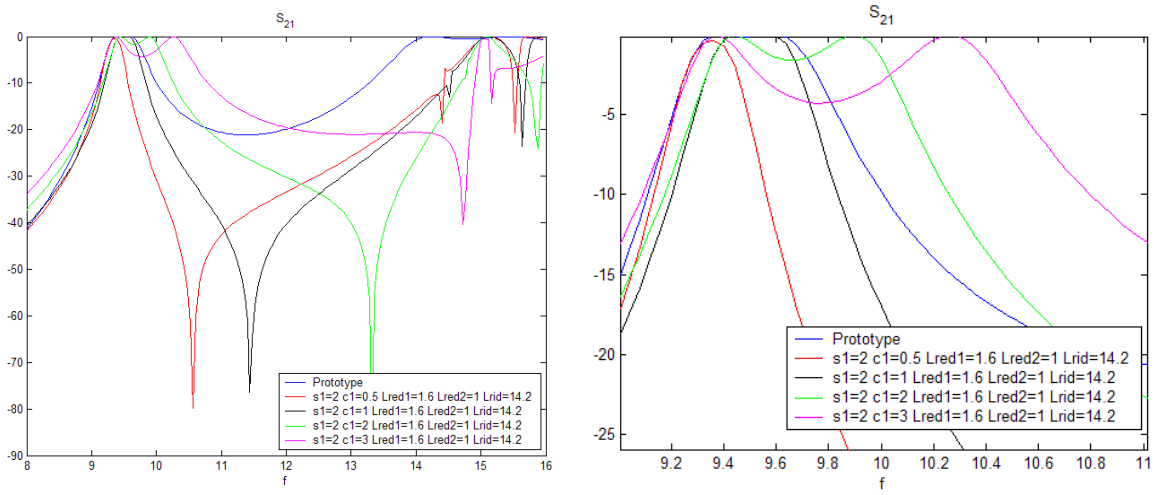


(a) (b)

*Figure 6-18: $S_{21}$ for different values of C1 (a), and a zoom of it in the passband(b)*

As a conclusion, the dimensions of the filter that has been made are given in *Table 6-13.*

| RWG FILTER | PROTOTYPE |
|---|---|
| S1=2 | |
| $C1_1$=1 ($C1_2$=7.16) | |
| Lred1=1.6 | Lred1=2.18800010322593 |
| Lred2=1 | Lred2= 6.85999984666705 |
| Lrid=14.2 | L=16.0271294973159 |

*Table 6-13: Dimensions of the filter and the prototype with two resonators*

Using the parameters of the *Table 6-13* a good response with the same passband than the prototype and with improved selectivity has been achieved, as it is exposed in *Figure 6-19*.

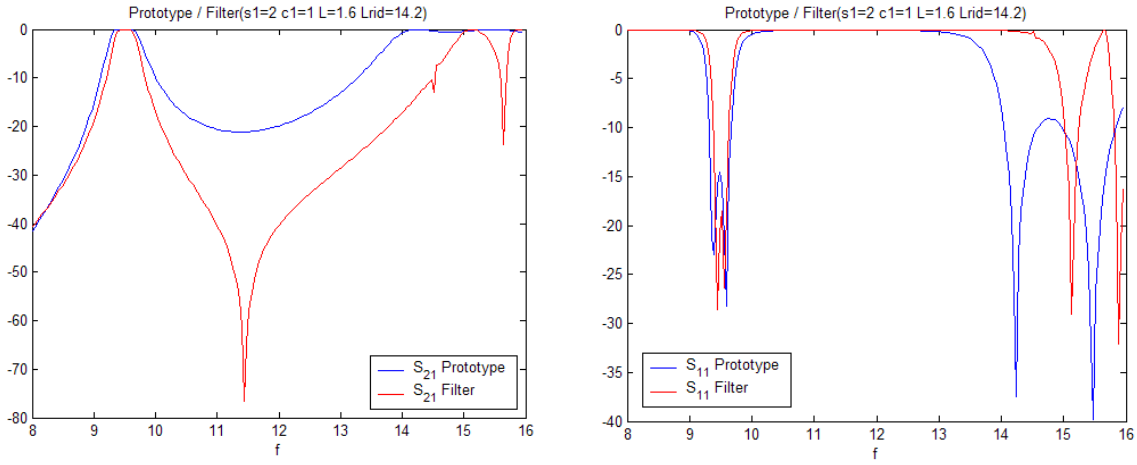


*(a)* *(b)*

*Figure 6-19: $S_{21}$ (a) and $S_{11}$ (b) for the prototype and the final filter*

The validated filter has two important advantages. One of these is that the filter is more selective, due to the high level of attenuation at the stopband and a transmission zero close to the passband. And the second one is that the total length of the filter has been reduced around 8.27mm with respect to the prototype.

| |
|---|
| Prototype length= 25.0751 mm |
| RWG filter length= 16.8000 mm |

The comparison of the response of the filter simulated in HFSS and Fortran is presented in *Figure 6-20*. Good agreement between the two simulations has been obtained.

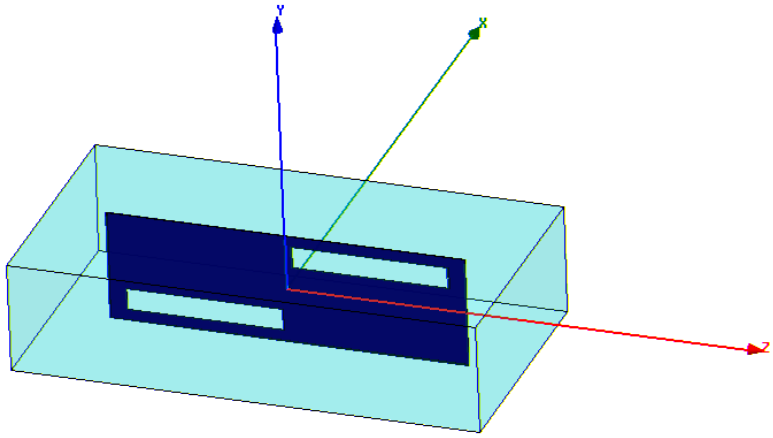


*(a)*

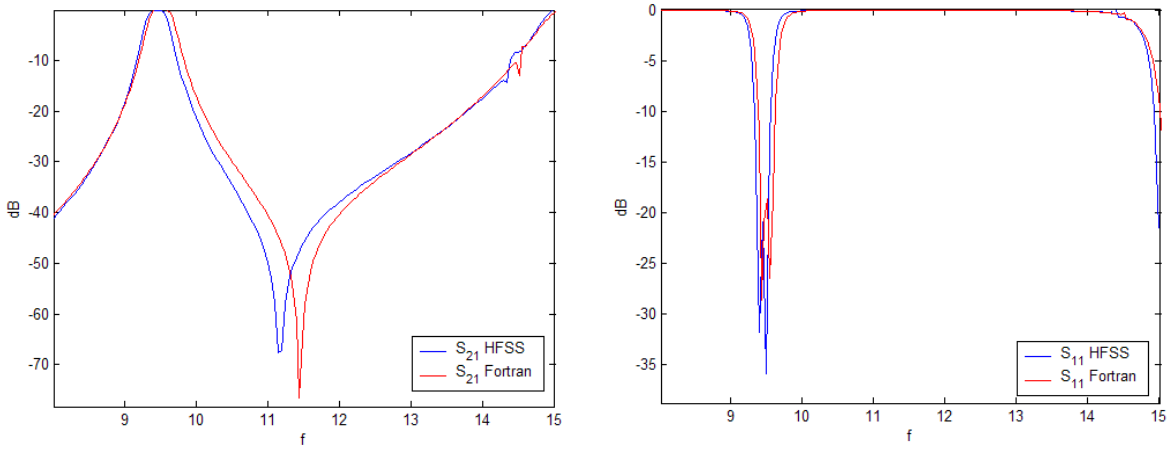


*(b)* *(c)*

*Figure 6-20: Sketch of the filter (a) and comparison of $S_{21}$ (b) and $S_{11}$ (c) obtained with HFSS and Fortran*

As in the previous chapter, the minimum deviations observed in *Figure 6-20* can be due to that HFSS needs more steps to converge to a more accurate response.

If it is compared the time needed to simulate the same filter in Fortran and HFSS on an AMD Athlon(tm) 64, 637 MHz, 1GB RAM, the results are extremely good as it is shown in *Table 6-14*.

| Fortran | HFSS |
|---|---|
| 24 sec. | 2400 sec. (40 min.) |

*Table 6-14: Time comparison*

# 7. ANALYSIS OF FILTERS WITH THREE RESONATORS

In this chapter the variation of the response of a E-Plane filter with three resonators is studied. Varying all the parameters that are shown in *Figure 7-1* we could have a complete analysis of this structures.

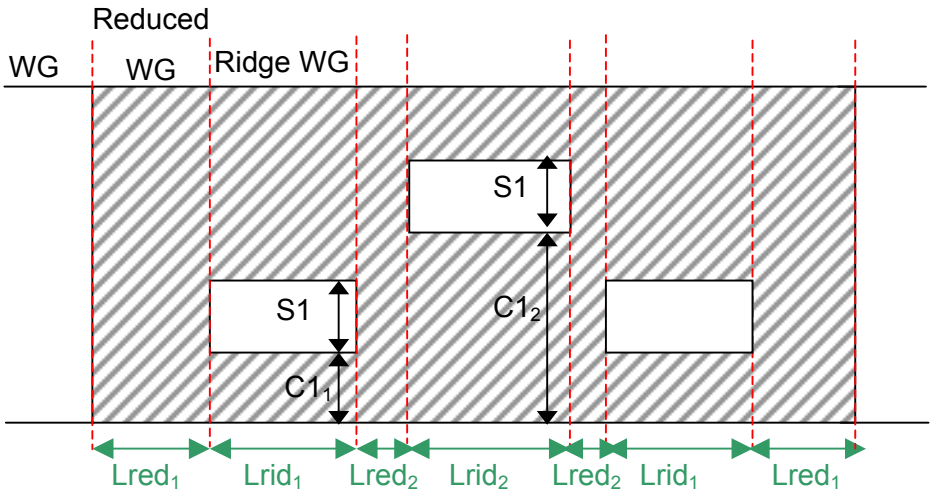


*Figure 7-1: Cross section in the Y-Z plane of a E-Plane Filter with three resonators*

In sections 7.1 and 7.2 a study of the variation of the filter response for a symmetric and asymmetric position of the resonators is presented.

A filter with a passband in 9.25-9.75 GHz is validated in section 7.3 using, in a first instant, the response of a prototype with all metal septa, and in a further stage the response of the same filter simulated with a commercial software, HFSS.

## 7.1. SYMMETRIC POSITION OF THE RESONATORS

### 7.1.1. VARIATION OF THE HEIGHT OF THE RESONATORS (S1, C1)

*Table 7-1* gives the dimensions of the filter under study. As previous chapters, the parameters that stand out in blue are the ones that experience changes.

| | |
|---|---|
| A=22.86 | 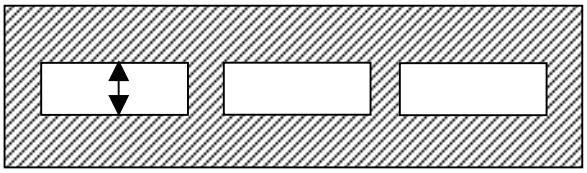 |
| B=10.16 | |
| $Lred_1$=2 | |
| $Lred_2$=2 | |
| $Lrid_1$=$Lrid_2$=15 | |
| T=0.1 | |
| C1=0-5 | |
| S1=0.16-10.16 | |

*Table 7-1: Dimensions of the E-Plane filter with three resonators*

*Figure 7-2* presents the S parameters for different values of the height of the resonators in a symmetric position. When the height decreases, the selectivity of the filter is improved. If the height is very thin we obtain a very high level of attenuation at the stopband. As in the case with one resonator, a transmission zero is obtained at finite frequencies, but it is not located close to the passband.

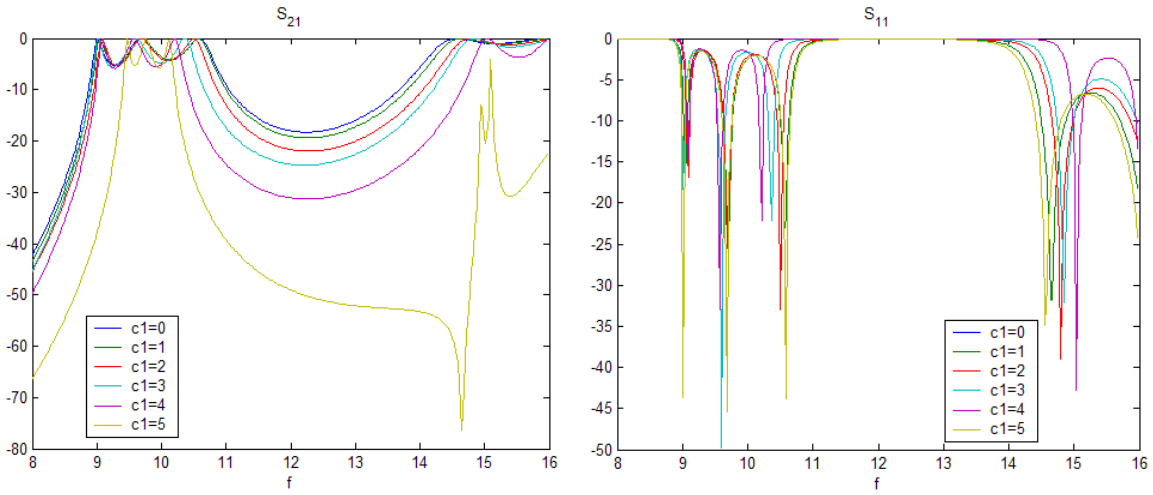


*(a)* *(b)*

*Figure 7-2: $S_{21}$ (a) and $S_{11}$ (b) for different values of c1 in a symmetric case*

### 7.1.2. VARIATION OF THE LENGTH OF THE RESONATORS ($LRID_1$=$LRID_2$)

As in the previous section *Table 7-2* presents the dimensions of the filter under study.

| | |
|---|---|
| A=22.86 | 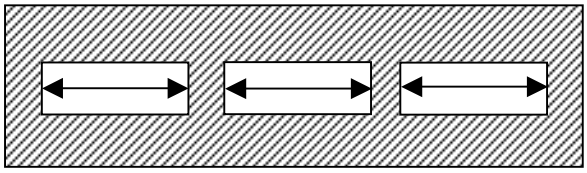 |
| B=10.16 | |
| $Lred_1$=2 | |
| $Lred_2$=2 | |
| $Lrid_1$=$Lrid_2$= 13-17 | |
| T=0.1 | |
| C1=4.08 | |
| S1=2 | |

*Table 7-2: Dimensions of the E-Plane filter with three resonators*

The S parameters for different values of the length of the resonators are shown in *Figure 7-3*. Hence, when Lrid increases, the central frequency decreases and the response is more selective.

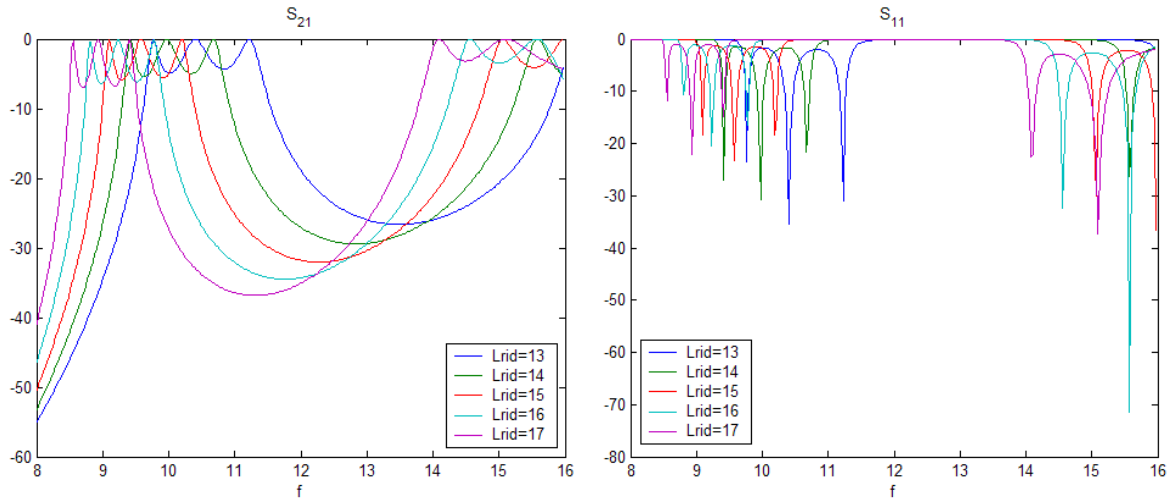


*(a)* *(b)*

*Figure 7-3: $S_{21}$ (a) and $S_{11}$ (b) for different values of Lrid in a symmetric case*

### 7.1.3. VARIATION OF THE LENGTH OF THE FIRST RESONATORS ($LRID_1$)

*Table 7-3* gives the dimensions of the filter under study.

| | |
|---|---|
| A=22.86 | 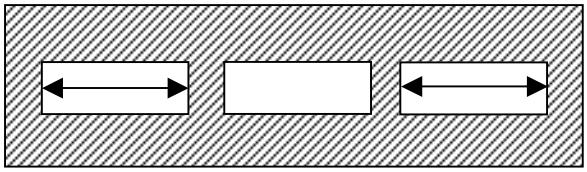 |
| B=10.16 | |
| $Lred_1$=2 | |
| $Lred_2$=2 | |
| $Lrid_1$= 13-17 | |
| $Lrid_2$=15 | |
| T=0.1 | |
| C1=4.08 | |
| S1=2 | |

*Table 7-3: Dimensions of the E-Plane filter with three resonators*

The S parameters for different values of the length of the first and third resonators are shown in *Figure 7-4*. In addition, when $Lrid_1$ is more dissimilar than $Lrid_2$ the ripple presents different shapes. Therefore, the value of the length of the resonators should be similar to each other.

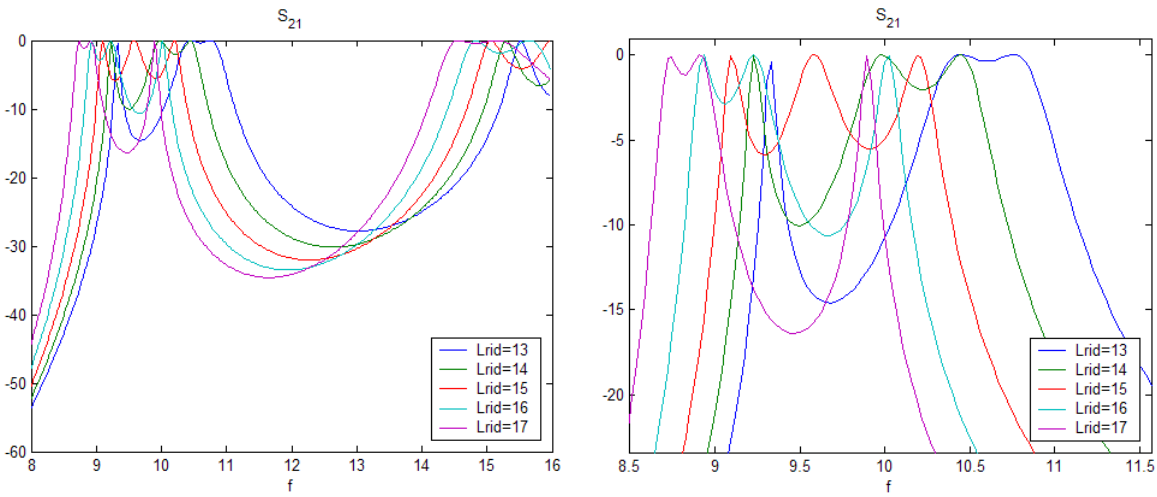


*(a)*

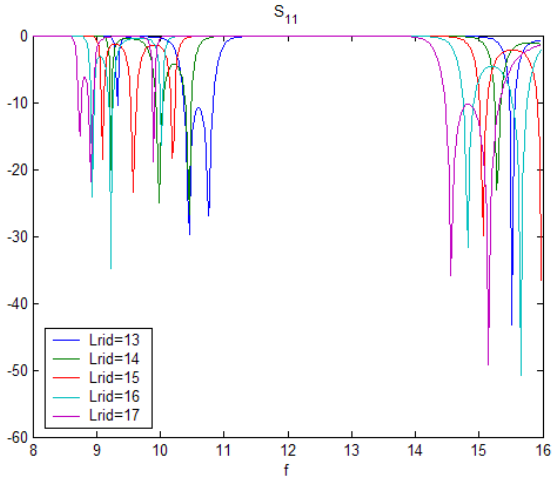


*(b)*

*Figure 7-4: $S_{21}$ (a) and $S_{11}$ (b) for different values of $Lrid_1$ in a symmetric case*

### 7.1.4. VARIATION OF THE LENGTH OF THE SECOND RESONATOR ($LRID_2$)

The dimensions of the filter under study are given in *Table 7-4*.

| | |
|---|---|
| A=22.86 | 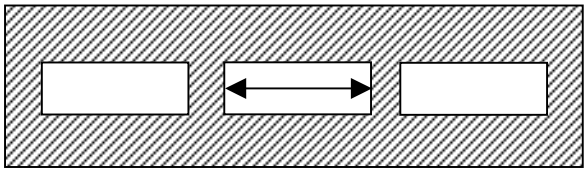 |
| B=10.16 | |
| $Lred_1$=2 | |
| $Lred_2$=2 | |
| $Lrid_1$= 15 | |
| $Lrid_2$=13-17 | |
| T=0.1 | |
| C1=4.08 | |
| S1=2 | |

*Table 7-4: Dimensions of the E-Plane filter with three resonators*

The S parameters for different values of the length of the second resonator are represented in *Figure 7-5*. When $Lrid_2$ is more different than $Lrid_1$ the ripple presents different shapes, as in the previous section 7.1.3.

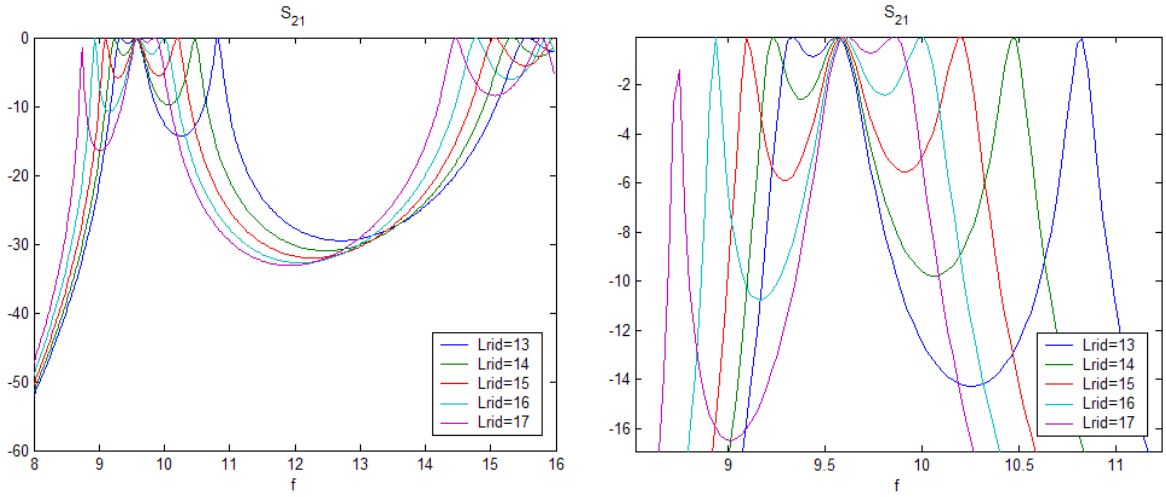


*(a)*

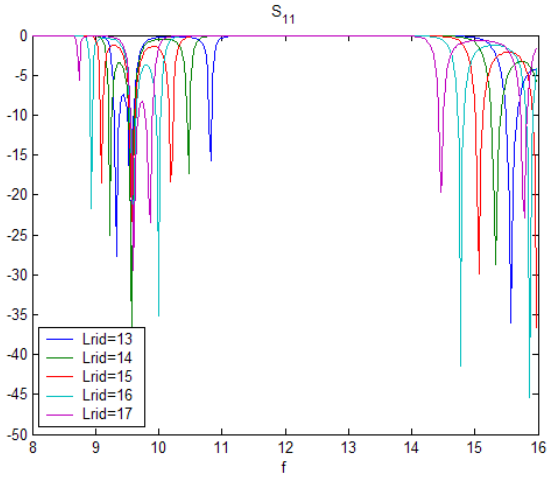


*(b)*

*Figure 7-5: $S_{21}$ (a) and $S_{11}$ (b) for different values of Lrid in a symmetric case*

### 7.1.5. VARIATION OF THE LENGTH OF THE FIRST METAL INSERTS ($LRED_1$)

*Table 7.5* gives the dimensions of the filter and in *Figure 7-6* the S parameters for different values of the length of the external metal inserts are presented. As it is shown in this figure, when $Lred_1$ increases the selectivity is improved because the discontinuity is more reflective and the coupling is weaker.

| | |
|---|---|
| A=22.86 | 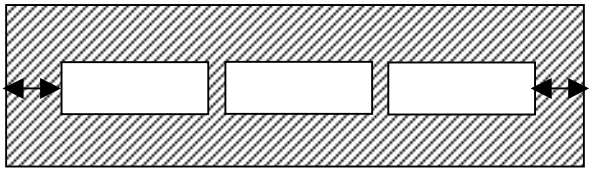 |
| B=10.16 | |
| $Lred_1$=1-6 | |
| $Lred_2$=2 | |
| $Lrid_1$=$Lrid_2$= 15 | |
| T=0.1 | |
| C1=4.08 | |
| S1=2 | |

*Table 7-5: Dimensions of the E-Plane filter with three resonators*

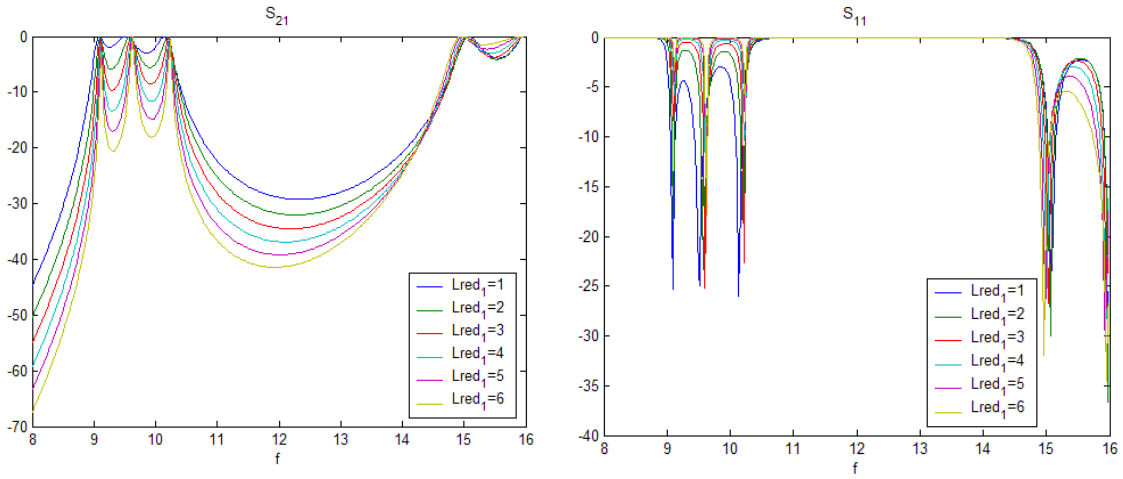


*(a)* *(b)*

*Figure 7-6: $S_{21}$ (a) and $S_{11}$ (b) for different values of $Lred_1$ in a symmetric case*

### 7.1.6. VARIATION OF THE LENGTH OF THE SECOND METAL INSERTS ($LRED_2$)

As in the previous section *Table 7-6* shows the dimensions of the filter under study.

| | |
|---|---|
| A=22.86 | 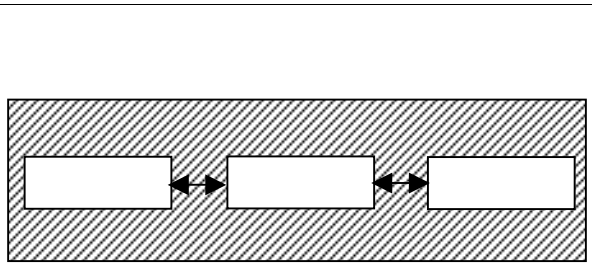 |
| B=10.16 | |
| $Lred_1$=2 | |
| $Lred_2$=1-6 | |
| $Lrid_1$=$Lrid_2$= 15 | |
| T=0.1 | |
| C1=4.08 | |
| S1=2 | |

*Table 7-6: Dimensions of the E-Plane filter with three resonators*

The S parameters for different values of the length of the internal metal inserts are represented in *Figure 7-7*. When $Lred_2$ increases, the response is more selective with a lower bandwidth, due to the coupling is weaker. In this case, the central frequency stay with a constant value.

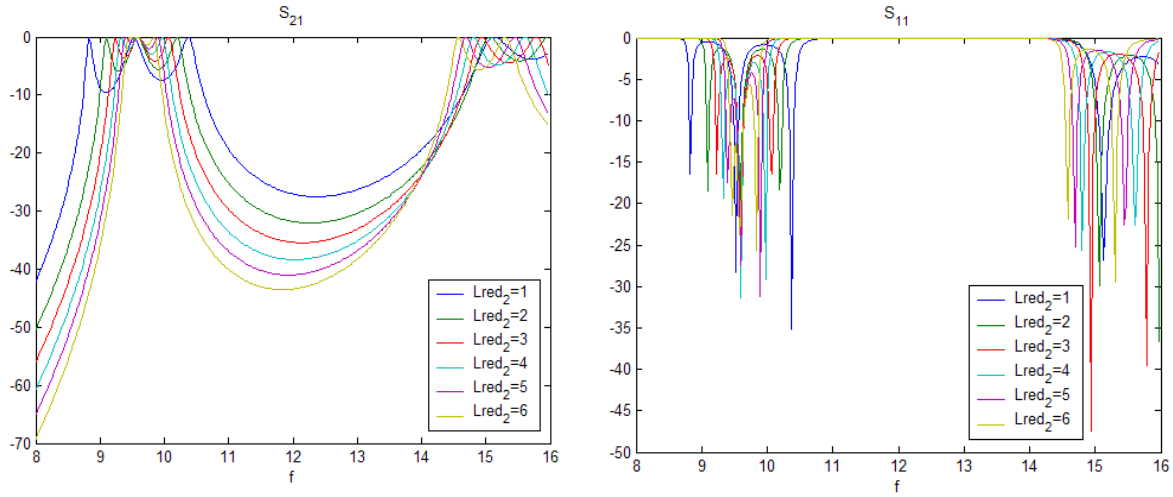


*(a)* *(b)*

*Figure 7-7: $S_{21}$ (a) and $S_{11}$ (b) for different values of $Lred_1$ in a symmetric case*

## 7.2. ASYMMETRIC POSITION OF THE RESONATORS

### 7.2.1. VARIATION OF THE POSITION OF THE RESONATORS ($C1_1$=$C1_2$) WITH A FIXED HEIGHT

*Table 7-7* shows the dimensions of the filter under study, where the height of the resonators is fixed to 2 mm.

| | |
|---|---|
| A=22.86 | 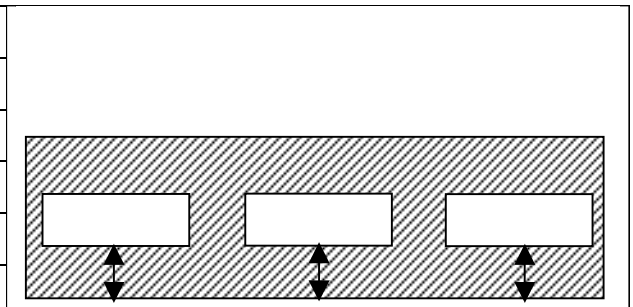 |
| B=10.16 | |
| $Lred_1$=2 | |
| $Lred_2$=2 | |
| $Lrid_1$=$Lrid_2$=15 | |
| T=0.1 | |
| $C1_1$= $C1_2$=0-4 | |
| S1=2 | |

*Table 7-7: Dimensions of the E-Plane filter with three resonators*

*Figure 7-8* presents the S parameters for different values of the position of the resonators, keeping the same value for all the resonators. When the resonators are far for the central position, the central frequency is lower, the level of losses is higher at the stopband. Furthermore, transmission zeros have been obtained in the extreme cases against to the filter with two resonator studied in section 6.2.1.

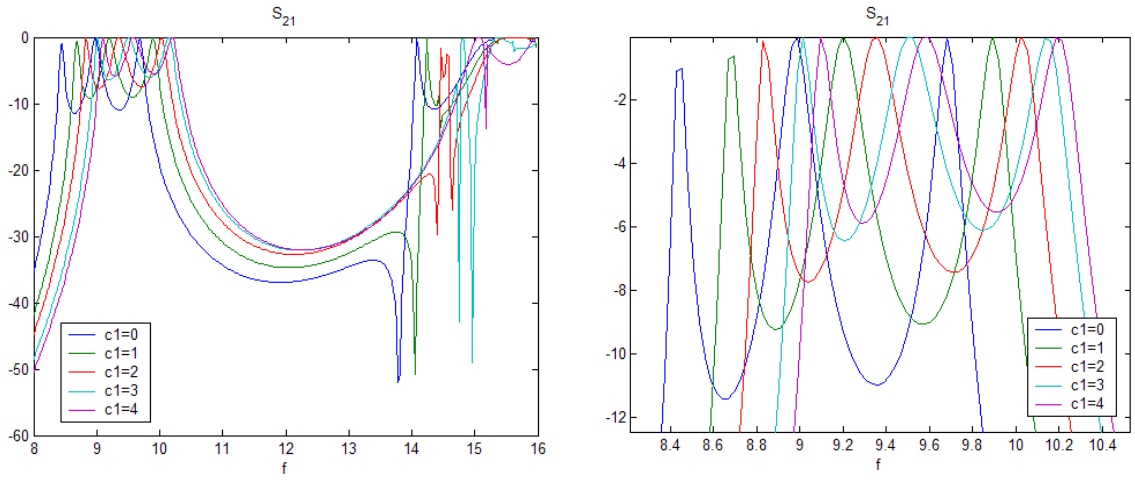


*(a)*

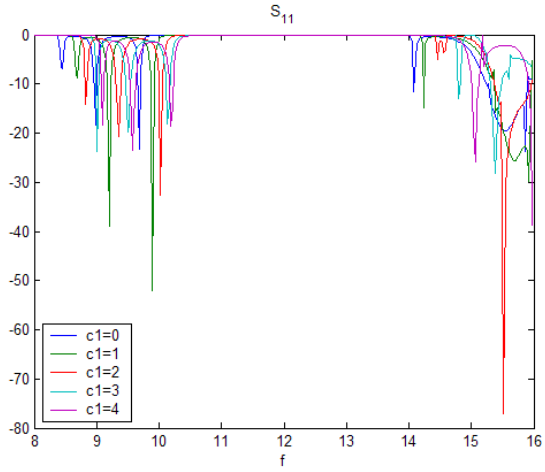


*(b)*

*Figure 7-8: $S_{21}$ (a) and $S_{11}$ (b) for different values of c1 in an asymmetric case*

### 7.2.2. VARIATION OF THE POSITION OF THE RESONATORS ($C1_1 \neq C1_2$) WITH A FIXED HEIGHT

As in the previous section *Table 7-8* gives the dimensions of the filter under study, where the height of the resonator is fixed to 2 mm. The difference is that in this case the values of the position of the resonators change in an opposite way.

| | |
|---|---|
| A=22.86 | 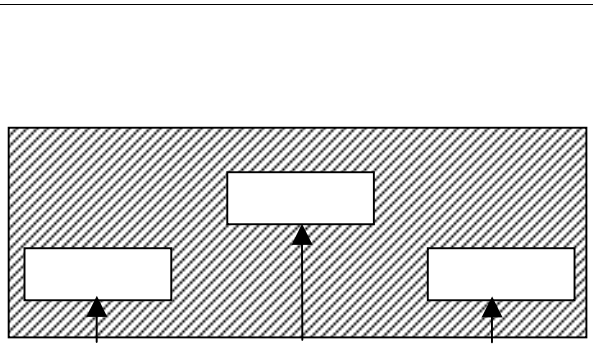 |
| B=10.16 | |
| $Lred_1$=2 | |
| $Lred_2$=2 | |
| $Lrid_1$=$Lrid_2$=15 | |
| T=0.1 | |
| $C1_1$=0-4 | |
| $C1_2$=B-$C1_1$-S1 | |
| S1=2 | |

*Table 7-8: Dimensions of the E-Plane filter with three resonators*

If *Figure 7-9* is analysed similar comments to section 6.2.2 can be made in this section. If *Figure 7-9* is compare with *Figure 6-7* it is appreciated that the responses obtained with three resonators are more selective than using two resonators.

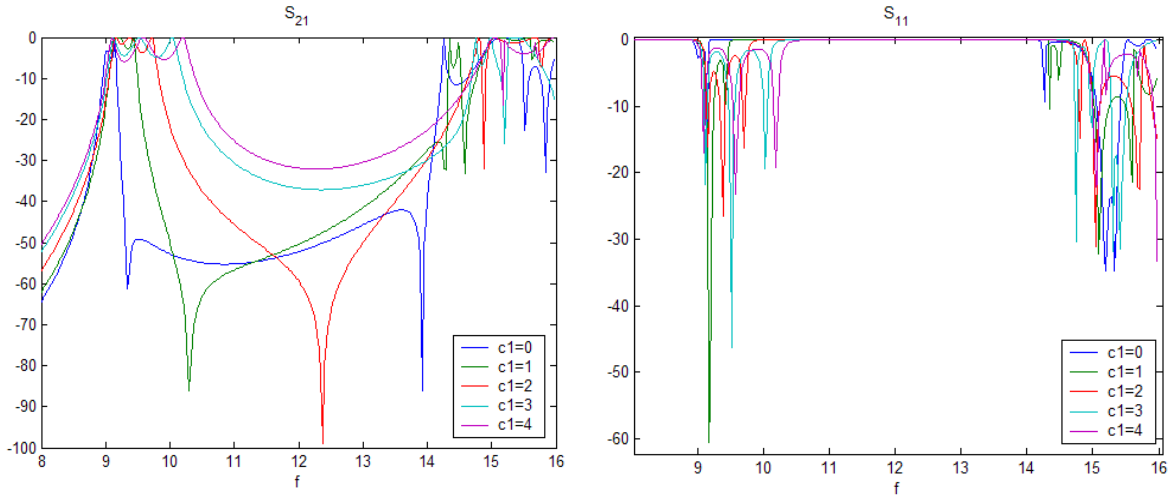


*(a)* *(b)*

*Figure 7-9: $S_{21}$ (a) and $S_{11}$ (b) for different values of c1 in an asymmetric case*

### 7.2.3. VARIATION OF THE HEIGHT OF THE RESONATORS (S1) WITH A FIXED POSITION ($C1_1$=$C1_2$)

The dimensions of the filter are given in *Table 7-9*.

| | |
|---|---|
| A=22.86 | 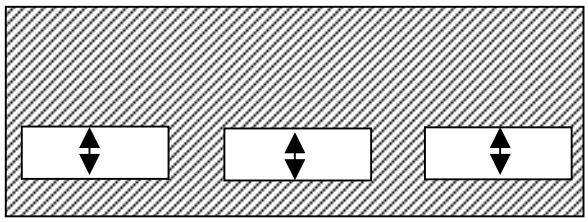 |
| B=10.16 | |
| $Lred_1$=2 | |
| $Lred_2$=2 | |
| $Lrid_1$=$Lrid_2$=15 | |
| T=0.1 | |
| $C1_1$= $C1_2$=1 | |
| S1=1-9 | |

*Table 7-9: Dimensions of the E-Plane filter with three resonators*

*Figure 7-10* shows the S parameters for different values of the height of the resonators when they are in the same asymmetric position. When the value of the height is small, the selectivity is improved, the central frequency is lower and a transmission zero appears. If *Figure 7-10* is compared with *Figure 6-8*, the main difference is that the transmission zero is obtained using three resonators instead two for a small value of the height.

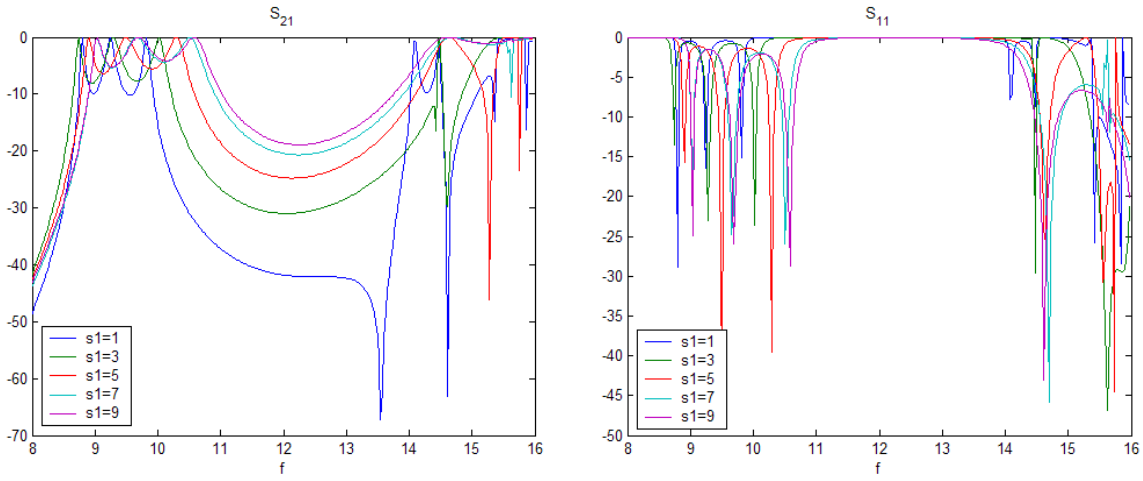


*(a)* *(b)*

*Figure 7-10: $S_{21}$ (a) and $S_{11}$ (b) for different values of the thickness of the resonators in an asymmetric case*

### 7.2.4. VARIATION OF THE HEIGHT OF THE RESONATORS (S1) WITH A FIXED POSITION ($C1_1 \neq C1_2$)

*Table 7-10* shows the dimensions of the filter under study, where the resonators are placed in the opposite asymmetric position.

| | |
|---|---|
| A=22.86 | 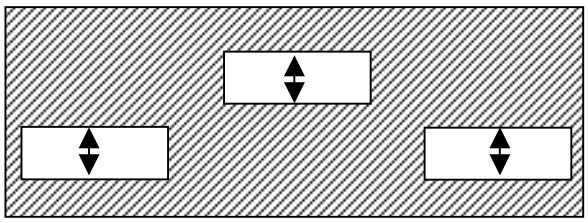 |
| B=10.16 | |
| $Lred_1$=2 | |
| $Lred_2$=2 | |
| $Lrid_1$=$Lrid_2$=15 | |
| T=0.1 | |
| $C1_1$= 1 | |
| $C1_2$=B- $C1_1$-S1 | |
| S1=1-9 | |

*Table 7-10: Dimensions of the E-Plane filter with three resonators*

The S parameters for different values of the height of the resonators are represeted in *Figure 7-11*. When the value of the height is small (the distance between the resonator is

higher), similar conclusions than in section 7.2.2 can be made. The selectivity is improved, the central frequency is lower and we can obtain a transmission zero at lower frequencies.

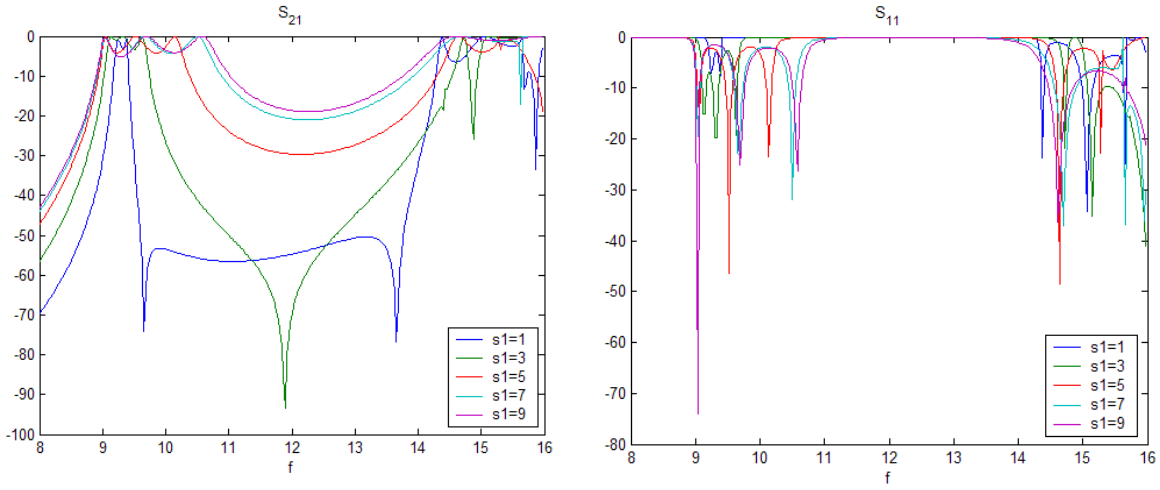


*(a)* *(b)*

*Figure 7-11: $S_{21}$ (a) and $S_{11}$ (b) for different values of the thickness of the resonators in an asymmetric case*

### 7.2.5. VARIATION OF THE LENGTH OF THE SECOND METAL INSERTS ($LRED_2$) WHEN $C1_1$=$C1_2$

As in other sections *Table 7-11* gives the dimensions of the filter under study, where the three resonator are in the same position with a fixed height equal to 2 mm.

| | |
|---|---|
| A=22.86 | 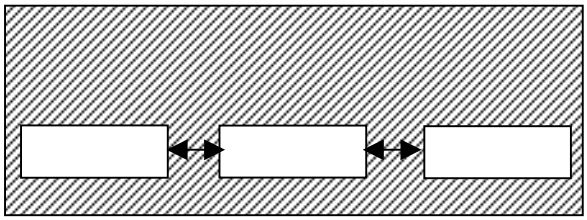 |
| B=10.16 | |
| $Lred_1$=2 | |
| $Lred_2$=1-6 | |
| $Lrid_1$=$Lrid_2$=15 | |
| T=0.1 | |
| $C1_1$= $C1_2$= 1 | |
| S1=2 | |

*Table 7-11: Dimensions of the E-Plane filter with three resonators*

*Figure 7-12* shows the S parameters for different values of the second metal inserts when the resonators are in the same asymmetric position. Similar comments to section 6.2.5 can be written and a transmission zero appears at a constant frequency due to in this case it depends on the position of the resonator, not on the length of the couplers.

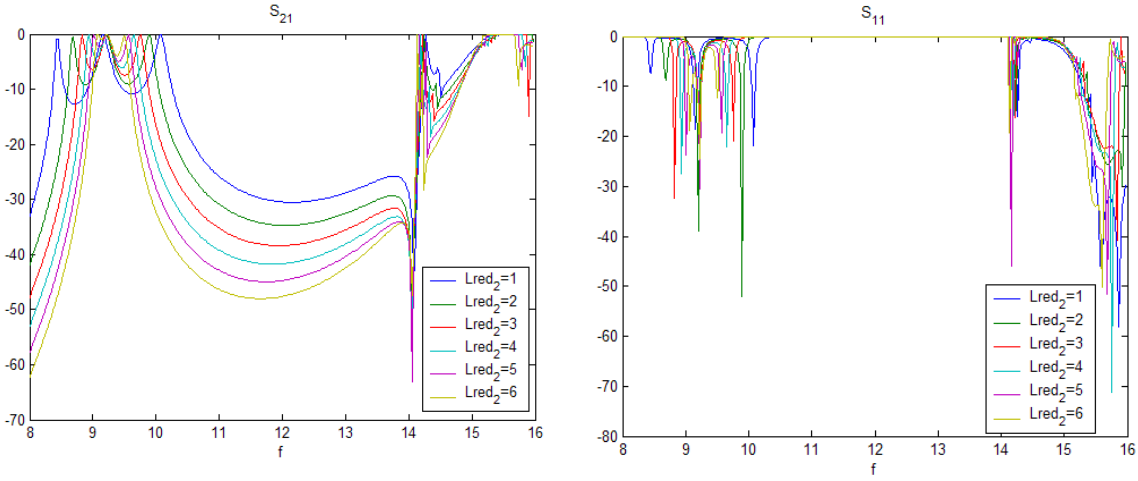


*(a)* *(b)*

*Figure 7-12: $S_{21}$ (a) and $S_{11}$ (b) for different values of the middle metal insert*

### 7.2.6. VARIATION OF THE LENGTH OF THE SECOND METAL INSERTS ($LRED_2$) WHEN $C1_1 \neq C1_2$

*Table 7-12* gives the dimensions of the filter under study, where the resonators are placed in the opposite asymmetric position with a fixed height equal to 2 mm.

| | |
|---|---|
| A=22.86 | 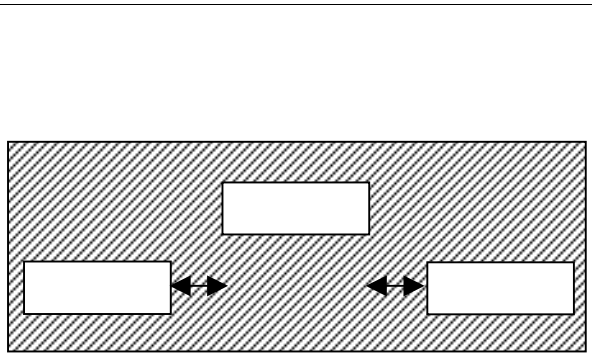 |
| B=10.16 | |
| $Lred_1$=2 | |
| $Lred_2$=1-6 | |
| $Lrid_1$=$Lrid_2$=15 | |
| T=0.1 | |
| $C1_1$= 1 | |
| $C1_2$= 7.16 | |
| S1=2 | |

*Table 7-12: Dimensions of the E-Plane filter with three resonators*

The S parameters for different values of the central metal insert when the resonators are in the opposite asymmetric position are represented in *Figure 7-13*. The differences in the passband are not very relevant as in section 6.2.6. The only thing that it can be stand out is that the transmission zero is shifted to lower frequencies close to the pass band when the central metal inserts are thinner. As it was shown in previous sections, when the resonators are placed in opposite position a transmission zero at finite frequencies appears improving the selectivity.

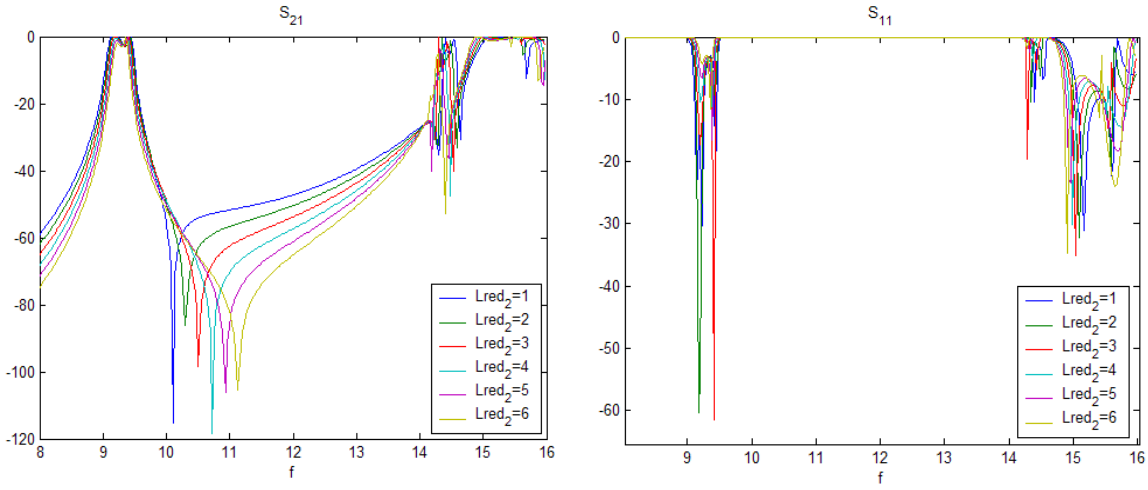


*(a)* *(b)*

*Figure 7-13: $S_{21}$ (a) and $S_{11}$ (b) for different values of the middle metal insert*

## 7.3. VALIDATION OF A FILTER: 9.25-9.75 GHZ PASSBAND

The parameters and the response of the prototype in [2-10] with three resonators are given in *Table 7-13*.

| PROTOTYPE | |
|---|---|
| A=22.86 | |
| B=10.16 | |
| T=0.1 | |
| Ripple=0.5 | |
| $Lred_1$=2.18800010322593 | |
| $Lred_2$=6.85999984666705 | |
| $L_1$-$L_3$=16.0271294973159 | |
| $L_2$=16.2252497988806 | |

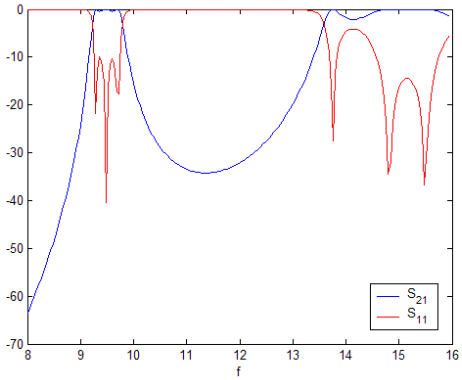


*Table 7-13: Dimensions of the prototype with three resonators*

The values of A, B and T for the validated filter will be the same than for the prototype.

To validate this filter we are going to keep the values of the two resonators filter for $Lred_1$=1.6, $Lred_2$=1, Lrid ($L_1$)=14.2, $C1_1$=1 ($C1_2$=8.16) and S1=2, but now we have to choose the value for Lrid2 to get a similar response to the prototype.

In previous sections, as 7.1.3 and 7.1.4, one of the conclusions after study the resultant figures was that the lengths of the resonators should be around the same value. Furthermore, the values of $Lrid_1$ and $Lrid_2$ for the prototype have a difference of 0.2 mm approximately. If the selected value is $Lrid_2$=14.4, a better response is obtained in comparison with $Lrid_2$= 14.2, as it is shown in *Figure 7-14*.

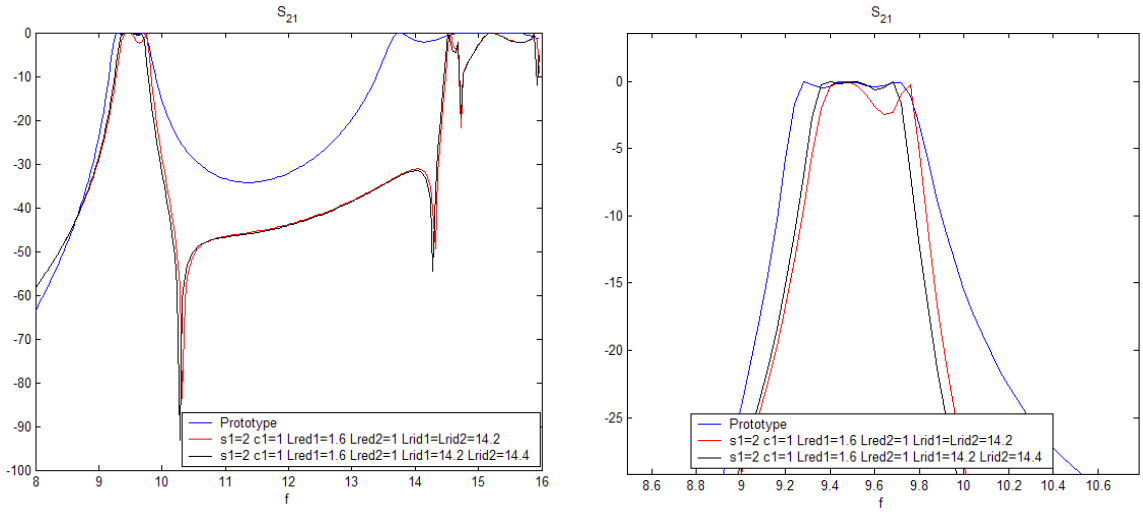


(a) (b)

*Figure 7-14: $S_{21}$ for different values of Lrid2 (a), and a zoom of it in the passband(b)*

As a conclusion, the dimensions of the filter that has been made are given in *Table 7-14.*

| RWG FILTER | PROTOTYPE |
|---|---|
| S1=2 | |
| C1=1 | |
| $Lred_1$=1.6 | $Lred_1$=2.18800010322593 |
| $Lred_2$=1 | $Lred_2$=6.85999984666705 |
| $Lrid_1$=14.2 | $L_1$-$L_3$=16.0271294973159 |
| $Lrid_2$=14.4 | $L_2$=16.2252497988806 |

*Table 7-14: Dimensions of the filter and the prototype with three resonators*

Using the parameters of the *Table 7-14* a good response with the same passband than the prototype and with improved selectivity has been achieved, as it is exposed in *Figure 7-15*.

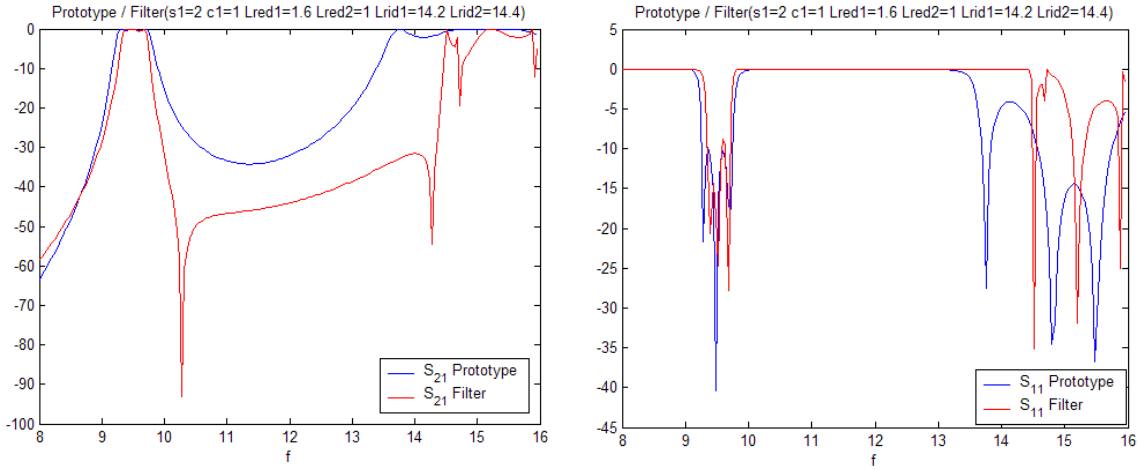


*(a)* *(b)*

*Figure 7-15: $S_{21}$ (a) and $S_{11}$ (b) for the prototype and the final filter*

The validated filter has two important advantages. One of these is that the validated filter is more selective, due to the high level of attenuation at the stopband and a transmission zero very close to the passband. And the second one is that the total length of the filter has been reduced around 18.3mm with respect to the prototype.

| |
|---|
| Prototype length= 66.3 mm |
| RCWG filter length= 48 mm |

*Figure 7-16* shows the comparison of the response of the filter simulated in HFSS and Fortran. Good agreement between the two simulations has been achieved.

In this case, a remark has to be done because to obtain good results in HFSS a discrete simulation is required, therefore more time is needed to converge to the response of the filter.

For that reason, when the number of resonator increases a more accurate and complex simulation is required to converge to the final results.

In addition, we can observe in *Figure 7-16* that there are some differences between the simulation in Fortran and HFSS. These deviations can be due to that HFSS needs more steps to converge to a more accurate response, or also that Fortran needs more number of TE and TM modes to converge to the final response of the filter.

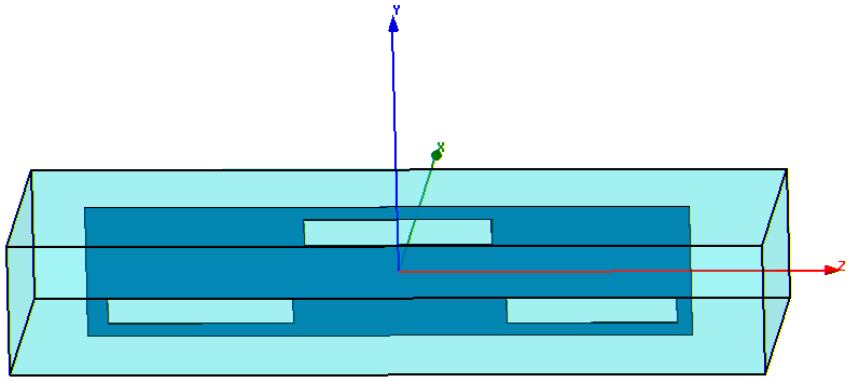


*(a)*

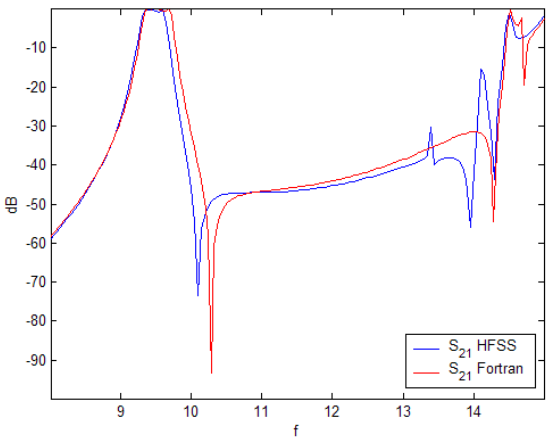


*(b)*

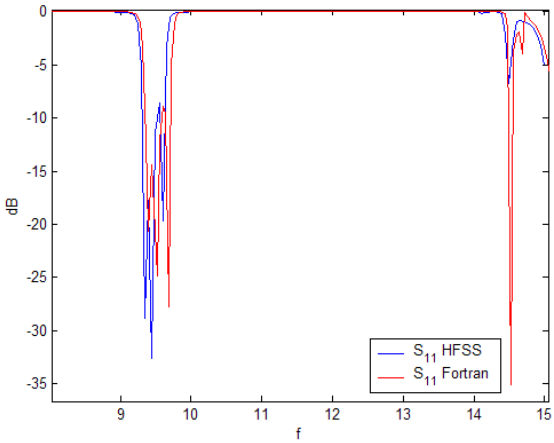


*(c)*

*Figure 7-16: Sketch of the filter (a) and comparison of $S_{21}$ (b) and $S_{11}$ (c) obtained with HFSS and Fortran*

*Table 7-15* presents the comparison of the time needed to simulate the same filter in Fortran and HFSS on an AMD Athlon(tm) 64, 637 MHz, 1GB RAM. The results are exceptionally good.

| Fortran | HFSS |
|---|---|
| 40 sec. | 17820 sec. (297 min.) |

*Table 7-15: Time comparison*

# 8. MEASUREMENTS

## 8.1. INTRODUCTION

In this chapter some comparisons between simulated and measured responses of the filters have been done.

To carry out the measurements it is necessary an analyzer, as it is shown in *Figure 8-1 (a)*. In this case the analyzer is *Anritsu 37397D, Vector Network Analyzer, 40 MHz-65 GHz*.

In addition, two adaptors are required to make the joint between the analyzer and the waveguide, as it is presented in *Figure 8-1 (b)*. Before doing the measurements it is necessary to calibrate the ports of the analyzer, to eliminate possible losses. Different types of calibrations exist, and the way to do the calibration can affect to the final results.

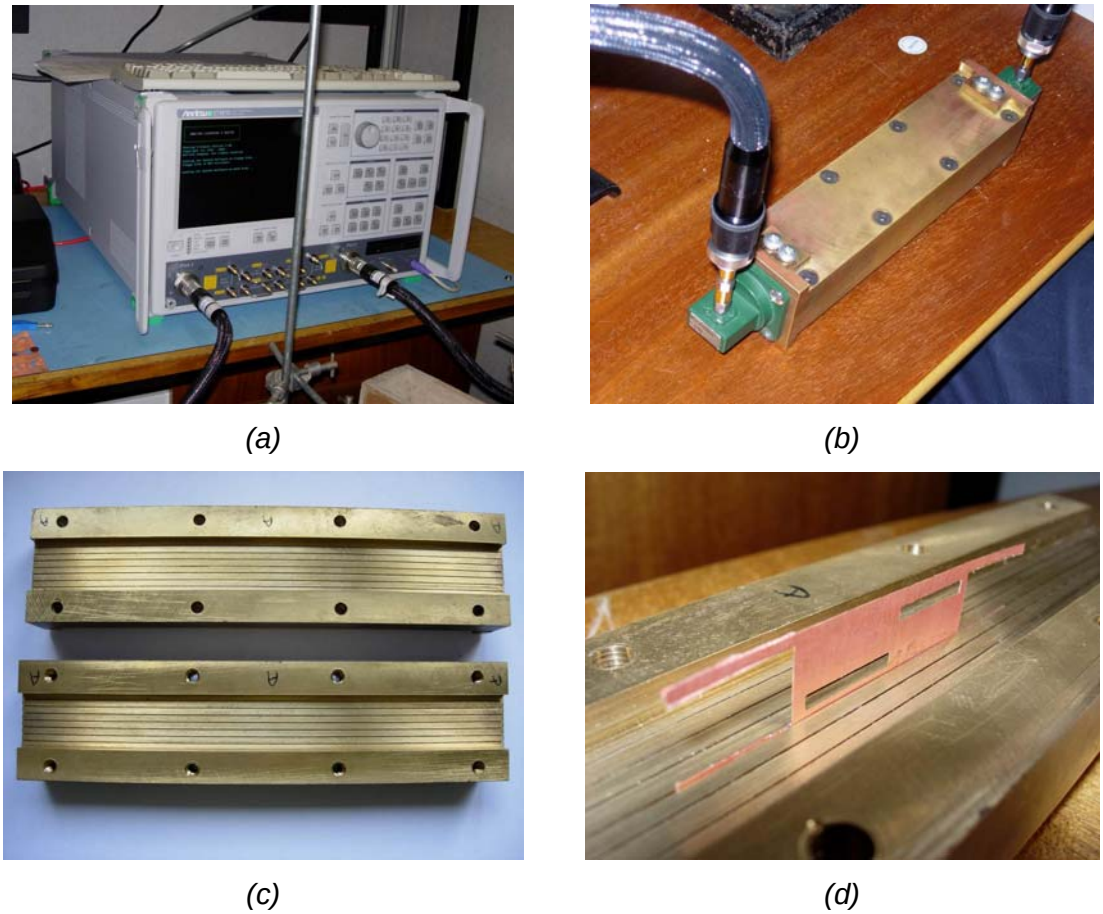

*(a)* *(b)*

*(c)* *(d)*

*Figure 8-1: Analyzer (a), Adaptors (b), Waveguide (c) and All metal septa (d) used to carry out the measurements.*

*Figure 8-1 (c)* introduces the waveguide that is used. It consists in a split block waveguide housing with slots parallel to the E-Plane of the waveguide. In this case, the

metal insert is placed in the central slot, as it is shown in *Figure 8-1 (d)*. The total length of the waveguide is 203.2 mm, the height is a=22.68 mm, and the height is b=10.05 mm.

Therefore, in order to demonstrate the feasibility of the bandpass component as well as the accuracy of developed mode matching simulator, a first and second order bandpass prototype have been fabricated. These filters will be explained in sections 8.2 and 8.3.

Section 8.4 presents some advices to improve the measurements, like using another type of split block waveguide housing.

## 8.2. FILTER WITH ONE RESONATOR

Dimensions in (mm) of a first simple structure are given in *Table 8-1*. In addition, a photograph of the fabricated metal insert is shown in this table. This metal insert is put in the central slot of the waveguide and operates as a first order filter. The extensions of metal at both sides of the main plaque help to make a better connection between the waveguide and the metal insert.

| | |
|---|---|
| B=10.05 | 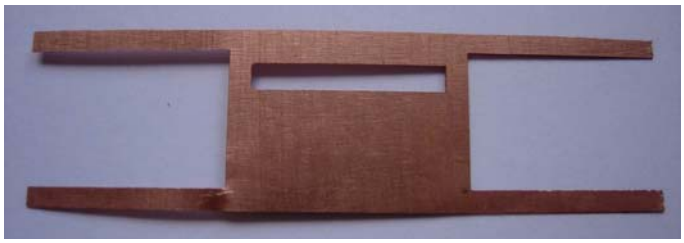 |
| Lred=1.6 | |
| Lrid=14.2 | |
| T=0.1 | |
| C1=1 | |
| S1=2 | |

*Table 8-1: Dimensions of the fabricated E-Plane filter with one resonator*

To obtain the simulated response, the same dimensions and mode matching with 20 TE and 15 TM modes have been used.

The simulated and measured results are shown in *Figure 8-2*. Some discrepancies are found in the measurement. For example, at the passband there are some losses around 0.6702 dB and the central frequency is shifted to a lower frequency. Although, that amount of losses is acceptable and the shape of the measured response follow the simulated response. Therefore, we can say that good agreement between simulation and measurement has been achieved and the found differences can be due to a bad contact between the metal insert and the waveguide.

The losses that are indicated in *Figure 8-2* are ohmic losses and they are explained in the following expression:

$$|S_{11}|^2 + |S_{21}|^2 + \underbrace{e^2}_{losses} = 1$$

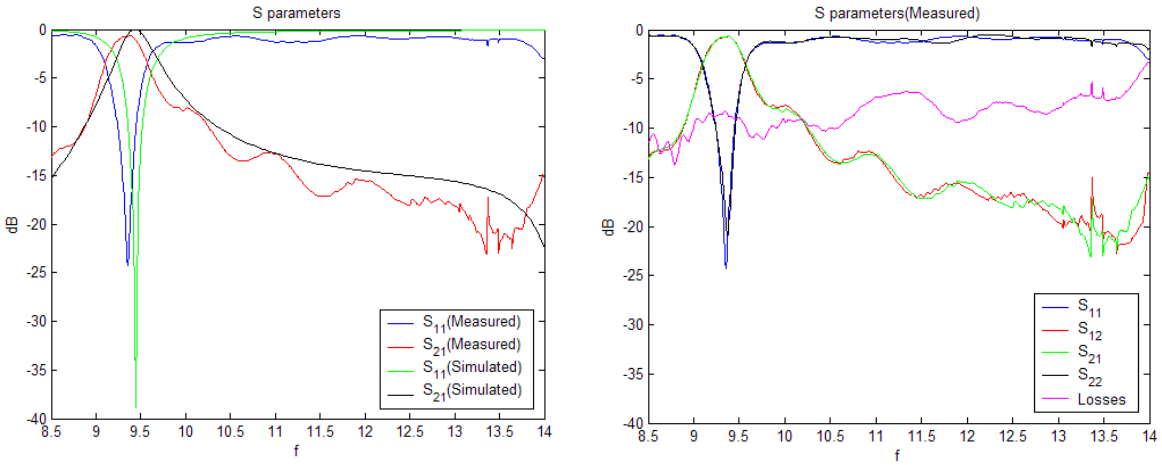


*(a)* *(b)*

*Figure 8-2: Simulated and measured response (a), and S parameters (b) of the fabricated filter*

## 8.3. FILTER WITH TWO RESONATORS

In this case two metal inserts have been fabricated keeping up the same main plaque. One of them has extensions of metal at both sides of the main plaque, and the other one is a metal plaque without the extensions.

The dimensions in (mm) of the fabricated metal insert with two resonators are given in *Table 8-2*. This metal insert is put in the central slot of the waveguide and operates as a second order filter.

| B=10.05 | T=0.1 | C1=1 | S1=2 | $Lred_1$=1.6 | $Lred_2$=1 | Lrid=14.2 |
|---|---|---|---|---|---|---|

*Table 8-2: Dimensions in (mm) of the fabricated E-Plane filter with two resonators*

To obtain the simulated response to compare with the measured response, the same dimensions and mode matching with 20 TE and 15 TM modes have been used.

### 8.3.1. FILTER WITHOUT METALLIC EXTENSIONS

*Figure 8-3* presents a photograph of the fabricated metal insert without metallic extensions. It is appreciable the two holes that operate like two resonators.

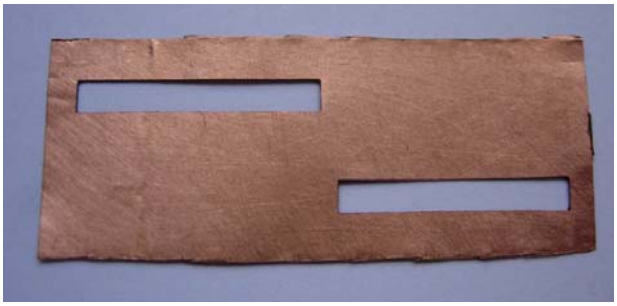

*Figure 8-3: Photograph of the fabricated metal insert*

The simulated and measured results are shown in *Figure 8-4 (a)*. More discrepancies are found in the measurement than in the previous case. For example, at the passband there are more losses around 5.5 dB and also the central frequency is shifted to a lower frequency. This amount of losses is not acceptable.Therefore, we can say that not very good agreement between simulation and measurement has been achieved.

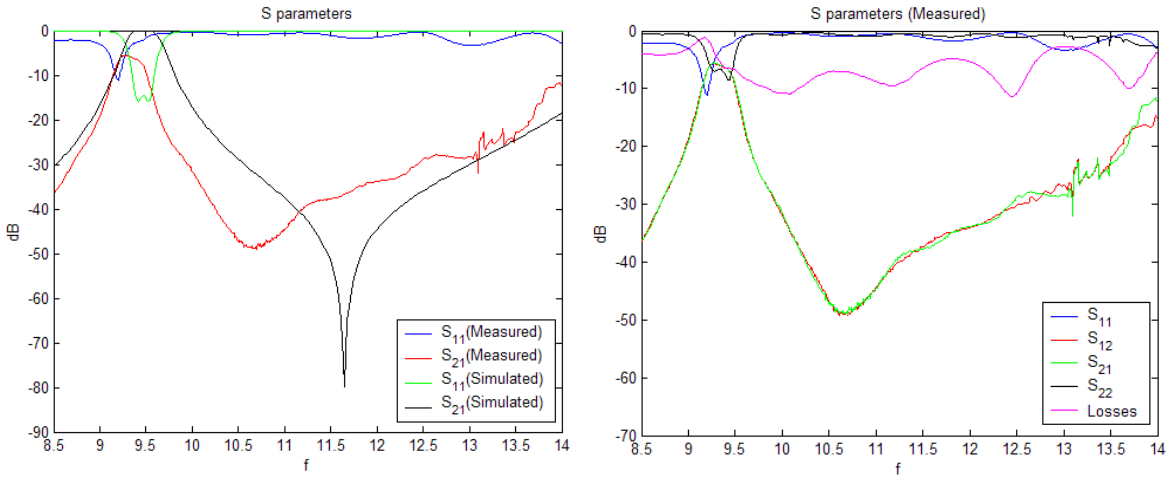


*(a)* *(b)*

*Figure 8-4: Simulated and measured response (a), and S parameters (b) of the fabricated filter*

### 8.3.2. FILTER WITH METALLIC EXTENSIONS

*Figure 8-5* presents a photograph of the fabricated metal insert with metallic extensions at both sides of the main plaque.

*Figure 8-5: Photograph of the fabricated metal insert*

*Figure 8-4 (a)* shows the simulated and measured results. As in the previous case, some deviations are found in the measurement. There are some losses at the passband around 6.6dB and the central frequency is shifted to a lower frequency. As in the previous case, this amount of losses is not acceptable, although the shape of the measured response follow the simulated response. Therefore, we can say that the losses at the passband can come from a bad contact between the metal insert and the waveguide, or from an error during the fabrication process.

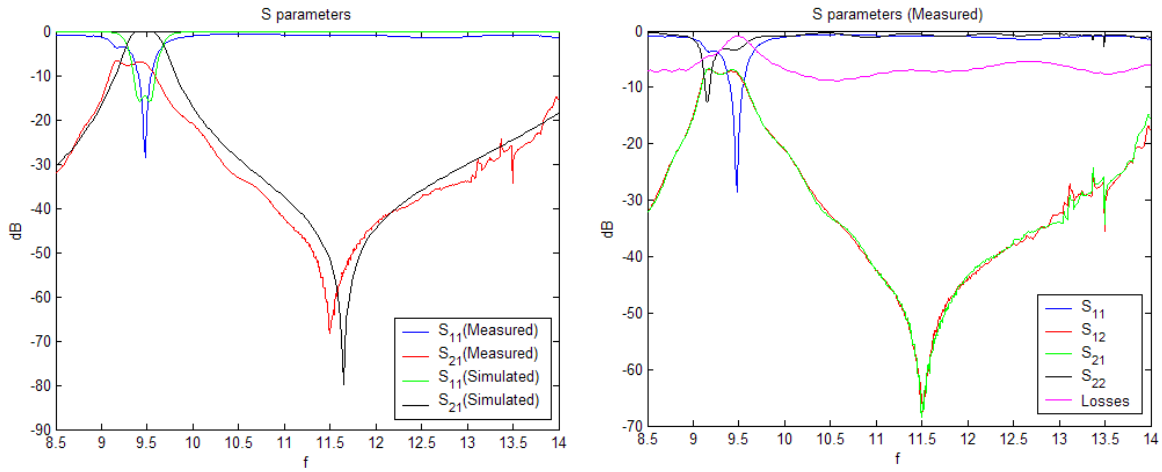


*(a)* *(b)*

*Figure 8-6: Simulated and measured response (a), and S parameters (b) of the fabricated filter*

## 8.4. CONCLUSIONS AND ADVICES

A part from some deviations, good agreement between simulation and measurement has been achieved for the fabricated filter with one resonator. The looses found in the passband are smaller than 1dB, therefore the results are acceptable.

On the opposite hand, the results achieved for the two fabricated configurations with two resonators are not acceptable due to the losses in the passband are bigger than 5dB.

As it was said in chapter seven, when the number of resonator increases a more accurate and complex simulation is required. In the case of the measurements something similar occurs. When there is some error in the fabrication of the model or there is a bad contact between the waveguide and the metal insert, the losses increase according to the number of resonators.

Attending to the previous remarks, the conclusions to remind for future fabrications are that it is important to improve the contact between the metal insert and the waveguide, and also it is important the accuracy of the fabrication process.

One proposal to improve the contact between the waveguide and the metal insert is to use another kind of waveguide split in its E-plane. This waveguide is presented in *Figure 8-7*.

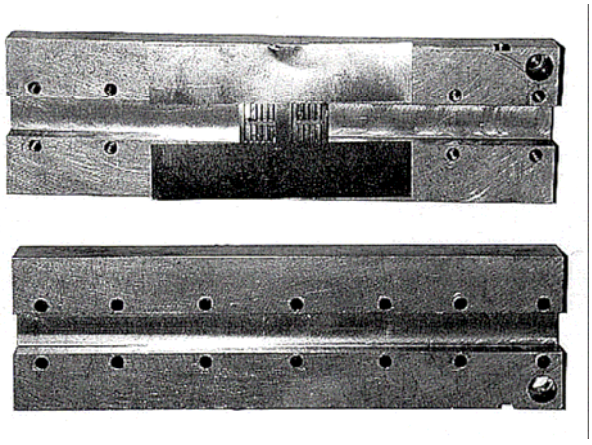

*Figure 8-7: Split block waveguide*

# 9. FUTURE WORKS

## 9.1. DESIGN TOOL

Having developed a mean of simulating waveguide E-plane structures, there emerges the need for designing E-plane filters. The randomised design of E-plane filters (e.g. by optimisation assuming random or very rough initial values) is an inefficient way of designing this type of filters, since the number of parameters that determine the geometry of a filter is large and increasing with the filter order, combined with the vast amount of calculations required for a single simulation of the filter response.

A design procedure that yields some initial values for this parameters depending on some predefined specifications is therefore essential. Distributed filter design for the microwave range of frequencies (and higher) has been extensively studied with a large literature on the subject. A variety of methods have been proposed [9-1]-[9-10], but the most relevant for direct coupled half wavelength filters is the one proposed by [9-2]. Since E-plane filters fall into this type of microwave filters, this method can be employed. This method starts from the ideal transfer function (Chebyshev filters) and builds an equivalent circuit consisting of half wavelength resonators and impedance inverters, which can readily be realised in E-plane technology.

## 9.2. MINIATURIZATION

Apart from the favourable characteristics, E-plane filters suffer from bulky size. [9-11] proposes a novel configuration that reduces the physical dimension of bandpass E-plane filters to approximately half. A 3rd order design is presented as an example in *Figure 9-1*. The proposed filter is completely compatible with the low-cost and mass-producible fabrication process of all-metal insert E-plane filters [9-12] and can be directly integrated with lowpass waveguide components for suppression of the spurious harmonic resonances [9-13]. This structure introduces parallel coupling between the resonators of ridge waveguide filters. Narrow gap resonators are coupled both in series and in parallel. This results in a significant reduction of the total size of the filter. Furthermore, the topology allows for cross-coupling between the resonators, thus introducing transmission zeros at finite frequencies as it was obtained in this project, using topologies with ridge waveguide in an asymmetric position.

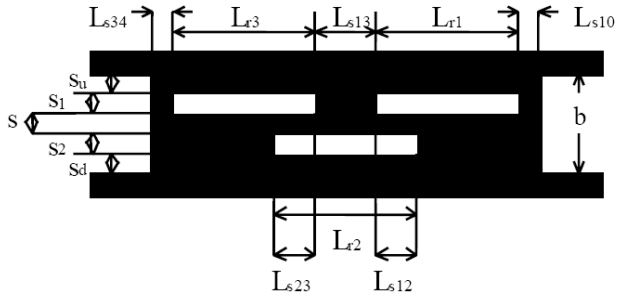


*Figure 9-1: Cross section of proposed configuration*

The proposed configuration was simulated with commercial programs, but that is not efficient. For that reason it is important to follow the same procedure develop in this project with the case of E-Plane filter with asymmetric ridge waveguide. To obtain the response of the topology presented in *Figure 9-1* it is necessary to apply the Mode Matching Method (MMM) for the discontinuity created between Ridge Coaxial waveguide (RCWG), in [9-14], and the Asymmetric Ridge waveguide (RWG). The rest of the discontinuities were solved during this project and in section 9.3 the MMM is applied for the RCWG-RWG discontinuity.

## 9.3. MODE MATCHING: RIDGE COAXIAL WG - RIDGE WG

The discontinuity between RCWG and RWG will be analysed by the MMM, taking as a reference [9-15] and section 2.5.

*Figure 9-2* shows the cross sections of the structures at both sides of the discontinuity that is going to be analysed.

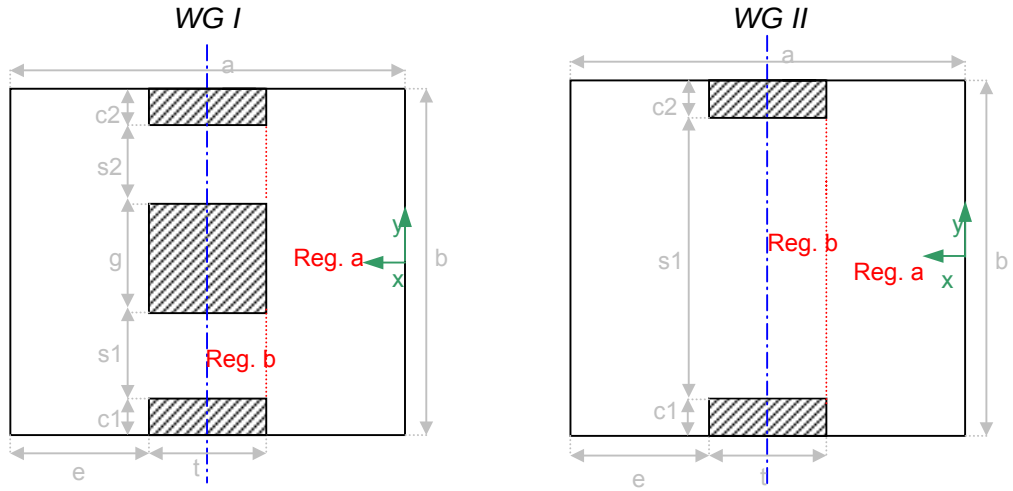


*(a)* *(b)*

*Figure 9-2: Cross section of Ridge Coaxial Waveguide (a) and Ridge Waveguide (b)*

Firstly, we have to remind that increasing cutoff frequencies, the lowest mode is the TEM mode for RCWG.

Following the same procedure than in section 2.5, the expressions for the vector potential relative to TEM, TE and TM modes for each structures have to be known.

The structures, Ridge Coaxial WG (*WG-II*) and Ridge WG (*WG-II*), can be divided in simple regions, 'a'-'b'-'c' and 'a'-'b' respectively. The field distribution for the TEM mode in each region of the RCWG was obtained in [9-16]. Furthermore, the field distribution for the TE and TM modes, the cutoff wavenumbers, *K*, and the amplitude coefficients, *A* and *D*, in each regions of the RCWG and RWG were obtained in [9-14]. The expressions for the field distribution for TE and TM modes in each structures are remembered in Appendix I.

After that, we have to solve the coupling matrix, M, for the respective discontinuity, that is arranged as:

$$M = \begin{bmatrix} 0 & J_{Te} \\ J_{hh} & 0 \\ J_{eh} & J_{ee} \end{bmatrix}$$

where the number of columns is given by the mode spectrum of the ridge waveguide and the number of rows by that of the ridge coaxial waveguide. Note that $J_{eT}$ is a single-column matrix, which disappears if the TEM mode is not present, as the case study in chapter 2.

The expressions of the $J_{hh}$, $J_{eh}$ and $J_{ee}$ submatrices were shown before as (2.3-16), (2.3-17) and (2.3-19), and have been calculated in Apendix II.

The last submatrix that has to be calculated in a future work is the $J_{eT}$ , and its expression is given by:

$$\left(J_{Te}\right)_p = \iint_{SII} (\nabla T_T^I)(\nabla T_{ep}^{II}) \cdot dS$$

After the coupling matrix have been calculated it is possible to apply the MMM in the RCWG-RWG discontinuity and implement it in Fortran to obtain a fast tool to simulate the kind of structures proposed in section 9.1.

*Figure 9-3* try to explain how the TEM mode is excited in a discontinuity between RWG and RCWG. First of all, *Figure 9-3 (b)* presents the first mode of a RWG, the $TE_1$, and the two first modes in a RCWG, the TEM and the $TE_1$. After that, in a RWG-RCWG discontinuity the coupling between the resonators can be in phase or in phase opposition. When the coupling is made in phase, the mode that is propagated in the RCWG is the $TE_1$. If the coupling is made in phase opposition, the propagated mode is the TEM. We can compare the shapes of the modes between *Figure 9.3 (a)* and *(b)*.

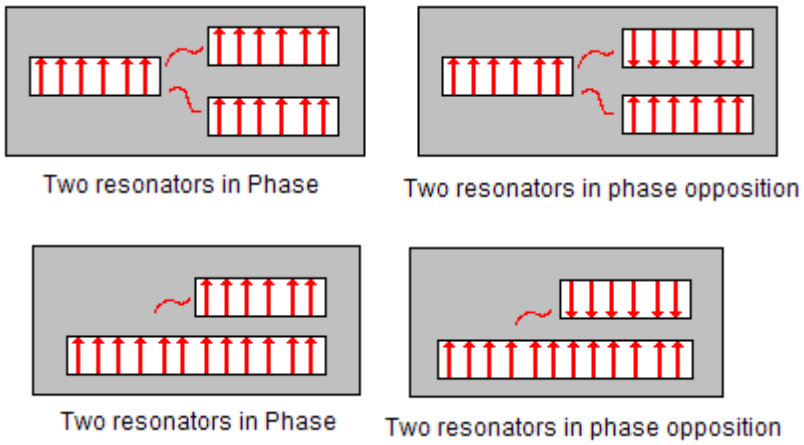


*(a)*

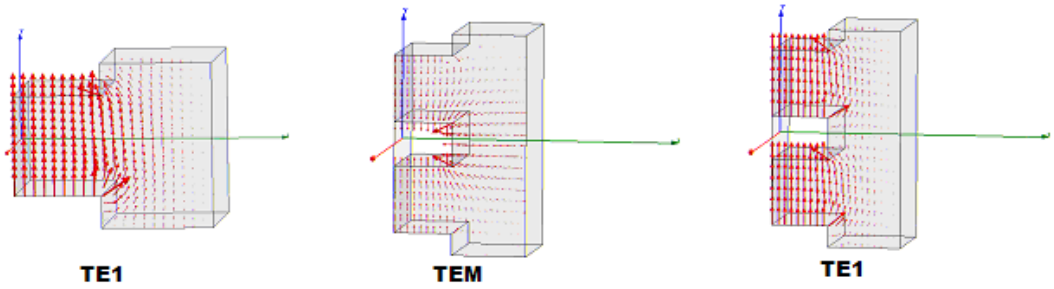


*(b)*

*Figure 9-3: Coupling in a RWG-RCWG discontinuity (a), and first modes in a RWG and in a RCWG (b)*

In addition, to verify that the MMM is applied correctly a structure with the cross section presented in *Figure 9-4* is simulated in HFSS.

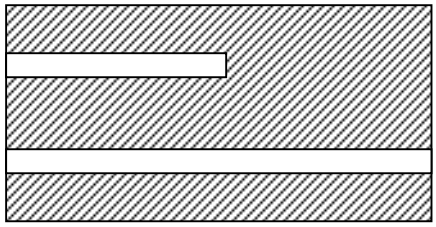

*Figure 9-4: Cross section of the structure used to verify the MMM in RCWG-RWG discontinuity*

If the TEM mode is not excited when it suffers the RCWG-RWG discontinuity, there is not coupling between the first modes of RCWG and RWG, the transmission is zero.

*Figure 9-5* shows the coupling between the first mode of RWG and the first mode of the RCWG. There is coupling between both modes, due to energy is transmitted from one port to the other. For that reason the TEM mode has to be taken into account.

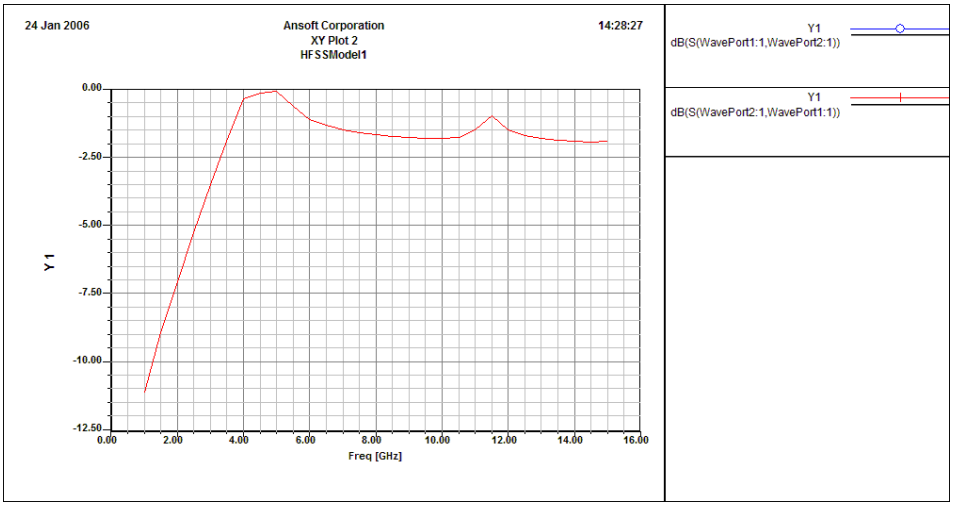


*Figure9-5: Coupling between first modes of RCWG and RWG*

## 9.4. REFERENCES

[9-1] G. L. Matthaei, L. Young, E. M. T. Jones, Microwave Filters, Impedance-Matching Networks and Coupling Structures, McGraw-Hill

[9-2] J.D. Rhodes, *"Microwave circuit realizations"*, in Microwave Solid State Devices and Applications, D.V. Morgan and M.J. Howes, Eds. England: Peregrinus, pp.49-57, 1980

[9-3] J. Uher, J. Bornemann, U. Rosenberg, Waveguide Components for Antenna Fed Systems: Theory and CAD, Artech House, Boston, 1993

[9-4] Levy R., *"Theory of Direct Coupled Cavity Filters"*, IEEE Trans. Microwave Theory and Techniques, Vol. MTT-15, No 6, pp 340-348, June 1967

[9-5] Levy R., *"A Generalised Design Technique for Practical Distributed Reciprocal Networks"*, IEEE Trans. Microwave Theory and Techniques, Vol. MTT-21, No 8, pp 519-526, August 1973

[9-6] Postoyalko V. and Budimir D., *"Design of Waveguide E-Plane Filters with All-Metal Inserts by Equal Ripple Optimisation"*, IEEE Trans. Microwave Theory and Techniques, Vol. MTT-42, No 2, pp 217-222, February 1994

[9-7] Budimir D. and Postoyalko V., *"EPFILTER: A CAD Package for E-Plane Filters", Microwave Journal",* pp. 110-114, August 1996

[9-8] Budimir D., *"Design of E-Plane Bandpass Filters with Improved Stopband Performance"*, PhD Thesis, University of Leeds, Department of Electronic and Electrical Engineering, July 1994

[9-9] G. Goussetis and D. Budimir, *"Simple Tuning Procedure for Coupled-Resonator Filters"*, Asia Pacific Microwave Conference (AMPC'2001), Taipei, Taiwan, December 3-6, 2001

[9-10] M. Guglielmi, *"Simple CAD Procedure for Microwave Filters and Multiplexers"*, IEEE Trans. Microwave Theory and Techniques, Vol. 42, No 2, pp 1347-1352, July 1994

[9-11] G. Goussetis, A.P. Feresidis, D. Budimir, and J.C. Vardaxoglou, *"A 3rd Order Ridge Waveguide Filter with Parallel Coupled Resonators"*

[9-12] D. Budimir, *"Generalized Filter Design by Computer Optimization"*, 1998, Artech House

[9-13] Goussetis G., Budimir D., *"Compact ridged waveguide filters with improved stopband performance",* IEEE MTT-S International Microwave Symposium Digest 2003, pp. 953 - 956, Vol. 2, Philadelphia, 8-13 June 2003

[9-14] MªÁngeles Ruiz Bernal, *"Modal analysis of Ridge Coaxial waveguide using the transverse resonance method and field matching to study microwave filters"*, Final Year Project, May 2006

[9-15] George Goussetis, *"Waveguide bandpass with improved performance"*, Ph.D. 2002.

[9-16] G.-U. Paul, *"Exact calculation of microwave filters composed of rectangular transmission line resonators (in German)"*, Frequenz 30 (1976), 335–339.

[9-17] Vladimir A. Labay, Jens Bornemann, Smain Amari, John M. Damaschke, *"Direct-Coupled Waveguide Filters for the Lower Gigahertz Frequency Range"*, received 25 January 2001; revised 17 August 2001

# 10. CONCLUSIONS

## 10.1. SUMMARY OF THE WORK

As it was pointed out in the introduction, the first main aim has been to explore the possibilities of improvement of the E-plane metal insert filters characteristics incorporating asymmetric Ridge waveguide. Moreover the main goals are to increase the selectivity and reduce the dimensions of the filter conserving the advantages that this filters provide, as low cost and mass producible filters. In order to achieve this, a first objective has been to develop a fast and accurate simulation tool for Ridge waveguide.

Following some literature review, many numerical methods have been introduced in the past two decades to describe the scattering phenomena of waves inside microwave passive components. The Mode Matching method was chosen as most appropriate to characterize the waveguides discontinuities with simple geometries because less memory and computing is required to converge to the solution.

As a next step, formulation and computer realisation of this method was made. The solutions for the surface discontinuities of Ridge WG to Reduced WG and WG to Reduced WG were combined with the propagation along the finite length sections in order to obtain a 3D structure simulator for E-plane filters.

Fortran code has been developed in order to realise this work. Moreover, the code in Fortran was later adapted to communicate it with Matlab to create an useful interface to simulate these configurations. Extensive convergence studies were then made. Investigation on the number of TE and TM modes required and the variation of these numbers with the geometry was made. Confidence that the simulator can work accurately was obtained.

Once the analysis and simulation tool were completed, a thorough investigation of the stopband improvement for several configurations was made and some configurations were fabricated to make the comparison between the obtained results with the measurements.

The final aim of the work has been to investigate a novel configuration for further improvement of E-plane filters like the reduction of the physical dimension of bandpass E-plane filters to approximately half.

## 10.2. FINAL CONCLUSIONS

This section aims to summarise the conclusions made by this project.

After analyse and verify the E-plane filters including asymmetric Ridge waveguide filters, the changes that the response of the filter suffers with respect all the parameters are known.

First of all, the length of the resonator (Lrid) is the parameter that can define the central frequency due to it is directly related to the frequency. Another important parameter is the height of the resonator (s1). In general, the selectivity and stopband improvements are maximised for narrower height of the resonator. Moreover, the length of the couplers (Lred) is important, because when Lred increases the configuration is more reflective and the coupling is weaker.

Secondly, one of the main objectives is to obtain a response with a transmission zero close to the passband to improve the selectivity. For this reason, we have to keep in mind that the resonators must be placed in opposite positions close to the up and bottom walls of the guide, the height of them should be thin and the length of the central metal insert must be short. Following these remarks we will be able to obtain a filter with a high selectivity and with a transmission zero at finite frequencies.

Moreover, two specific factors have been studied due to their importance at the future stage of the design, they are the quality factor (Q) and the coupling coefficient (K). The conclusion about Q is that it is increased when the resonator is positioned close to the up or bottom walls of the guide, and also when the length of the metal insert is large. Furthermore, the K coefficient is increased when the resonators are close each other, and also when the length of the second metal insert is small.

It is interesting to remark that to carry out the objective of the selectivity improvement the resonators has to be in opposite positions to make the coupling weaker, as it was said before. In addition, in this case the dependence of K with respect to the length of the second metal insert is very small, for that reason we can choose a small value for $Lred_2$ and achieve the other main objective reducing the size of the filter.

After the basic analysis of these configurations, the results have been validated taking a prototype and a commercial software (HFSS) as a reference. Therefore, the validated filter has two important advantages over the prototype. One of these is that the validated filter is more selective, due to the high level of attenuation at the stopband and a transmission zero very close to the passband. And the second one is that the total length of the filter has been reduced with respect to the prototype, as it is shown in *Table 10-1*.

| (mm) | All metal septa E-plane filter | Ridge WG E-plane filter | Difference |
|---|---|---|---|
| One resonator filter | 20.403 | 17.4 | 3.003 |
| Two resonators filter | 25.0751 | 16.8 | 8.2751 |
| Three resonators filter | 66.3 | 48 | 18.3 |

*Table 10-1: Size comparison between the analysed filter and the prototype*

In addition, *Table 10-2* present the comparison of time needed to simulate the same structure in Fortran and in HFSS on an AMD Athlon(tm) 64, 637 MHz, 1GB RAM, and very good results have been obtained. It is important to remark that when the number of resonator increases a more accurate and complex simulation is required.

| (sec.) | Fortran | HFSS | $Time_{HFSS}/Time_{Fortran}$ |
|---|---|---|---|
| One resonator filter | 15 | 1260 | 84 |
| Two resonators filter | 24 | 2400 | 100 |
| Three resonators filter | 40 | 17820 | 445.5 |

*Table 10-2: Time comparison between the filter simulated in Fortran and in HFSS*

Apart from the verification, some measurements have been made. Good agreement between simulation and measurement has been achieved for the fabricated filter with one resonator. The looses found in the passband have been smaller than 1dB, therefore the results are acceptable. On the opposite hand, the results achieved for the two fabricated configurations with two resonators are not acceptable due to the losses at the passband are bigger than 5dB. As in the simulation case, when the number of resonator increases a more accurate fabrication is required due to when there is some error in the fabrication of the model or there is a bad contact between the waveguide and the metal insert, the losses increase according to the number of resonators.

Attending to the previous remarks, the conclusions to remind for future fabrications are that it is important to improve the contact between the metal insert and the waveguide, and also it is important the accuracy of the fabrication process.

Finally, among the conclusions of this project has also been to propose future works to explore the advantages of Ridge waveguide filters and E-plane technology. The most interesting work is to analyse a novel structure that is completely compatible with the low-cost and mass-producible fabrication process of all-metal insert E-plane filters. In addition, it introduces parallel coupling between the resonators of ridge waveguide filters. Narrow gap resonators are coupled both in series and in parallel. This results in a significant reduction of the total size of the filter. Furthermore, the topology allows for cross-coupling between the resonators, thus introducing transmission zeros at finite frequencies as it was obtained in this project, using topologies with ridge waveguide in an asymmetric position.

# APPENDIX I: EXPRESIONS OF FIELD DISTRIBUTION FOR RCWG AND RWG

## RCWG (WG-I)

- TE

Region a:
$$T_{hq}^{Ia}(x,y)=\sum_{m=0}^{Ma} A_{qm}^{a}\cos\left(K_{xqm}^{a}x\right)\cdot\frac{\cos\left(\frac{m\pi}{b}\left(y+\frac{b}{2}\right)\right)}{\sqrt{1+\delta_{om}}}$$

Region b:
$$T_{hq}^{Ib}(x,y)=\sum_{m=0}^{Mb} A_{qm}^{b}\frac{1}{K_{xqm}^{b}}\sin\left(K_{xqm}^{b}\cdot(x-\frac{a}{2})\right)\cdot\frac{\cos\left(\frac{m\pi}{s1}\left(y+\frac{b}{2}-c1\right)\right)}{\sqrt{1+\delta_{om}}}$$

Region c:
$$T_{hq}^{Ic}(x,y)=\sum_{m=0}^{Mc} A_{qm}^{c}\frac{1}{K_{xqm}^{c}}\sin\left(K_{xqm}^{c}\cdot(x-\frac{a}{2})\right)\cdot\frac{\cos\left(\frac{m\pi}{s2}\left(y-\frac{b}{2}+c2+s2\right)\right)}{\sqrt{1+\delta_{om}}}$$

- TM

Region a:
$$T_{er}^{Ia}(x,y)=\sum_{m=1}^{Ma} D_{rm}^{a}\frac{1}{K_{xrm}^{a}}\sin\left(K_{xrm}^{a}x\right)\cdot\sin\left(\frac{m\cdot\pi}{b}\left(y+\frac{b}{2}\right)\right)$$

Region b:
$$T_{er}^{Ib}(x,y)=\sum_{m=1}^{Mb} D_{rm}^{b}\cos\left(K_{xrm}^{b}\cdot(x-\frac{a}{2})\right)\cdot\sin\left(\frac{m\cdot\pi}{s1}\left(y+\frac{b}{2}-c1\right)\right)$$

Region c:
$$T_{er}^{Ic}(x,y)=\sum_{m=1}^{Mc} D_{rm}^{c}\cos\left(K_{xrm}^{c}\cdot(x-\frac{a}{2})\right)\cdot\sin\left(\frac{m\pi}{s2}\left(y-\frac{b}{2}+c2+s2\right)\right)$$

## RWG (WG-II)

- TE

Region a:
$$T_{hs}^{IIa}(x,y)=\sum_{m=0}^{Ma} A_{sm}^{a}\cos\left(K_{xsm}^{a}x\right)\cdot\frac{\cos\left(\frac{m\pi}{b}\left(y+\frac{b}{2}\right)\right)}{\sqrt{1+\delta_{om}}}$$

Region b:
$$T_{hs}^{IIb}(x,y)=\sum_{m=0}^{Mb} A_{sm}^{b}\frac{1}{K_{xsm}^{b}}\sin\left(K_{xsm}^{b}\cdot(x-\frac{a}{2})\right)\cdot\frac{\cos\left(\frac{m\pi}{s1}\left(y+\frac{b}{2}-c1\right)\right)}{\sqrt{1+\delta_{om}}}$$

- TM

Region a:
$$T_{et}^{IIa}(x,y)=\sum_{m=1}^{Ma} D_{tm}^{a}\frac{1}{K_{xtm}^{a}}\sin\left(K_{xtm}^{a}x\right)\cdot\sin\left(\frac{m\cdot\pi}{b}\left(y+\frac{b}{2}\right)\right)$$

Region b:
$$T_{et}^{IIb}(x,y)=\sum_{m=1}^{Mb} D_{tm}^{b}\cos\left(K_{xtm}^{b}\cdot(x-\frac{a}{2})\right)\cdot\sin\left(\frac{m\cdot\pi}{s1}\left(y+\frac{b}{2}-c1\right)\right)$$

# APPENDIX II: J MATRICES FOR THE RCWG-RWG DISCONTINUITY

## $J_{hh}$ SOLUTION

After that, we can study each region '*a*' and *'b'* independently.

$$\left(J_{hh}\right)_{qs} = \underbrace{\int_{0}^{e}\int_{-\frac{b}{2}}^{\frac{b}{2}} (\nabla T_{hq}^{Ia} \times \hat{z})\cdot(\nabla T_{hs}^{IIa} \times \hat{z})dxdy}_{J_{hh}^{a}} + \underbrace{\int_{e}^{\frac{a}{2}}\int_{-\frac{b}{2}+c1}^{-\frac{b}{2}+c1+s1} (\nabla T_{hq}^{Ib} \times \hat{z})\cdot(\nabla T_{hs}^{IIb} \times \hat{z})dxdy}_{J_{hh}^{b}}$$

Furthermore we can separate $J_{hh}^{a}$ and $J_{hh}^{b}$ in two parts:

$$J_{hh}^{a} = \underbrace{\int_{0}^{e}\int_{-\frac{b}{2}}^{\frac{b}{2}} (\frac{\partial T_{hq}^{Ia}}{\partial y}\cdot\frac{\partial T_{hs}^{IIa}}{\partial y})dxdy}_{J_{hh}^{a1}} + \underbrace{\int_{0}^{e}\int_{-\frac{b}{2}}^{\frac{b}{2}} (\frac{\partial T_{hq}^{Ia}}{\partial x}\cdot\frac{\partial T_{hs}^{IIa}}{\partial x})dxdy}_{J_{hh}^{a2}}$$

$$J_{hh}^{b} = \underbrace{\int_{e}^{\frac{a}{2}}\int_{-\frac{b}{2}+c1}^{-\frac{b}{2}+c1+s1} (\frac{\partial T_{hq}^{Ib}}{\partial y}\cdot\frac{\partial T_{hs}^{IIb}}{\partial y})dxdy}_{J_{hh}^{b1}} + \underbrace{\int_{e}^{\frac{a}{2}}\int_{-\frac{b}{2}+c1}^{-\frac{b}{2}+c1+s1} (\frac{\partial T_{hq}^{Ib}}{\partial x}\cdot\frac{\partial T_{hs}^{IIb}}{\partial x})dxdy}_{J_{hh}^{b2}}$$

If we solve this integrals we obtain the following solutions:

$$J_{hh}^{a1} = \sum_{m=1}^{Ma} A_{qm}^{a}\cdot A_{sm}^{a}\cdot\frac{m^2\pi^2}{4\cdot b}\cdot\left[\frac{\sin\left(\left(k_{xqm}^{a}-k_{xsm}^{a}\right)\cdot e\right)}{\left(k_{xqm}^{a}-k_{xsm}^{a}\right)}+\frac{\sin\left(\left(k_{xqm}^{a}+k_{xsm}^{a}\right)\cdot e\right)}{\left(k_{xqm}^{a}+k_{xsm}^{a}\right)}\right]$$

$$J_{hh}^{a2} = \sum_{m=0}^{Ma} A_{qm}^{a}\cdot A_{sm}^{a}\cdot k_{xqm}^{a}\cdot k_{xsm}^{a}\,\frac{b}{4}\cdot\left[\frac{\sin\left(\left(k_{xqm}^{a}-k_{xsm}^{a}\right)\cdot e\right)}{\left(k_{xqm}^{a}-k_{xsm}^{a}\right)}-\frac{\sin\left(\left(k_{xqm}^{a}+k_{xsm}^{a}\right)\cdot e\right)}{\left(k_{xqm}^{a}+k_{xsm}^{a}\right)}\right]$$

$$J_{hh}^{b1} = \sum_{m=1}^{Mb} A_{qm}^{b}\cdot A_{sm}^{b}\cdot\frac{1}{k_{xqm}^{b}\cdot k_{xsm}^{b}}\,\frac{m^2\pi^2}{4\cdot s1}\cdot\left[\frac{\sin\left(\left(k_{xqm}^{b}-k_{xsm}^{b}\right)\cdot\frac{t}{2}\right)}{\left(k_{xqm}^{b}-k_{xsm}^{b}\right)}-\frac{\sin\left(\left(k_{xqm}^{b}+k_{xsm}^{b}\right)\cdot\frac{t}{2}\right)}{\left(k_{xqm}^{b}+k_{xsm}^{b}\right)}\right]$$

$$J_{hh}^{b2} = \sum_{m=0}^{Mb} A_{qm}^{b}\cdot A_{sm}^{b}\cdot\frac{s1}{4}\cdot\left[\frac{\sin\left(\left(k_{xqm}^{b}-k_{xsm}^{b}\right)\cdot\frac{t}{2}\right)}{\left(k_{xqm}^{b}-k_{xsm}^{b}\right)}+\frac{\sin\left(\left(k_{xqm}^{b}+k_{xsm}^{b}\right)\cdot\frac{t}{2}\right)}{\left(k_{xqm}^{b}+k_{xsm}^{b}\right)}\right]$$

## $J_{eh}$ SOLUTION

We solve that integral as we solved $J_{hh}$.

First of all, we can study each region '*a*' and '*b*' independently.

$$\left(J_{eh}\right)_{rs} = \underbrace{\int_{0}^{e}\int_{-\frac{b}{2}}^{\frac{b}{2}}(-\nabla T_{er}^{Ia})\cdot(\nabla T_{hs}^{IIa}\times\hat{z})dxdy}_{J_{eh}^{a}} + \underbrace{\int_{e}^{\frac{a}{2}}\int_{-\frac{b}{2}+c1}^{-\frac{b}{2}+c1+s1}(-\nabla T_{er}^{Ib})\cdot(\nabla T_{hs}^{IIb}\times\hat{z})dxdy}_{J_{eh}^{b}}$$

Furthermore we can separate $J_{eh}{}^{a}$ and $J_{eh}{}^{b}$ in two parts:

$$J_{eh}^{a} = \underbrace{-\int_{0}^{e}\int_{-\frac{b}{2}}^{\frac{b}{2}}(\frac{\partial T_{er}^{Ia}}{\partial x}\cdot\frac{\partial T_{hs}^{IIa}}{\partial y})dxdy}_{J_{eh}^{a1}} + \underbrace{\int_{0}^{e}\int_{-\frac{b}{2}}^{\frac{b}{2}}(\frac{\partial T_{er}^{Ia}}{\partial y}\cdot\frac{\partial T_{hs}^{IIa}}{\partial x})dxdy}_{J_{eh}^{a2}}$$

$$J_{eh}^{b} = \underbrace{-\int_{e}^{\frac{a}{2}}\int_{-\frac{b}{2}+c1}^{-\frac{b}{2}+c1+s1}(\frac{\partial T_{er}^{Ib}}{\partial x}\cdot\frac{\partial T_{hs}^{IIb}}{\partial y})dxdy}_{J_{eh}^{b1}} + \underbrace{\int_{e}^{\frac{a}{2}}\int_{-\frac{b}{2}+c1}^{-\frac{b}{2}+c1+s1}(\frac{\partial T_{er}^{Ib}}{\partial y}\cdot\frac{\partial T_{hs}^{IIb}}{\partial x})dxdy}_{J_{eh}^{b2}}$$

If we solve this integrals we obtain the following solutions:

$$J_{eh}^{a1} = \sum_{m=1}^{Ma} D_{rm}^{a}\cdot A_{sm}^{a}\cdot\frac{m\pi}{4}\cdot\left[\frac{\sin\left(\left(k_{xrm}^{a}-k_{xsm}^{a}\right)\cdot e\right)}{\left(k_{xrm}^{a}-k_{xsm}^{a}\right)}+\frac{\sin\left(\left(k_{xrm}^{a}+k_{xsm}^{a}\right)\cdot e\right)}{\left(k_{xrm}^{a}+k_{xsm}^{a}\right)}\right]$$

$$J_{eh}^{a2} = -\sum_{m=1}^{Ma} D_{rm}^{a}\cdot A_{sm}^{a}\cdot\frac{k_{xsm}^{a}}{k_{xrm}^{a}}\cdot\frac{m\pi}{4}\cdot\left[\frac{\sin\left(\left(k_{xrm}^{a}-k_{xsm}^{a}\right)\cdot e\right)}{\left(k_{xrm}^{a}-k_{xsm}^{a}\right)}-\frac{\sin\left(\left(k_{xrm}^{a}+k_{xsm}^{a}\right)\cdot e\right)}{\left(k_{xrm}^{a}+k_{xsm}^{a}\right)}\right]$$

$$J_{eh}^{b1} = -\sum_{m=1}^{Mb} D_{rm}^{b}\cdot A_{sm}^{b}\cdot\frac{k_{xrm}^{b}}{k_{xsm}^{b}}\cdot\frac{m\pi}{4}\cdot\left[\frac{\sin\left(\left(k_{xrm}^{b}-k_{xsm}^{b}\right)\cdot\frac{t}{2}\right)}{\left(k_{xrm}^{b}-k_{xsm}^{b}\right)}-\frac{\sin\left(\left(k_{xrm}^{b}+k_{xsm}^{b}\right)\cdot\frac{t}{2}\right)}{\left(k_{xrm}^{b}+k_{xsm}^{b}\right)}\right]$$

$$J_{eh}^{b2} = \sum_{m=1}^{Mb} D_{rm}^{b}\cdot A_{sm}^{b}\cdot\frac{m\pi}{4}\cdot\left[\frac{\sin\left(\left(k_{xrm}^{b}-k_{xsm}^{b}\right)\cdot\frac{t}{2}\right)}{\left(k_{xrm}^{b}-k_{xsm}^{b}\right)}+\frac{\sin\left(\left(k_{xrm}^{b}+k_{xsm}^{b}\right)\cdot\frac{t}{2}\right)}{\left(k_{xrm}^{b}+k_{xsm}^{b}\right)}\right]$$

## $J_{ee}$ SOLUTION

As the previous cases we obtain $J_{ee.}$

Initially, we can study each region '*a*' and *'b'* independently.

$$(J_{ee})_{rt} = \underbrace{\int_0^e \int_{-\frac{b}{2}}^{\frac{b}{2}} (\nabla T_{er}^{Ia}) \cdot (\nabla T_{et}^{IIa}) dxdy}_{J_{ee}^a} + \underbrace{\int_e^{\frac{a}{2}} \int_{-\frac{b}{2}+c1}^{-\frac{b}{2}+c1+s1} (\nabla T_{er}^{Ib}) \cdot (\nabla T_{et}^{IIb}) dxdy}_{J_{ee}^b}$$

Furthermore we can separate $J_{ee}{}^a$ and $J_{ee}{}^b$ in two parts:

$$J_{ee}^a = \underbrace{\int_0^e \int_{-\frac{b}{2}}^{\frac{b}{2}} \left(\frac{\partial T_{er}^{Ia}}{\partial x} \cdot \frac{\partial T_{et}^{IIa}}{\partial x}\right) dxdy}_{J_{ee}^{a1}} + \underbrace{\int_0^e \int_{-\frac{b}{2}}^{\frac{b}{2}} \left(\frac{\partial T_{er}^{Ia}}{\partial y} \cdot \frac{\partial T_{et}^{IIa}}{\partial y}\right) dxdy}_{J_{ee}^{a2}}$$

$$J_{ee}^b = \underbrace{\int_e^{\frac{a}{2}} \int_{-\frac{b}{2}+c1}^{-\frac{b}{2}+c1+s1} \left(\frac{\partial T_{er}^{Ib}}{\partial x} \cdot \frac{\partial T_{et}^{IIb}}{\partial x}\right) dxdy}_{J_{ee}^{b1}} + \underbrace{\int_e^{\frac{a}{2}} \int_{-\frac{b}{2}+c1}^{-\frac{b}{2}+c1+s1} \left(\frac{\partial T_{er}^{Ib}}{\partial y} \cdot \frac{\partial T_{et}^{IIb}}{\partial y}\right) dxdy}_{J_{ee}^{b2}}$$

If we solve this integrals we obtain the following solutions:

$$J_{ee}^{a1} = \sum_{m=1}^{Ma} D_{rm}^a \cdot D_{tm}^a \cdot \frac{b}{4} \cdot \left[ \frac{\sin\left(\left(k_{xrm}^a - k_{xtm}^a\right) \cdot e\right)}{\left(k_{xrm}^a - k_{xtm}^a\right)} + \frac{\sin\left(\left(k_{xrm}^a + k_{xtm}^a\right) \cdot e\right)}{\left(k_{xrm}^a + k_{xtm}^a\right)} \right]$$

$$J_{ee}^{a2} = \sum_{m=1}^{Ma} D_{rm}^a \cdot D_{tm}^a \cdot \frac{1}{k_{xrm}^a \cdot k_{xtm}^a} \frac{m^2\pi^2}{4 \cdot b} \cdot \left[ \frac{\sin\left(\left(k_{xrm}^a - k_{xtm}^a\right) \cdot e\right)}{\left(k_{xrm}^a - k_{xtm}^a\right)} - \frac{\sin\left(\left(k_{xrm}^a + k_{xtm}^a\right) \cdot e\right)}{\left(k_{xrm}^a + k_{xtm}^a\right)} \right]$$

$$J_{ee}^{b1} = \sum_{m=1}^{Mb} D_{rm}^b \cdot D_{tm}^b \cdot k_{xrm}^b \cdot k_{xtm}^b \cdot \frac{s1}{4} \cdot \left[ \frac{\sin\left(\left(k_{xrm}^b - k_{xtm}^b\right) \cdot \frac{t}{2}\right)}{\left(k_{xrm}^b - k_{xtm}^b\right)} - \frac{\sin\left(\left(k_{xrm}^b + k_{xtm}^b\right) \cdot \frac{t}{2}\right)}{\left(k_{xrm}^b + k_{xtm}^b\right)} \right]$$

$$J_{ee}^{b2} = \sum_{m=1}^{Mb} D_{rm}^b \cdot D_{tm}^b \cdot \frac{m^2\pi^2}{4 \cdot s1} \cdot \left[ \frac{\sin\left(\left(k_{xrm}^b - k_{xtm}^b\right) \cdot \frac{t}{2}\right)}{\left(k_{xrm}^b - k_{xtm}^b\right)} + \frac{\sin\left(\left(k_{xrm}^b + k_{xtm}^b\right) \cdot \frac{t}{2}\right)}{\left(k_{xrm}^b + k_{xtm}^b\right)} \right]$$